Dynamics of the Shear Margin of Ice Stream B, West Antarctica

Thesis by

Miriam Jackson

In Partial Fulfillment of the Requirements

for the Degree of

Doctor of Philosophy

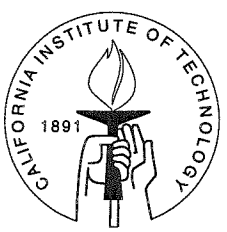

Caltech

Pasadena, California

1999

(Submitted April 2, 1999)

Acknowledgements

There are many people I wish to thank who have helped me during my somewhat extended residence in this division.

My advisor, Barclay Kamb, showed much patience in teaching me about glaciological theory and practice. His depth of understanding of the subject and tenacity with which he tried to solve problems that arose are an inspiration. Our apparent language differences, such that Barclay claims to have understood very little of what I said to him, do not seem to have slowed us down too much.

Rob Clayton, my academic advisor, not only gave good advice but also helped me deal with the occasional bureaucratic hurdles that arose.

Dr. Charles Raymond of the University of Washington provided the basic finite element code that was used in this study and helped with the initial problems in getting it to run successfully.

I wish to thank thank Hermann Engelhardt for carrying out the core drilling that furnished the core studied here, and also for providing the temperature profile in Figure 8b and for help with preparation of the test apparatus and instrumentation. He was ably assisted in the difficult job of drilling in the highly crevassed Dragon by Keith Echelmeyer, Will Harrison, and several field assistants (Chris Larsen, Keri Petersen, Keith-Nels Swenson, Sabina Schmidt, and others). Several of those field assistants made field seasons not only bearable but fun, most especially Leanne Allison, Darius Siemmens, Deborah Baldwin and Sam Webb.

Will Harrison provided Figure 3.5 and he and Keith Echelmeyer provided preprints of their work, including the newer velocity date in Chapter 3, and were always willing to answer any questions that arose.

I think Richard Alley for occasional discussions about ice fabrics, for encouraging me to do the fabric mapping in Chapter 4 and for generously offering me a postdoctoral position at Penn. State.

The work in chapter 3 was made possible by grants OPP-9018703 and OPP-9319018 from the National Science Foundation.

The secretarial staff of the division, especially Ann Freeman, Donna Sackett, Cheryl Contopolous and Kathy Lima, were always helpful with paperwork and my many questions, and Kathy never got sick of me asking the whereabouts of missing faculty.

Many students made my tenure in this division a more pleasant experience. Sharon Kedar deserves special mention for inviting me over to South Mudd from solitary confinement in North Mudd, although his ceaseless chatter and endless arguments that he always lost did nothing to shorten my stay here. Tim Melbourne either joined in of took up the slack when Sharon wasn't around, but also taught me some basic things about UNIX, LaTeX and computers in general that other students here appear to learn by osmosis. Despite my above complaints about them, Sharon and Tim have always been not only great office-mates but also very good friends. Craig Scrivner also answered various latex and other computer-related questions, and generally made life more bearable. I shared my office with various other students, including Jeanne Hardebeck, Linda Rowan, Anu Venkataraman and Lupei Zhu, some of who also had to occasionally share the office with one of my sons, Joseph, who wasn't always the quietest child. Indeed, I think everyone in seismolab who has put up with Joe and Luke as they explored various offices and corridors.

My two children have helped very little with this thesis, except to get sick or have sleepless nights at the most inopportune times. I thank them anyway just for being here and for being the greatest two kids in the world, even though they never see as much of me as they would like.

Lastly, I thank my husband Graeme Whittington, who has followed my academic wanderings around the globe, missed soccer games when I needed to work, and who has always believed in me.

Abstract

The ice streams in the West Antarctica Ice Sheet flow at several hundred metres per year. The lateral increase in speed from typical inland ice sheet speeds of a few metres per year to ice stream speeds of several hundred metres per year occurs over a short distance ($\sim$ 2 km) in the outer part of the ice stream known as the marginal shear zone (MSZ). The ice in this zone is highly crevassed and chaotically jumbled. This thesis is an effort to understand the dynamics of the MSZ and to find out whether the velocity of the ice stream is controlled primarily by the stresses in its MSZs or by stresses at the base. This is done by determining the marginal shear stress in one of the marginal shear zones using the ice itself as a stress meter. The observed marginal shear strain rate of 0.14 a^{-1} is used to calculate the marginal shear stress from the flow law of ice determined by creep tests on ice cores from a MSZ. The test specimen orientation relative to the stress axes in the tests is chosen on the basis of *c*-axis fabrics so that horizontal shear across vertical planes parallel to the margin is applied to the ice specimens in the test. The resulting marginal shear stress is $(2.2 \pm 0.3) \times 10^5$ Pa. This implies that 63 to 100% of the ice stream's support against gravitational loading comes from the margins and only 37 to 0% from the base, so that the margins play an important role in controlling the ice stream motion. The marginal shear stress value is twice that given by the ice-stream model of Echelmeyer *et al.* (1994), and the corresponding strain-rate enhancement factors differ greatly ($E \approx 1-2$ from the creep tests vs. $E \approx 10-12.5$ from the model of Echelmeyer *et al.* (1994)). This large discrepancy may possibly be explained by recrystallization of the ice during or shortly after coring. Estimates of the expected recrystallization time scale range widely but include the $\sim$ 1-hour time scale of coring and leave the likelihood of recrystallization uncertain. However, the observed two-maximum fabric type is not what is expected for annealing recrystallization from the sharp single-maximum fabric that would be expected in situ at the high shear strains involved ($\gamma \sim 20$). Experimental data from

Wilson (1982) suggest that if the core did recrystallize, the prior fabric was a two-maximum fabric not substantially different from the observed one, which implies that the measured flow law and derived marginal shear stress are applicable to the in-situ situation.

An ice-stream flow model was developed to explore the discrepancy in enhancement factors. Using this model, which is similar to the model of Echelmeyer *et al.* (1994), it is possible to match the observed surface velocity profile across the ice stream using a strain rate enhancement factor of 5. This is more than four times the value found in the experimental work but half the value from the modelling results of Echelmeyer *et al.* The flow model suggests that the lateral shear stress integrated over the margins is larger than the basal shear stress integrated over the base, so that the ice stream is controlled at the sides rather than at the base.

It was thus not possible to reconcile fully the results from the experimental work and from modelling, since the modelling still suggests that there is substantial flow enhancement in the MSZ. There may be variation of the enhancement factor with depth, so that at 300 m depth the enhancement factor is close to 1, but increases at greater depths.

c-axis measurements in ice from the middle of the MSZ reveal that there is an asymmetrical two-maxima fabric, as expected for ice under simple shear. 600 m away, between the middle of the MSZ margin and its outer edge, there is still a two-maxima fabric but the secondary maximum is much smaller and the primary maximum is much bigger. 500 m further, right at the boundary between the shear margin and the ice stream, there is only a single maximum. Outside the ice stream the fabrics show a single, very diffuse maximum.

Contents

List of Figures

List of Tables

Chapter 1 Introduction

The ice streams in West Antarctica are one of the most fascinating features of the West Antarctic Ice Sheet. They flow at several hundred metres per year. Why do they flow so fast? Standard glaciological theory predicts a speed of less than a metre per year based on ice stream surface slope and ice thickness. The inland part of the ice sheet in this region flows at speeds of less than 10 metres per year. However, Ice Stream B flows at more than 400 metres per year in the region studied and faster than 800 metres per year farther downstream, despite its very low surface slope.

These ice streams may play an important role in the stability of the ice sheet (e.g., Alley and Whillans, 1991). It is thought that the ice streams themselves could be unstable. To understand the stability of the ice streams, it is necessary to understand how forces are partitioned within the ice stream. Whereas valley glacier behavior is controlled by flow processes both at the base and at the margins, in ice streams the width-thickness ratio is so much greater that it was generally considered that ice stream motion must be controlled mainly by resistive drag at the base, and that the margins were relatively unimportant. However, it is known that Ice Stream B is underlain by a layer of water-saturated till (Alley *et al.*, 1986, 1987). This till is very weak, especially at the high water pressures that exist beneath the ice stream, and its shear strength is too low to support the downslope component of gravity acting on the ice stream (Kamb, 1991). Some authors (e.g., Alley, 1993) have suggested that the ice stream is supported by "sticky spots" where the till is either stronger than elsewhere or is absent and the bed is composed of bedrock instead. An alternative suggestion by Echelmeyer *et al.* (1994) and by Ian Whillans (pers. com.) is that the marginal shear zones (MSZs) that mark the boundaries of the sides of the ice stream play an important role in supporting the ice stream and controlling its flow.

An important consequence of the high flow velocities of the ice streams is that if the ice streams were to increase in speed, there could be a negative mass balance of

ice in West Antarctica (as there already is in some places such as Ice Stream B). If ice is drained from the interior of the ice sheet much faster than it is replenished, this could lead to the collapse of the ice sheet. In order to understand the possibility of collapse we need to understand how the ice streams flow so fast, the forces that are restraining them and the potential for change in ice stream dynamics.

A mechanism for the fast flow of ice streams was proposed by Hughes (1975). He suggested softening of the ice within the MSZs. It wasn't until ten years later that velocity measurements were made on the ice streams, using Magnavox Doppler (Transit) satellite receivers. These receivers took a long time to measure a position and this measurement then had to be repeated after a substantial interval to get a reliable velocity measurement. Using this technique alone it was difficult to measure how the velocity varies across the MSZ of an ice stream. However, it was possible to use this technique in conjunction with others to collect velocity data within the MSZ. Jackson (1991) used repeat aerial photography with ground control provided locally by the satellite receivers to collect hundreds of flow-velocity measurements across the ice stream. This was done by tracking the positions of features such as crevasses over a period of one year. Echelmeyer *et al.* (1994) were able to measure velocity in a transect across the MSZ by using a theodolite and electronic distance meter to survey markers that they had placed in a profile across the margin. They then used this velocity profile to develop various numerical models for the velocity field. From these models they were able to place a numerical value on the strain rate enhancement within the MSZ. The amount of enhancement is a measure of how much faster the ice stream flows than would be predicted by standard glaciological theory.

Chapter 2 describes mechanical experiments that were performed on ice samples from within an ice stream MSZ (the Dragon, the southern MSZ of this part of Ice Stream B). The strain rate within the MSZ is known from the two sets of velocity measurements described above. By applying to the ice samples a stress sufficient to produce a strain rate that matches that observed in the MSZ, it is possible to calculate the shear stress within the MSZ. From this, the partitioning of stresses within the ice stream can be deduced.

The mechanical experiments indicate that there is little or no enhancement in the shear margin and that the high shear strain rate within the shear margin must be due to some other aspect of ice stream flow. In contrast, Echelmeyer *et al.* (1994) found by numerical modelling of the ice stream that substantial flow-law enhancement is necessary in the MSZ, with flow enhancement factor rising to a peak of $E = 12.5$ within the MSZ. In order to better understand the discrepancy between the enhancement factors $E \approx 1$ from laboratory testing and $E \approx 12.5$ from numerical modelling, and to see if it is possible to use the laboratory value of E in a numerical model that successfully reproduces the measured surface velocity profile, I here develop my own model of the flow distribution in and adjacent to the MSZ using the finite element method, and compare it with the model of Echelmeyer *et al.* (1994) and with the measured velocity profile. This is done in Chapter 3.

In order to orient the ice correctly to perform the mechanical tests, it is necessary to study the c-axis orientations of the individual crystals within the ice. The c-axis orientations are plotted on a Schmidt diagram to give the ice fabric, which is a measure of the degree of alignment of the different c-axes. As well as being used to orient the ice for the mechanical tests, these measurements are also intrinsically interesting because the ice fabric tells us something about the past and present stresses to which the ice has been subjected and about the possible recrystallization that may have occurred in the ice specimens during or subsequent to the coring operation.

Ice samples were taken from different drill holes in a transect that goes from the middle of the MSZ, where the velocity increases over a short distance and the strain rate is a maximum, to the intra ice-stream region called the Unicorn where the ice is flowing very slowly. Each drill site is in a different stress regime from the other drill sites. The ice fabrics give some indication of what the stress regime is and how much it differs from a neighbouring site. If the stress regime represented by the fabrics differs from that suggested by the measured velocity field, this implies that the ice was previously under a different state of stress. The response of the fabric to such a change in the stress state in the MSZ is probably about 3 years. As there is a lateral component of ice flow which moves ice laterally through the MSZ, as well as

the dominant longitudinal component of velocity which moves the ice along the ice stream, it is not unexpected that the ice from at least some of the boreholes would have previously been under a different state of stress. The challenge is to understand the stress history described by the ice fabrics and how this relates to the dynamics of the MSZ. The fabrics are described in Chapter 4.

Chapter 2 The Marginal Shear Stress

2.1 Introduction

One of the major issues concerning the stability of the ice streams is whether they are mainly supported by the shear margins or whether most of the support is at the bed. This thesis addresses this issue by undertaking a determination of the marginal shear stress of Ice Stream B2 at a point in its southern shear margin (the "Dragon"; see Figure 2.1). From this stress we can estimate how the support of the ice stream against gravitational loading is partitioned between the base and margins, which provides a measure of the relative importance of the base and margins in controlling the flow.

The method of measuring the marginal shear stress is to use the ice itself as a stress meter. The marginal shear strain rate is measured, and the shear stress is calculated from the ice flow law. To determine the flow law we obtained core samples of ice from the marginal shear zone and subjected them to creep tests in the laboratory.

This work is part of a comprehensive study of ice stream mechanics by means of borehole geophysics (Engelhardt *et al.*, 1990; Kamb, 1991; Kamb and Engelhardt, 1991; Engelhardt and Kamb, 1994, 1997, 1998), and it bears directly on modelling of ice flow in the marginal shear zones (Echelmeyer *et al.*, 1994; Raymond, 1996).

2.2 Field Data

The above procedure for shear stress measurement is carried out for a location (borehole site) "93-6" near the center of the Dragon about 10 km from camp Up B, as shown in Figures 2.1 and 2.2. At this site the marginal shear strain rate is at a level that is at or near its maximum in a transverse profile through the site (see Figure 2.2). The shear strain rate has been measured by two different methods. One method used

repeat aerial photogrammetry and tracked crevasses over a one year interval to give the velocities of the crevasses and hence the strain rates (Jackson, 1991; Whillans *et al.*, 1993). The marginal strain rate near Up B was found to be approximately 0.14 a^{-1}, expressed as engineering shear strain rate $\dot{\gamma} = \partial u_x / \partial u_y$, where u_x is the absolute flow velocity in the x (downstream) direction and y is the transverse coordinate (perpendicular to x). In the second method, Echelmeyer *et al.* (1994) made repeated ground surveys of a profile of marker poles placed across the shear margin, through site 93-6, obtaining the velocity profile reproduced in Figure 2.2. According to Echelmeyer *et al.* (1994, Figure 2b) the shear strain rate at site 93-6 is 0.15 a^{-1}. In our evaluation of the marginal shear stress we take $\dot{\gamma} = 0.14$ a^{-1}.

2.3 Ice Samples

The ice tested to determine the flow law was obtained in late December 1993 from a depth of 300 m in borehole 93-6, by means of a hot water ice core drill used in conjunction with standard hot water drilling from the surface down to 300 m. The core drill retrieves azimuthally unoriented ice cores of maximum diameter 9.5 cm and maximum length 2 m. Two cores, each of length 2 m, were obtained from depths 300-304 m in borehole 93-6, where the total ice thickness is approximately 950 m. The 300 m depth of the cores was chosen as a depth great enough to have ice of suitable texture and be below the disturbing effects of crevasses and yet shallow enough that the marginal shear strain rate measured at the surface is expected to be applicable. It is also a depth tolerable for drilling under the restrictive conditions in the Dragon. Access to site 93-6 for people and equipment (manhauled) required special precautions and involved special difficulties because of the very extensive crevassing.

After retrieval the ice cores were kept as cold as possible (ca. $-10°C$) for two days in insulated Tilson boxes buried in the snow and shielded from solar radiation with plywood sheets. The boxes were then taken by air (cold deck LC-130 flight) to McMurdo Station, where they were stored at $-22°C$ for about 1.5 months, and where preliminary studies of the ice were made. The boxes were then shipped by sea to the

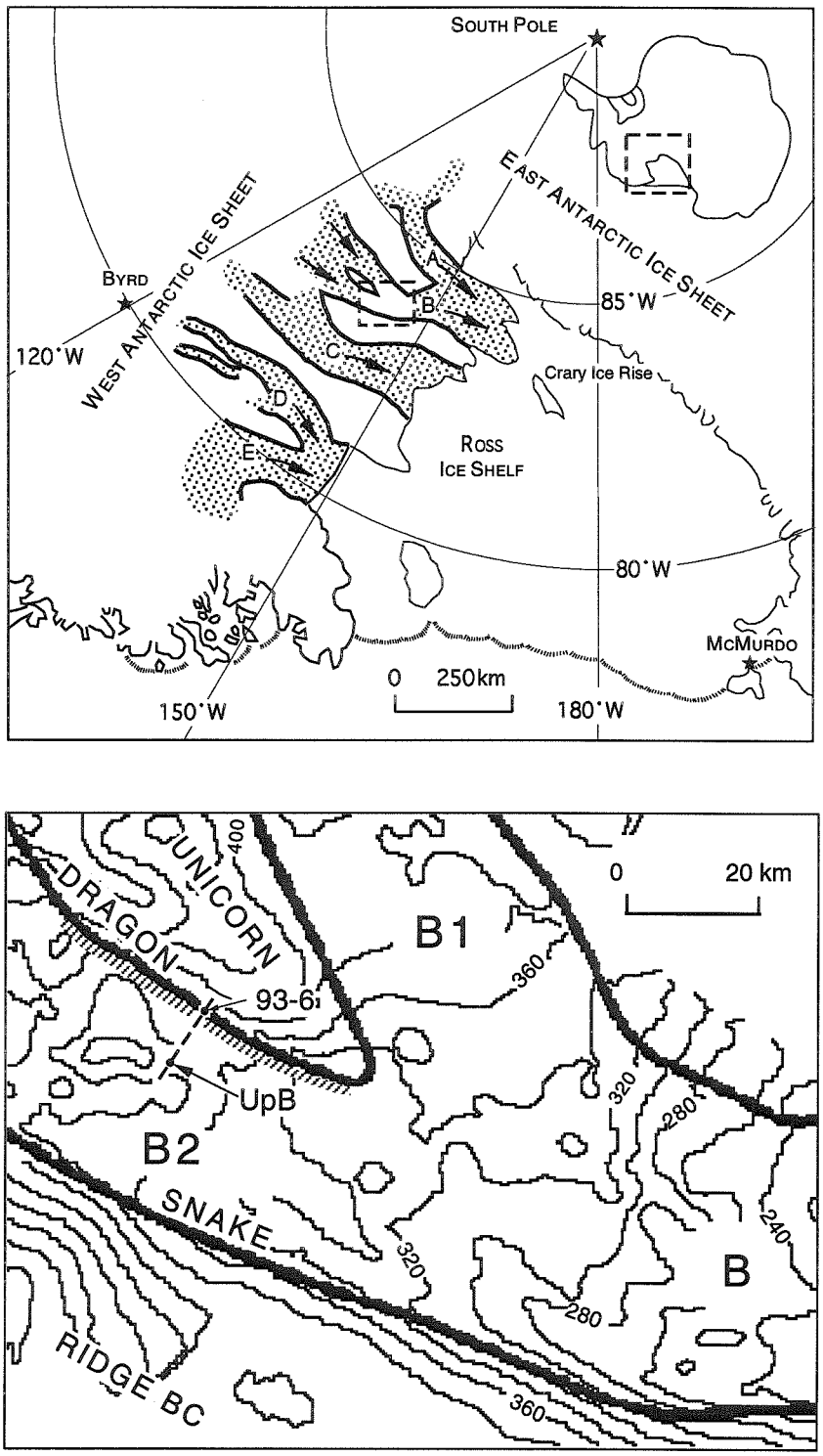

Figure 2.1: Location map showing core hole 93-6 on a profile (dotted) across the south half of Ice Stream B2, passing through camp Up B, based on Retzlaff *et al.* (1993, Fig. 7). Marginal shear zones are shown schematically with heavy lines; the Dragon is shown with added cross-hatching to approximate its actual width. Surface contour elevations are in meters.

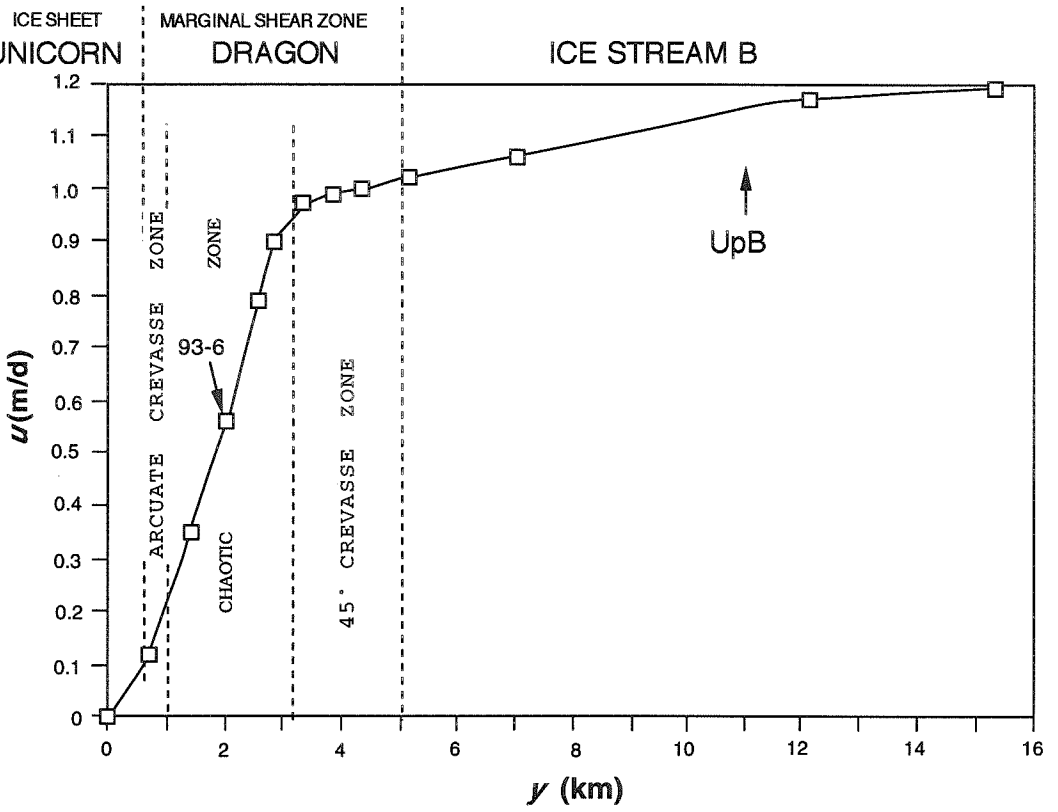

Figure 2.2: Ice-stream flow velocity u along the dotted profile in Figure 2.1, showing the relation between the velocity profile and the marginal shear zone of Ice Stream B2 (the Dragon). On the left (south) is the interstream ridge called the "Unicorn" (Fig. 1). The locations of Up B and core hole 93-6 on the profile are marked. The lightly dashed lines show subdivision of the shear zone into three subzones. The flow velocities are preliminary values kindly supplied by Keith Echelmeyer (pers. com.). The (transverse) y coordinate is measured from 0 at the south end of the profile.

U.S. in a refrigerated shipping container at −20°C, and delivered to Pasadena from Port Hueneme (transport time 1.5 hours) where they were put into cold-room and deep-freeze storage at −23°C. The total elapsed time from retrieval to testing of the samples used in this study was 1.5–2.5 years, most of it at a temperature of −23°C. This temperature history makes it unlikely that the ice underwent recrystallization before being tested (Gow, 1994), except possibly during the hot-water core-drilling operation as discussed in Section 2.7.

In the present study, ice from one of the two cores from borehole 93-6, core no. 93-6-1, was used in the creep tests. Using only a single core made it possible to keep track of the relative orientations of all thin sections and test specimens.

From the ice core, 11 oriented thin sections (ca. 0.5 mm thick) were made with a microtome from slabs of ice cut from the core with a band saw and cemented to glass plates with cyanoacrylate glue. An example of the grain texture shown in the sections is given in Figure 2.3. The mean grain area, as measured by counting all the grains within a given area of a vertical thin section, is 15 mm^2, but some grains are up to 70 mm^2 in area. The grain shapes are irregular (non-tessellate) and interlocking, with suturing of grain boundaries, as is normal for ice that has recrystallized during deformation. The grain size and shape are comparable to that for presumably shear-deformed ice from depth $\sim$ 1500 m in the Byrd core (Gow and Williamson, 1976, Figs. 2,3) and from depth $\sim$ 1100 m in the Camp Century core (Herron and Langway, Jr., 1982). Some grains contain planar basal cleavage cracks, seen in thin section and also when the core was first brought to the surface; they doubtless formed on release of pressure, either during the core sampling or during thin sectioning.

c-axis fabrics were measured for 7 of the above thin sections, some in horizontal and some in vertical orientations. Although there is statistical fluctuation in the fabric diagrams from section to section, the general pattern is consistent: two fairly broad, unequally strong maxima, both centered approximately in the horizontal plane, and at an angle of about 50° ± 10° between them. An example is shown in Figure 2.4. This is the general type of pattern expected for simple shear in a horizontal direction across vertical planes (Kamb, 1972, p. 236), which is the strain geometry expected in

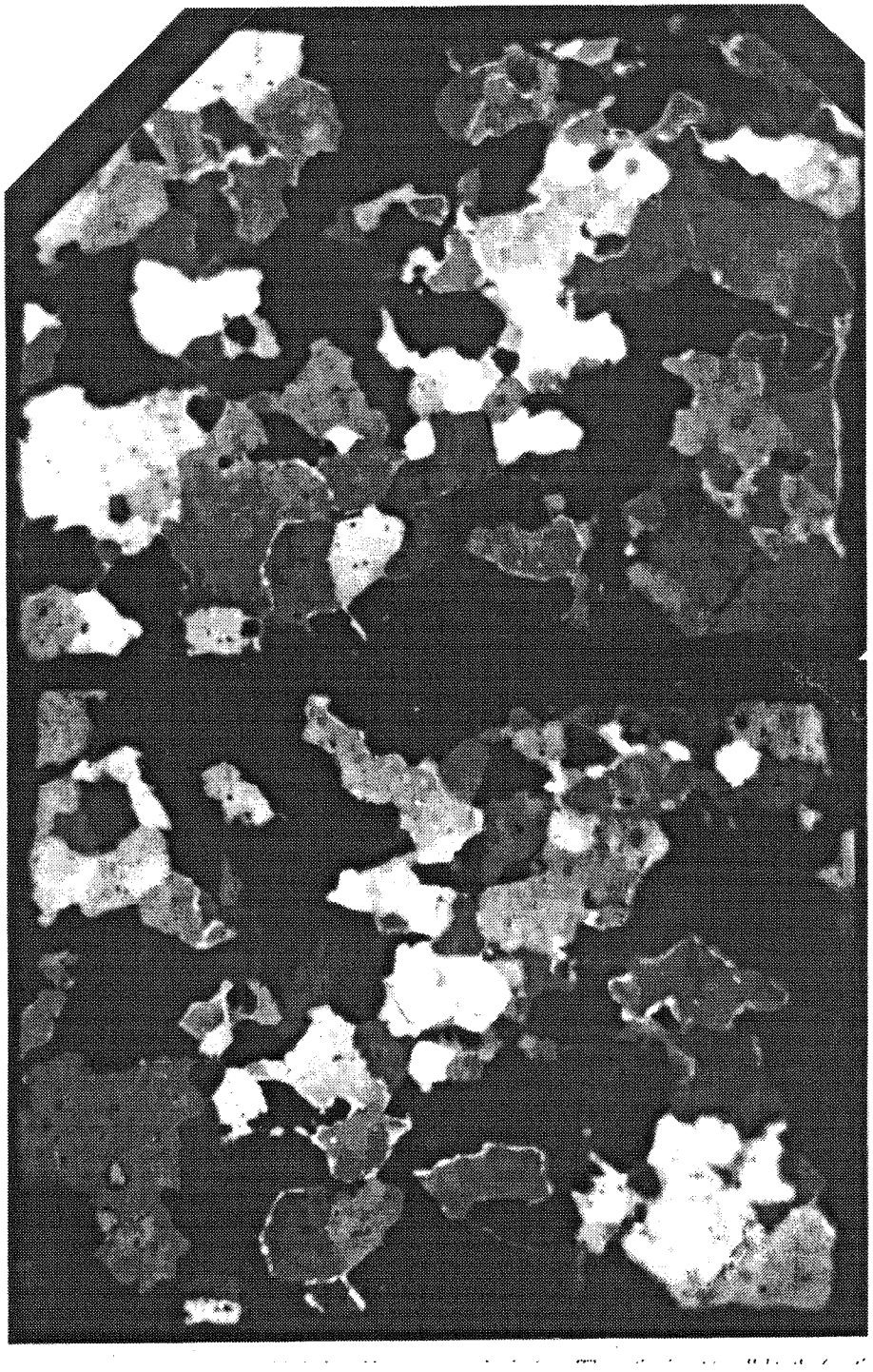

Figure 2.3: Thin section of ice from specimen no. 2 viewed between crossed polarizers. The section is cut parallel to the (vertical) core axis, which runs left and right across the photo. For scale, the ice measures 5.9 cm in that direction. In order to make all of the grains visible, the photo shows the section twice: in the upper half, and then repeated in the lower half with the direction of polarization rotated 45° with respect to the first.

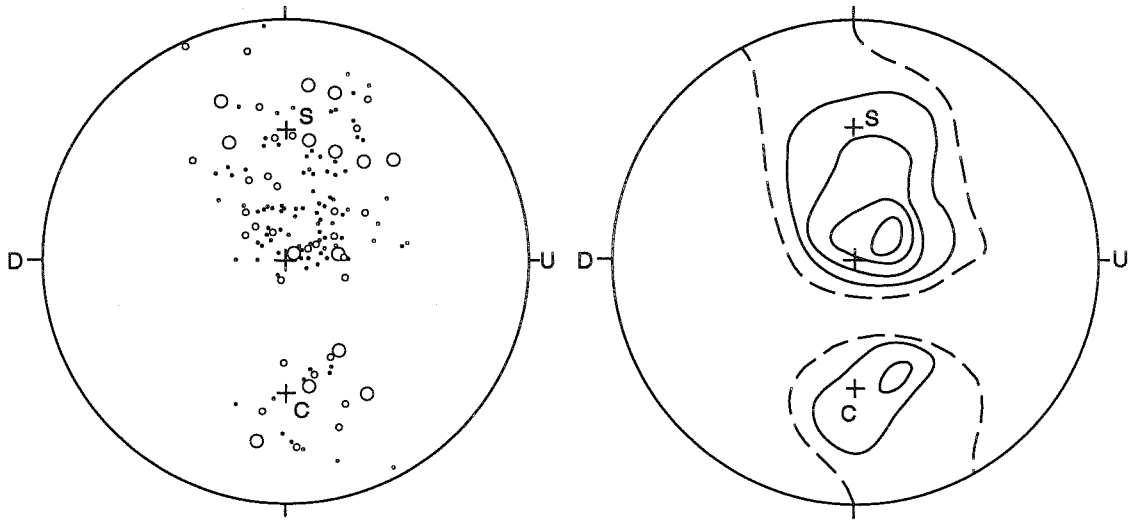

Figure 2.4: *c*-axis fabric of ice from the thin section shown in Figure 2.3. Equal area plot, on the lower hemisphere. 139 *c*-axes are plotted. The size of each crystal is indicated by the plotting symbol as follows: a large open circle indicates a grain whose longest dimension is ≥ 1 cm; small open circle, longest dimension in the range 0.5 to 1 cm; dot, longest diameter < 0.5 cm. For the contoured diagram the points were counted with a counting area of 2.4% of the area of the hemisphere. (2.4% was used rather than the more usual 1% to give a better representation of the fabric, following the methods of Kamb (1959)). Solid contours are at 1, 2, 3, 4% per 1% of area, dashed contour at 0.3% per 1%. The core axis runs from U (up) to D (down). The axis of compression in the creep test is the unlabelled tick at the top of the equatorial circle (or at the bottom). The pole of the shear plane (or plane of maximum resolved shear stress) is at S, 45° from the compression axis, and its conjugate plane is at C.

the shear margin. A complete treatment of fabric data from within and outside the shear margin is given in Chapter 4.

2.4 Creep Tests

The ice core to be tested was cut with a band saw into rectangular parallelepipeds in the required orientation (see below), and the faces of the parallelepipeds were smoothed with a file. The pieces were tested in unconfined uniaxial compression between plane parallel stainless steel platens (figure 2.5). Test pieces were of average height 4.1 cm parallel to the compressional axis and average cross-sectional area 22 cm^2 in the plane perpendicular to that axis. The test pieces were cut from the core in

an orientation such that the core axis was perpendicular to the compression axis and the stronger of the two c-axis fabric maxima was at 45° to the compression axis, i.e., centered at point S in Figure 2.4. (Because of statistical fluctuations in fabric from one thin section to another cut in the same orientation with respect to the core, in some sections the maximum is found to deviate somewhat from the intended position at S, which was established from another thin section. This is the case in Figure 2.4.) This makes the compression test apply maximum shear stress to the test specimen in the same orientation as marginal shear stress was applied to it in the ice sheet, namely, in a horizonal direction across vertical planes parallel to the margin. This relation holds because the stronger c-axis maximum is normal to the plane of simple shear (Kamb, 1972, p. 236).

Although a measurement of shear stress is the objective, the creep test used is a compression test because of the well known difficulties associated with direct shear type tests. The compression test is a permissible substitute because of the insensitivity of the flow law to the mean stress, because of the equivalence of simple shear and pure shear for the small strains involved in the tests, and because of the expected effect of flow anisotropy due to the c-axis fabric (discussed in Section 2.5). The testing apparatus is shown schematically in Figure 2.5. Compressive stress is applied to the upper platen by weights acting through a lever of mechanical advantage 11.5. The applied load is measured with a load cell, and the displacement of the upper, moveable platen is measured with two Mitutoyo 543 digital displacement indicators, which can resolve displacements of 0.001 mm. The gauges are located symmetrically on opposite sides of the load axis in order to measure the movement of the loading platen on the center line by averaging the readings of the two indicators and thus eliminating the effect of any slight tilting that occurs. The shortening displacement, load, and temperature near the specimen are recorded on a data logger as a function of time. The apparatus is enclosed in a thermally insulated compartment to damp the temperature fluctuations within the room caused mainly by the cyclic operation of the refrigeration defrost system. The rms variation in temperature in the air near the test specimens is 0.1°C.

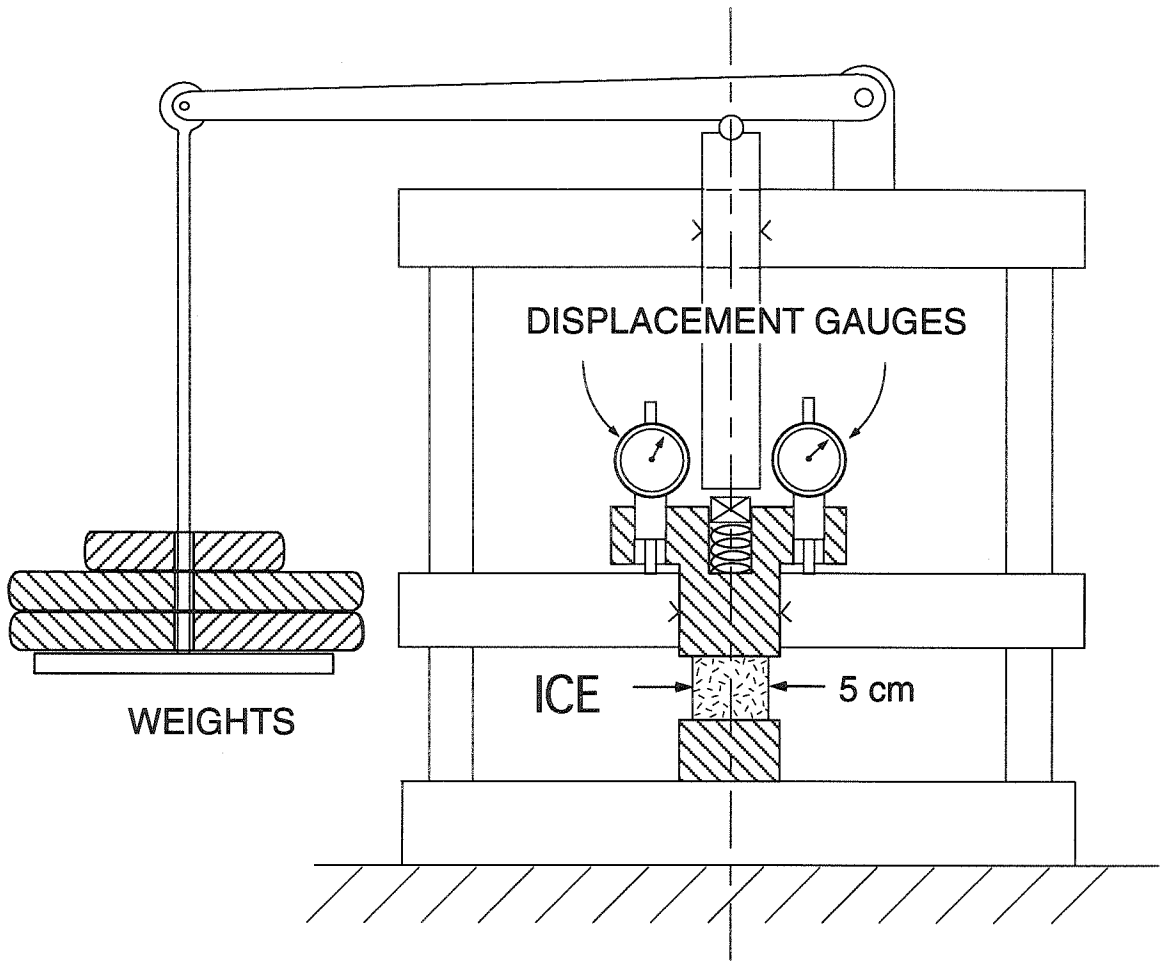

Figure 2.5: Diagram of test apparatus. The test specimen, approximately a cube of size 5 cm, is compressed between the upper and lower platens, shown cross-hatched. The upper platen is loaded by the weights via the lever and upper loading shaft, which presses on a load cell (identified by the symbol "×" in the diagram) and in turn on a load-transfer spring to protect the ice from loading shocks. The displacement gauges (Mitutoyo 543) measure the motion of the upper platen relative to the loading frame. The frame dimension is 0.4 m. Surfaces marked with a "V" are close sliding fits for mechanical stability in loading.

In carrying out creep tests to define the marginal shear stress, each specimen was tested at two stress levels, such that the resulting two shear strain rates bracketed (or nearly bracketed) the observed marginal shear strain rate of 0.14 a^{-1}. The marginal shear stress is then obtained by nonlinear interpolation between (or slight extrapolation from) the two data points, as explained in the Section 2.5.1. The shear stress across the shear plane is one-half of the compressive stress acting at 45° to this plane in the test, and for pure shear the compressive shear strain rate sought in the test is one-half the observed marginal shear strain rate of 0.14 a^{-1}, hence the compressional stress levels in the tests were chosen to give measured longitudinal strain rates $\dot{e}$ bracketing the value $\dot{e} = 0.07a^{-1}$. (These relations follow from Mohr's circle.)

Four ice specimens from core no. 93-6-1 were tested in the above way. The temperature for all tests was $-22.0° \pm 0.1°C$, fairly close to the observed temperature of $-24.1°C$ at depth 300 m in borehole no. 93-5, adjacent to no. 93-6 (Harrison and Echelmeyer, 1994). Test parameters and results are listed in Table 2.1. Test l refers to the creep test at the lower stress, test h to that at the higher stress. Typical test data are given in Figure 2.6, which shows platen displacement, load, and temperature vs. time for the tests on specimen no. 1. Each test at a given stress was allowed to run uninterrupted for 8 to as long as 14 days (individual figures in Table 2.1), until the strain rate stabilized once the large initial transient creep rate had died away. The criterion for steady strain rate was that the average strain rate over the last day of the test be no more than 0.003 a^{-1} smaller than the average over the last 3 days. The strain-rate value given for each test in Table 2.1 is the last-three-day average value.

As illustrated in Figure 2.6, the testing of each specimen began with the preliminary application of a load considerably below the test l load, for a period of several to 10 days. The strain rates at these low loads did not reach a steady state as reliably as at the higher stresses of test l and test h, hence the results of the low-load tests are not used in determination of the marginal shear stress. However, the time spent in the preliminary low-load part of each run was of value, we think, in counting toward the accumulation of primary creep strain needed to reach steady state in tests l and

Specimen number	Height	Area	Test duration		Applied stress (compression)		Compressive strain rate		Overall decrease in specimen dimensions		
	L_z	L_xL_y			σ		$\dot{e}$		$-\Delta L_x$	$-\Delta L_y$	$-\Delta L_z$
	cm	cm^2	d		10^5 Pa		a^{-1}	a^{-1}	%	%	%
			(l)	(h)	(l)	(h)	(l)	(h)			
1	3.9	22	8	9	4.94	5.45	0.073	0.097	3.3	1.1	1.7
2	3.7	21	8	8	4.42	5.14	0.056	0.091	3.2	1.3	2.6
3	4.5	23	9	9	4.26	4.60	0.053	0.066	-	-	-
4	4.4	22	10	14	4.75	5.31	0.068	0.093	12.8	1.3	3.5

Table 2.1: Specimen dimensions and test data, (l) at lower stress level and (h) at higher stress level.

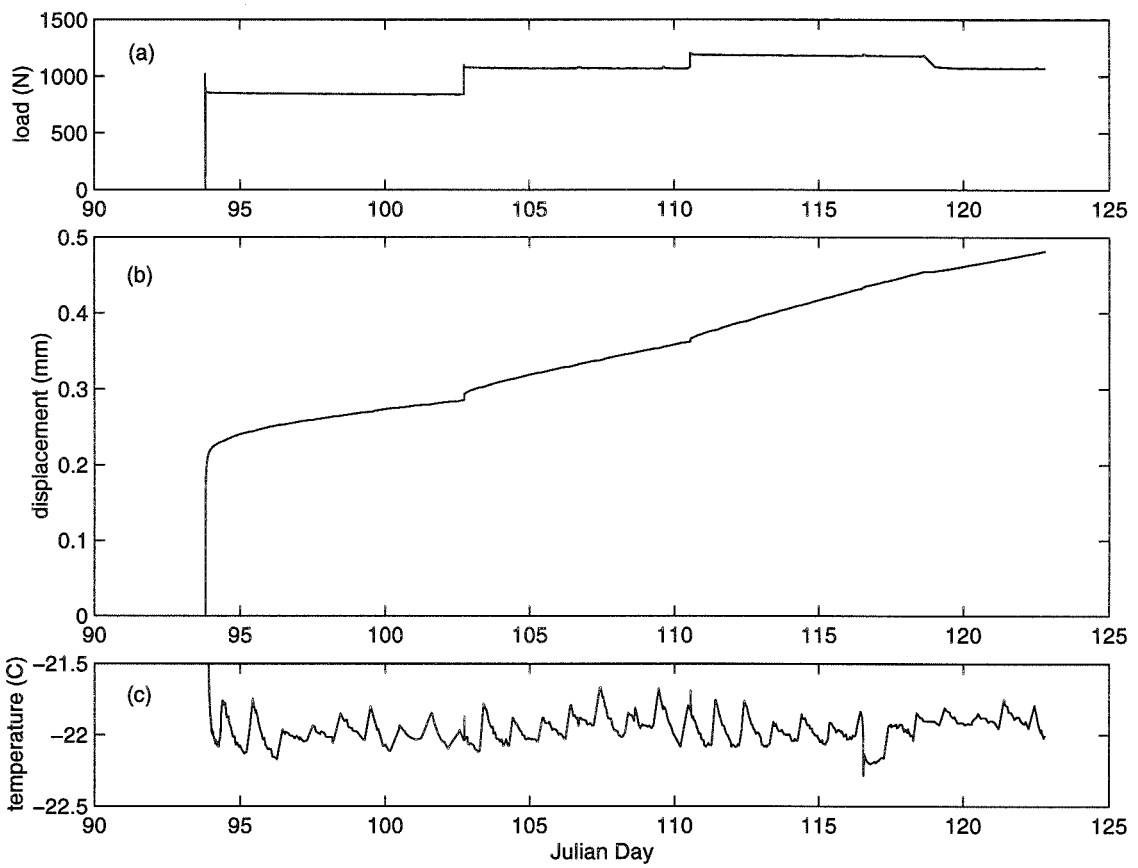

Figure 2.6: Test data for specimen no. 1. (a) shows the applied load and (b) the response in terms of displacement of the upper platen vs. time. (c) records the air temperature alongside the specimen. Test l runs from J.D. 102 to 110, and Test h from J.D. 110 to 119, after which a run at a stress level near that of Test 1 is done as a check. The run from J.D. 94 to 102 is an example of the type of low-load preliminary test mentioned in the text.

h.

In interpreting the results in Table 2.1 in terms of the marginal shear stress, as done in Section 2.5, we assume that the core sampling procedure captured the ice in its in situ structural state, in tertiary creep at very large shear strain. Thus in the laboratory creep tests the stationary stain rate that was reached once the transient creep had died away is the rate for renewed tertiary creep, as has been observed for stopped and restarted laboratory tests (Budd and Jacka, 1989, pp. 116, 126, and Fig. 8, curves L3). It is thus the strain rate appropriate to the in situ flow of the ice prior to core sampling. In Section 2.7 the possibility that the above assumption is violated

due to annealing recrystallization is considered.

2.5 Interpretation

2.5.1 Marginal shear stress, τ_M

The strain-rate vs. stress data in Table 2.1 can be interpreted in a straightforward way by assuming that a Glen-type flow law applies to the ice in shear across vertical planes parallel to the margin (e.g. Paterson, 1994, Chapter 5):

$$\dot{\gamma} = C\tau^n \tag{2.1}$$

where $\dot{\gamma}$ is engineering shear strain rate across the marginal planes, τ is the shear stress across these planes, and C is a flow-law constant similar to the A that is usually used. The marginal shear stress τ_M is the value of τ that produces the observed marginal shear strain rate of $\dot{\gamma}_M = 0.14\text{a}^{-1}$:

$$\tau_M = (\dot{\gamma}_M/C)^{\frac{1}{n}}. \tag{2.2}$$

The straightforward way to obtain C from the creep tests is to assume that the c-axis fabric is accompanied by a flow anisotropy such that the axial compression σ in the tests, applied at 45° to the marginal shear planes, produces a simple shear strain rate across these planes. In this case, from Mohr's circle $\tau = \sigma/2$ and $\dot{e} = \dot{\gamma}/2$ where $\dot{e}$ is the axial shortening strain rate produced by σ. Hence, from (2.1)

$$\dot{e} = B\sigma^n \tag{2.3}$$

$$B = C/2^{n+1}. \tag{2.4}$$

Specimen number	Marginal shear stress τ_M 10^5Pa	Flow-law exponent n	Enhancement factor E Pat. E_P	B. & J. E_J
1	2.43	2.8	1.12	2.31
2	2.37	3.2	1.19	2.48
3	2.35	2.9	1.22	2.55
4	2.40	2.7	1.14	2.39

Table 2.2: Derived results (anisotropic evaluation).
Pat.: E is referred to the flow law of Paterson (1994, p. 97).
B. & J.: E is referred to the flow law of Jacka and Budd (1989, Fig. 1).

The reason for introducing B as a separate flow parameter will become apparent in Section 2.5.2. If we now use (2.3) to interpret the data for tests l and h,

$$\dot{e}_l = B\sigma_l^n, \ \dot{e}_h = B\sigma_h^n \tag{2.5}$$

we can obtain B and n by solving (2.5):

$$n = \frac{\log \dot{e}_h - \log \dot{e}_l}{\log \sigma_h - \log \sigma_l} \tag{2.6}$$

$$\log B = \frac{\log \sigma_l \log \dot{e}_h - \log \sigma_h \log \dot{e}_l}{\log \sigma_l - \log \sigma_h} \tag{2.7}$$

Then C is obtained from (2.4) and the marginal shear stress from (2.2). The above method uses the Glen-type relation (2.3) as a means of interpolating (or slightly extrapolating) non-linearly between the data of test l and test h (Table 2.1) to find the stress τ_M that corresponds to the observed $\dot{\gamma}_M$.

The results are listed in Table 2.2. They indicate a marginal shear stress of $(2.2 \pm 0.3) \times 10^5$ Pa. There is only a modest scatter in the results from the four specimens. The indicated value $n = 2.9 \pm 0.3$ is as expected for a shear zone dominated by simple shear (Alley, 1992).

2.5.2 Effects of isotropy/anisotropy on the evaluation of τ_M

The above derivation of τ_M from the test data implicitly treats the flow of the ice as "perfectly anisotropic" in the way it would be if the fabric were so strong that the ice flowed like a single crystal with its (0001) planes aligned parallel to (or perpendicular to) the marginal planes (see Figure 2.7), and with flow law (2.1) relating shear stress τ and shear strain rate $\dot{\gamma}$ across (0001). There is indeed a well developed fabric with roughly these features, as discussed in Section 2.3. (In Figure 2.7 the (0001) planes for crystals of the second, weaker maximum in Figure 2.4 are omitted for clarity; these crystals would contribute to the flow in the same way as the crystals of the first maximum do, if the second maximum were perpendicular to the first.)

There is some qualitative experimental evidence for the assumed flow anisotropy: the extensional strain rate perpendicular to the compression axis (centerline in Figure 2.5) is smaller in the direction parallel to the marginal planes (x axis in Figure 2.7) than in the direction at 45° to the marginal plane (y axis in Figure 2.7). This relationship is indicated in Figure 2.7 by the heavy arrows, which represent the extensional/compressional strain rates in the three perpendicular directions (x, y, z) parallel and perpendicular to the compression axis of the tests. The extensional strain rates $\dot{e}_x$ and $\dot{e}_y$ (Figure 2.7) cannot be measured quantitatively in our test specimens because the x and y faces are free faces that become slightly ablated by sublimation during the test, but the final specimen dimensions are always reduced relative to the initial dimensions by a larger amount in the x direction than in the y direction, indicating that $\dot{e}_x < \dot{e}_y$. The magnitude of the inequality $\dot{e}_x < \dot{e}_y$ is of the same order as the magnitude of $\dot{e}_z$, to judge from figures in the last three columns of Table 2.1, which give the overall changes in dimensions of each specimen tested (except no. 3, for which the measurements were inadvertently omitted).

Because $\dot{e}_x$ and $\dot{e}_y$ cannot be measured quantitatively, we cannot make an evaluation of the test data on the basis of a model of parametrically adjustable flow anisotropy (Johnson, 1977; Paterson, 1994; Lliboutry, 1993, p. 412), which would include the foregoing treatment of "perfect anisotropy" as a limiting case. We can,

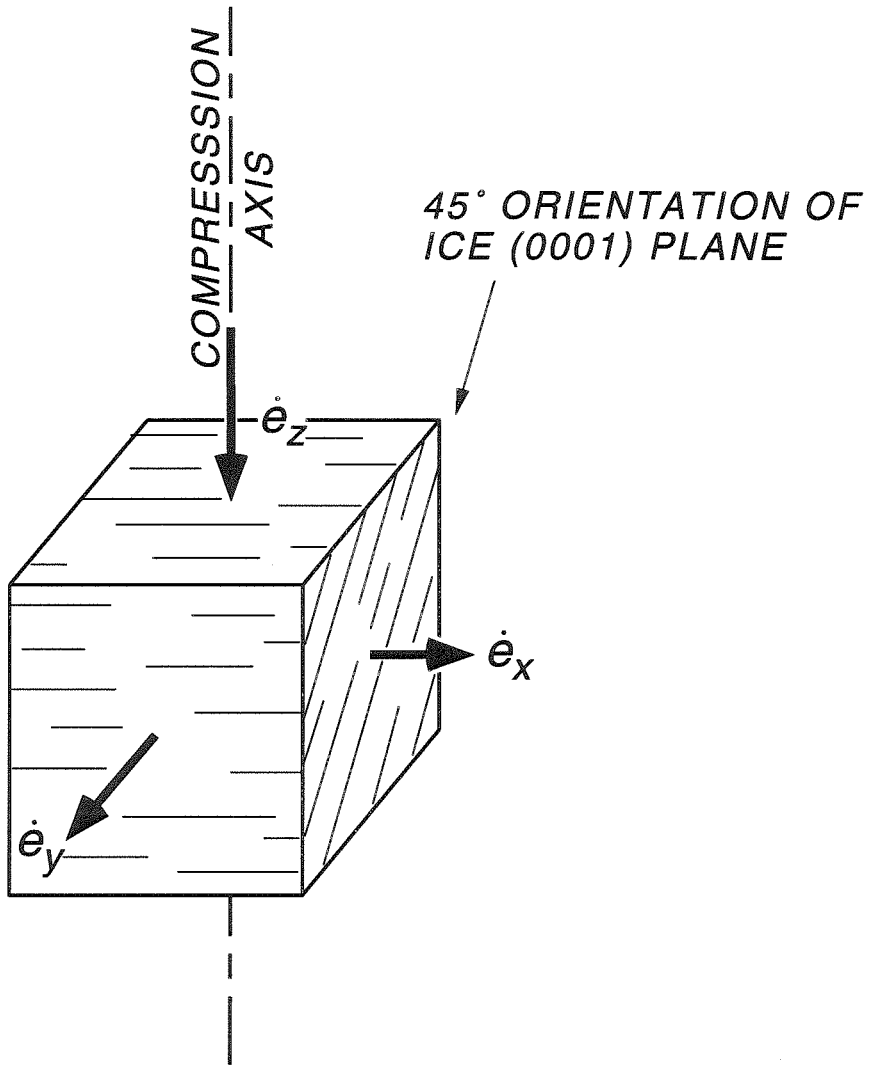

Figure 2.7: Schematic illustration of a typical test block, with ice (0001) planes of the main maximum of the c-axis fabric dipping 45° relative to the top (z) face of the block, which is perpendicular to the compression axis. The planes of the secondary maximum, not shown, would have the same strike and would dip $x \sim 20°$ in the opposite direction. The strike direction is the core axis, parallel to the x axis. The heavy arrows depict schematically the shortening strain rate parallel to the z axis and the extensional strain rates parallel to the x and y directions, with $\dot{e}_x < \dot{e}_y$. (The y axis of Figure 2.2 is different; if shown here it would be perpendicular to the (0001) planes.)

however, assess the possible effect of "imperfect anisotropy" on the evaluation by treating the limiting case of complete isotropy of the flow law, the other extreme in the anisotropy/isotropy spectrum. This is done in the standard way (Paterson, 1994, p. 92): the flow law is given in the form

$$\dot{e_{ij}} = A\tilde{\tau}^{n-1}\tau'_{ij} \tag{2.8}$$

$$\tilde{\tau}^2 = \frac{1}{2}\tau'_{ij}\tau'_{ij} \tag{2.9}$$

where $\tilde{\tau}^2$ is the second invariant of the stress deviator tensor τ'_{ij} (with tensor summation convention). A is the standard flow parameter. When (2.8) and (2.9) are evaluated for unconfined uniaxial compression in the z direction, with $\sigma = -\tau_{zz}$, all other $\tau_{ij} = 0$, and $\dot{e}_{zz} = -\dot{e}$, we obtain

$$\dot{e} = B\sigma^n \tag{2.10}$$

with

$$B = 2A/3^{n+1/2} \tag{2.11}$$

(2.10) has the same form as (2.3), so the evaluation of B from the test data is the same whether we assume anisotropy or isotropy. The difference is that the isotropic flow parameter A in (2.8) is calculated from B by (2.11), whereas the anisotropic flow parameter C in (2.1) is calculated from B by (2.4). The marginal shear stress τ_{MI} for the isotropic evaluation is calculated from (2.8) and (2.9) under the assumption that the flow in the marginal shear zone is pure shear with $\dot{e}_{xx} = 0$ (x axis vertical), $\dot{e}_{yy} = \dot{\gamma_M}/2$ and $\tau'_{yy} = \tau_{MI}$ (from Mohr's circle), and $\tilde{\tau} = \tau'_{yy}$, giving

$$\dot{\gamma_M} = 2A\tau^n_{MI} \tag{2.12}$$

If we take A from (2.12) and substitute into (2.11), then take B from (2.11) and substitute into (2.4), and finally take C from (2.4) and substitute into (2.2), we

obtain

$$\tau_{MA} = \left(\frac{\sqrt{3}}{2}\right)^{n+1/n} \tau_{MI} \tag{2.13}$$

In (2.13), τ_{MA} on the left, which is the same as τ_M on the left in (2.2), has been redesignated τ_{MA} to call attention to the fact that it is based on the anisotropic treatment in Section 2.5.1. From (2.13) we see that for $n = 3$, $\tau_{MA} = 0.83\tau_{MI}$, or $\tau_{MI} = 1.21\tau_{MA}$. Thus the maximum correction to the anisotropic evaluation on account of "imperfect" anisotropy is a 21% increase in the marginal shear stress over the values listed in Table 2.2. The corrected value could be increased in this way at most to $(2.9 \pm 0.2) \times 10^5$ Pa. However, the flow indication of anisotropy $\dot{e}_x < \dot{e}_y$, noted above, suggests that the value is not increased this much.

2.5.3 Flow enhancement factor

Benchmarks for comparison with the foregoing results are the marginal shear stress values τ_{MP} and τ_{MJ} that would be implied if the ice in the marginal zone deformed in accordance with standard minimum-strain-rate isotropic flow relations such as the one of Paterson (1994, p. 91) or the one of Jacka and Budd (1989, Fig. 1; also given by Budd and Jacka, 1989, Fig. 6). At $-22°$C the Paterson relation is (2.8) with $n = 3$, and $A = A_P = 1.4 \times 10^{-16}\text{s}^{-1}(\text{kPa})^{-3}$, and the Jacka and Budd relation (converted from its expression in terms of octahedral shear values) is the same with $A = A_J = 0.67 \times 10^{-16}$ s^{-1} (kPa)$^{-3}$. The benchmark stresses τ_{MP} and τ_{MJ} are obtained from

$$\dot{\gamma}_M = 2A_P\tau_{MP}^n, \ \dot{\gamma}_M = 2A_J\tau_{MJ}^n \tag{2.14}$$

which are based on (2.12), with A replaced by A_P or A_J, and τ_{MI} replaced by τ_{MP} or τ_{MJ}. The results are $\tau_{MP} = 2.51 \times 10^5$ Pa and $\tau_{MJ} = 3.21 \times 10^5$ Pa. These values, especially τ_{MP}, are only modestly greater than the value $\tau_{MA} = (2.4 \pm 0.2) \times 10^5$ Pa obtained in Section 2.5.1, which implies that the c-axis fabric has only a slight effect in weakening the actual ice relative to the standard, or else that such weakening is counteracted by other effects that strengthen the ice. The discrepancy between

the two benchmark values $\tau_{MP} = 2.5 \times 10^5$ Pa and $\tau_{MJ} = 3.2 \times 10^5$ Pa indicates that we cannot take these values as an absolute reference to use in the assessment of weakening in the marginal shear zone.

An alternative representation of these results is in terms of a flow enhancement factor E, which is the factor by which the observed marginal shear strain rate is increased over the shear strain rate that is given by a standard minimum-strain-rate isotropic flow law at the same shear stress. Making use of the similarity between (2.1) and (2.14), we set $C = 2EA$ so that

$$\dot{\gamma}_M = 2EA\tau_{MA}^n \tag{2.15}$$

From (2.14) and (2.15) it follows that

$$E_P = (\tau_{MP}/\tau_{MA})^n, \; E_J = (\tau_{MJ}/\tau_{MA})^n \tag{2.16}$$

Values of E from (2.16) are listed in Table 2.2.

The Paterson benchmark shear stress $\tau_{MP} = 2.5 \times 10^5$ Pa is smaller than the marginal shear stress $\tau_{MI} = (2.9 \pm 0.2) \times 10^5$ Pa based on the isotropic evaluation of our test data. The corresponding enhancement factor $E_I = (\tau_{MP}/\tau_{MI})^n$ is 0.64. Thus according to the isotropic evaluation the flow is suppressed, not enhanced, relative to the benchmark. Such suppression could in principle occur, due for example to a c-axis fabric unfavorable to flow (e.g., Paterson, 1994, Fig. 5.7; Shoji and Langway Jr., 1988, Fig. 5), but we think it more likely that the result indicates that the anisotropic evaluation is closer to being valid than the isotropic one is. This problem does not arise for the Budd and Jacka (1989) benchmark stress τ_{MJ}, which is greater than τ_{MI} and corresponds to $E_I = 1.8$.

2.5.4 Effect of vertical temperature profile

The value of the marginal shear stress obtained above applies specifically to depth 300 m, where the ice core was obtained and where the temperature is close to the

temperature of the laboratory tests. Because the control of the overall ice stream motion is exercised in terms of the depth-averaged marginal shear stress, and because the flow of ice is sensitive to the temperature, which increases substantially in the lower half of the ice mass, we need to estimate a temperature correction from the 300-m shear stress value τ_M to a depth-averaged value $\bar{\tau}_M$. This is done with the measured temperature profiles in Figure 2.8. A profile to depth 500 m was measured by Harrison and Echelmeyer (1994) in borehole 93-5, adjacent to the core hole 93-6. It is given in Figure 2.8. A profile from depth 500 m to the bottom at 914 m was measured by Engelhardt (pers. com.) in borehole 93-10 near the outer edge of the marginal zone at coordinate y = 1.0 km in Figure 2.2, 1 km south of 93-6; it is given in Figure 2.8. These profiles were combined into a single vertical absolute-temperature profile T(z), where z is depth; in this combination the ice at hole 93-6 was assumed to be 950 m thick and the temperature curve in Figure 2.8 was accordingly shifted downward by 36 m.

The temperature dependence of the ice flow law (2.1) is taken in the standard form (Paterson, 1994, e.g.) where T_1 is 251 K and C_1 is the value indicated by the tests, at $T = T_1$. R is the gas constant.

$$C(z) = C_1 \exp\left[\frac{Q_1}{R}\left(\frac{1}{T_1} - \frac{1}{T(z)}\right)\right]. \tag{2.17}$$

The activation energy Q_1 is taken to be 60 kJ mol^{-1} for T below 263 K $= T_2$, and 139 kJ mol^{-1} $= Q_2$ for T above T_2 (Weertman, 1973, Table2), where (2.17) is replaced by

$$C(z) = C_1 \exp\left[\frac{Q_1}{R}\left(\frac{1}{T_1} - \frac{1}{T_2}\right) + \frac{Q_2}{R}\left(\frac{1}{T_2} - \frac{1}{T(z)}\right)\right]. \tag{2.18}$$

Below 263 K, Q is apparently equal to the *activation energy for volume self-diffusion* (Weertman, 1973, Table2). Above 263 K, there are probably several different creep processes operating, and the value of 139 kJ mol^{-1} K^{-1} that is used is the mean of four values (Weertman, 1973, Table2).

In calculating the depth-averaged shear stress $\bar{\tau}_M$ we assume that the marginal

shear strain rate $\dot{\gamma}_M$, which is measured at the surface, is constant with depth. This is probably a good assumption in the upper part of the ice mass but not near the bed. This is an aspect of the problem of strain-rate distribution in the marginal shear zone, which is considered in detail by Echelmeyer *et al.* (1994) and by Raymond (1996). Because of weakening of the ice near the bed, where the temperature approaches melting, the contribution from that part of the profile to the depth averaged $\bar{\tau}_M$ is small and the breakdown of the constant $\dot{\gamma}_M$ assumption is therefore not serious. Thus the averaging is done by introducing (2.17) and (2.18) into (2.2) and integrating over depth:

$$\begin{aligned}\frac{\bar{\tau}_M}{\tau_M} = \frac{1}{h} & \left\{\int_0^{z_2} \exp\left[\frac{Q_1}{nR}\left(\frac{1}{T(z)} - \frac{1}{T_1}\right)\right] dz \right. \\ + & \int_{z_2}^{h} \exp\left[\frac{Q_1}{nR}\left(\frac{1}{T_2} - \frac{1}{T_1}\right)\right. \\ & \left.\left. + \frac{Q_2}{nR}\left(\frac{1}{T(z)} - \frac{1}{T_2}\right)\right] dz\right\} \end{aligned} \tag{2.19}$$

h is the ice thickness (950 m) and z_2 is the depth at which $T(z_2) = T_2$. In obtaining (2.19) from (2.2) we replace $(\dot{\gamma}_M/C_1)^{1/n}$ by τ_M, the marginal shear stress at 300 m depth, discussed in Section 2.5.1.

When (2.19) is evaluated numerically with the $T(z)$ data in Figure 2.8, the temperature averaging factor $\bar{\tau}_M/\tau_M$ is found to have the value 0.98, hardly different from 1, so that there is no appreciable temperature correction for the depth-averaged marginal shear stress. Evidently the ice-weakening effect of the warmer temperatures below a depth of about 600 m (Figure 2.8) is offset by the strengthening due to the low temperatures (to $-36°$C) above 300 m depth (Figure 2.8); also, the actual temperature at 300 m is 2°C lower than the test temperature of $-22°$C.

The anomalous deep temperature minimum at $\sim$ 50 m depth is due, as explained by Harrison and Echelmeyer (1994), to the heat-pump action of thermal convection in the crevasses that pervade the marginal shear zone to a depth $\sim$ 50 m. (The temperature minimum at $\sim$ 30 m depth is an artifact of the thermal disturbance due to the freezing of the return water flow from the hot-water drilling which apparently

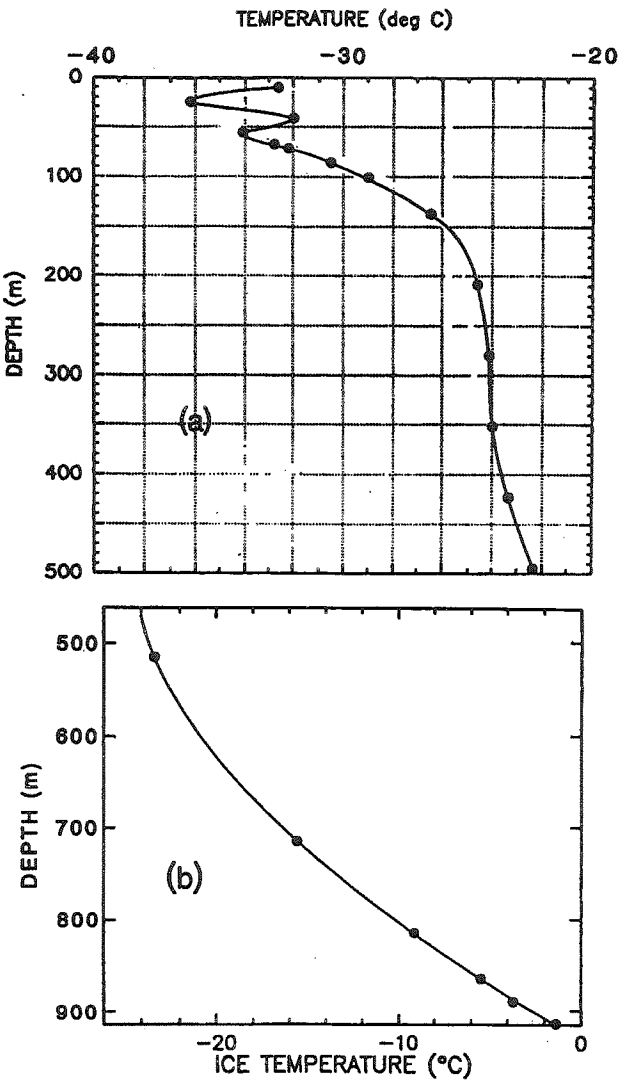

Figure 2.8: Temperature profile through the ice sheet near hole 93-6: (a) in the upper 500 m, from Harrison and Echelmeyer (1994); and (b) in the lower 400 m, in borehole 93-10, 1 km south of 93-6, by Hermann Engelhardt (pers. com.). There is no temperature profile to the base in the middle of the shear margin, hence the use of the profile from 93-10.

ponded in the bottoms of crevasses (Harrison *et al.*, 1998)). Because of the crevassing the uppermost 50 m of the ice mass must be weakened relative to the unfractured ice below. A very crude estimate of this weakening is a factor 0.5, on the basis that the tensile principal stress in the marginal shear zone is relieved by tensile fracture. If we apply this weakening factor to the upper 100 m of the ice column (choosing the overestimate 100 m to assess the maximum effect), and correct the calculation in (2.19) accordingly, we obtain a combined temperature-and-fracture correction factor of 0.91, and a depth-averaged shear stress $\bar{\tau}_M = 2.2 \times 10^5$ Pa for the anisotropic evaluation and $\bar{\tau}_M = \bar{\tau}_{MI} = 2.6 \times 10^5$ Pa for the isotropic evaluation.

2.6 Force Balance in the Ice Stream

The foregoing evidence and argument lead to a depth-averaged marginal shear stress $\bar{\tau}_M$ of about $(2.2 \pm 0.3) \times 10^5$ Pa. This is surprisingly large in relation to the maximum stresses of about 1×10^5 Pa that are normally found (from force balance calculation) in glaciers and ice sheets (Paterson, 1994, p. 242). The situation can be rationalized by noting that the marginal shear strain rate ($0.14 a^{-1}$) is comparable to that often observed in temperate glaciers (e.g., Meier *et al.*, 1974, Fig. 6), but the ice is much colder and its viscosity consequently higher.

Another contrast is that in normal glaciers, as distinct from ice streams, the marginal shear stress τ_M is almost always smaller than the basal shear stress τ_B (from force balance calculation), whereas here τ_M is much greater than τ_B. This is seen in the ice-stream mechanical model of Echelmeyer *et al.* (1994, Fig. 5), in which τ_B is only about 0.06×10^5 Pa. The low τ_B can be attributed to the weakness of the subglacial till, which has a measured strength $\sim 0.02 \times 10^5$ Pa (Kamb, 1991, p. 16,587).

The large marginal shear stress must play a major role in controlling the motion of the ice stream. This can be judged by calculating for a simple model the support provided by τ_M against the downslope component of gravity and comparing it with the support provided by τ_B. In a general way, the larger the fraction of support provided

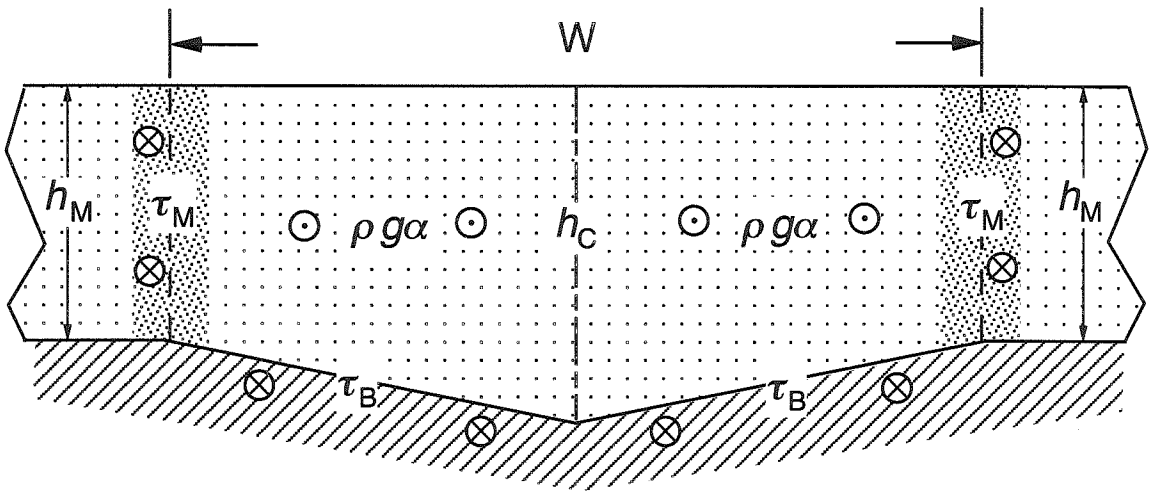

Figure 2.9: Idealized cross section of Ice Stream B at camp Up B, for calculation of the balance of longitudinal forces (not drawn to scale). The ice is dotted, and the marginal shear zones are shown heavily dotted. The bed is cross-hatched. The ice is taken to be 1200 m thick ($= h_C$) at the centerline and 900 m thick ($= h_M$) at the margins. The width of the ice stream is W = 31 km. The gravitational body force component $\rho g \sin \alpha$ acts on the ice in the downstream direction, perpendicular to the cross section; this is represented by the "arrow heads" seen end on — circles with dot in the center. The shear stress at the bed and margins (drag stress acting upstream on the ice, resisting the flow) is represented by the "arrow tails" (circles with a cross) just outside the periphery of the cross section.

by τ_B or τ_M, the greater the control exerted by the base or the margin on the flow velocity. The model (figure 2.9) treats an ice-stream of longitudinally constant cross section, assumes no longitudinal gradients of flow, and idealizes the cross section as composed of two quadrilaterals symmetrical across the center line. (The neglect of longitudinal gradients is discussed by Jackson (1991, p. 77) and by Echelmeyer *et al.* (1994, p. 530)). Based on borehole drilling and on a radar profile by Shabtaie and Bentley (1988, Fig. 4b), the centerline ice depth is $h_c = 1200$ m and the thickness at the margin is $h_m = 900$ m. The balance of forces for the cross section, balancing the down-slope component of gravity integrated over the cross section against the basal drag and the marginal drag over unit length of the ice stream, is

$$\rho g \frac{1}{2}(h_C + h_M)(\sin\alpha)W = \bar{\tau}_B W + 2\bar{\tau}_M h_M \tag{2.20}$$

where α is the surface slope, W is the ice stream width (31 km), g is gravity, and ρ is ice density. (The slight effect of the small transverse slope of the bed is neglected.) The factor 2 comes from the two margins (left and right), and $\bar{\tau}_M$ is averaged vertically as in Section 2.5.4. (2.20) can be usefully expressed in terms of the driving stress $\bar{\tau}_D = \rho g \bar{h} \sin\alpha$ (averaged over the cross section, with $\bar{h} = \frac{1}{2}(h_c + h_m) = 1050$ m):

$$\bar{\tau}_D = \bar{\tau}_B + 2\bar{\tau}_M h_M / W \tag{2.21}$$

The surface slope α of the ice stream is not well defined locally because of complex surface irregularities on a scale of a few kilometers (Jackson, 1991, Fig. 3). For illustrative purposes we first take the average slope over an approximately 45-km reach centered on Up B, which is $\alpha = 0.0013 \pm 0.0003$. This is based on a surface elevation map of Ice Stream B by Retzlaff *et al.* (1993, Fig. 7). The same value of α was used in the model of Echelmeyer *et al.* (1994, p. 531). It gives $\bar{\tau}_D = 0.12 \times 10^5$ Pa. When this value and $\bar{\tau}_M = 2.2 \times 10^5$ Pa are introduced into (2.21) and it is solved for τ_B, the result is $\tau_B = 0.0 \times 10^5$ Pa. Thus, according to this model, all of the mechanical support for the ice stream comes from the margins, and the basal

shear stress is negligible. If instead of $\alpha = 0.0013$ we use $\alpha = 0.00225$, which is our estimate of the local slope averaged over a longitudinal interval of ≈ 5 km about the dotted profile in Figure 2.1, we obtain $\tau_B = 0.08 \times 10^5$ Pa. This is nearly the same as $\tau_B = 0.06 \times 10^5$ Pa in the Echelmeyer *et al.* (1994, Fig. 5a) model (except near the margins, where τ_B decreases). In this case, the fraction of the driving force that is supported by the basal shear stress, $\bar{\tau}_B/\bar{\tau}_D$, is 37%, and the fraction supported by the margins, $2h_M\bar{\tau}_M/W\bar{\tau}_D$, is 63%. The value of α could possibly be even higher - Alley and others (1987) used 0.0027 - which would further lower the fractional support from the margins. The marginal-support fractions given by the different models of Echelmeyer *et al.* (1994) range from 35% to 93%.

Although this shows that the margins tend to dominate in controlling the motion of the ice stream in its present active configuration, we should not lose sight of the fact that the fundamental controlling mechanism that allows the ice stream to attain its rapid motion in the first place is the mechanism of basal lubrication, which causes the low basal shear stress.

2.7 Discrepancies and the Possible Role of Recrystallization

The value $\bar{\tau}_M = 2.2 \times 10^5$ Pa is high by a factor of almost 2 relative to the results of a mechanical model of the marginal shear zone by Echelmeyer *et al.* (1994, p. 535), which gives a marginal shear stress of about 1.2×10^5 Pa. The corresponding enhancement factor E for ice in the high- marginal zone is $E = 10$ to 12.5 (Echelmeyer *et al.*, 1994, Figs. 3b, 4), which is 5 to 10 times larger than the E values that we obtain (Table 2.2). These differences in τ_M and E constitute a fundamental discrepancy, which needs to be clarified. We first discuss two other seemingly related discrepancies and then consider their possible explanation in terms of recrystallization of the core.

The modest E values of 1.1–1.2 or 2.3–2.5 (Table 2.2) can be compared with the enhancement factor of $E = 2.5$ recommended by Paterson (1994, p. 98), or of up

to $E = 8$ reported by Jacka and Budd (1989) for ice recrystallized under shear in laboratory experiments, or up to $E = 17$ reported by Shoji and Langway (1988) for ice from depth in the Greenland Ice Sheet (Dye 3 core), tested shortly after core recovery. These high E values are associated with c-axis fabrics with a single sharp maximum, of radius $14 - 20°$, centered at the pole of the known or presumed shear plane (Fig. 3c, d Budd and Jacka, 1989; Herron *et al.*, 1985). The small enhancement shown by the marginal ice specimens probably results from the considerable breadth of the main c-axis maximum in Figure 2.4 (radius $\approx 31°$) and also from the displacement of the maxima from the poles S and C in Figure 2.4. (This displacement is partly unavoidable, because the two maxima are not at 90°, and it is partly due to the statistical fluctuations noted in Section 2.4.) The sensitivity of E to degradation with increase in breadth of a single fabric maximum is indicated by Budd and Jacka (1989, Fig. 9a). The degradation of E due to displacement of a maximum from S or C is treated by Paterson (1994, Fig. 5.7) and by Shoji and Langway (1988, Fig. 5).

The weak enhancement factor and the rather diffuse type of two-maximum fabric shown by the core specimens are what is expected for the early stages of fabric development under shear, with $\gamma \sim 0.1$, starting from ice with an isotropic fabric (Kamb, 1972, Figs. 13b, 15). The marginal ice studied here has been sheared to a far greater strain, $\gamma \sim 8 - 40$, according to the reasoning of Echelmeyer and others (1994, p. 532): it has spent about 100-500 years in the high $\dot{\gamma}$ zone, with $\dot{\gamma} \approx 0.14$ a^{-1}. A more recent paper by Echelmeyer and Harrison (1999) suggests that there has been outward lateral migration of the shear margin which would lower the estimate of strain undergone by the ice. However, at the measured strain rate and given the known position of the margin over the last 15 years, the shear is still greater than the $\gamma \sim 2$ that is sufficient in the laboratory (Bouchez and Duval, 1982) and in a natural shear zone in the Barnes Ice Cap (Hudleston, 1977, p. 145) to eliminate the secondary maximum and sharpen the main maximum to a radius $\approx 20°$, giving a large flow enhancement such as the $E = 8$ indicated by Jacka and Budd (1989) and the $E = 17$ found by Shoji and Langway (1988). The sharp single-maximum fabric and associated large flow enhancement expected for $\gamma \geq 2$ thus contrast strongly with

what the cores show. This is a discrepancy as fundamental as, and parallel to, the discrepancy noted above between our E values and those of Echelmeyer and others (1994).

At all stages of the fabric-development and flow-enhancement sequence seen experimentally from $\gamma \sim 0.1$ on, strain shadows and small-angle kink boundaries in the ice grains are abundant (Kamb, 1972; Wilson, 1986; Wilson *et al.*, 1986; Duval and Castelnau, 1995, p. 222, 228, 232). They indicate internal bending due to plastic deformation by (0001) glide within the individual crystal grains. They are also common in ice from the sharp-single-maximum fabric zone at depth in the ice sheets ((Gow, 1994, p. 232), (Rigsby, 1960, p. 605), (Gow and Williamson, 1976, p. 1675)). In contrast, strain shadows are very rare in our specimens, and kink bands are not observed.

If the marginal ice underwent annealing recrystallization between the time it was cored and the time we studied and tested it, the discrepancies discussed above could be explained, at least in a general way: post-kinematic recrystallization would probably eliminate a sharp single fabric maximum, reduce E to a modest value, and eliminate strain shadows and kinks. This would allow the unrecrystallized ice in situ to have a large E value and relatively small τ_M, as predicted by the model of Echelmeyer and others (1994, Figs. 3b, 4).

Although every precaution possible under the physical constraints of the field work was taken to avoid annealing recrystallization of the core, what is the possibility that the core recrystallized anyway? No recrystallization took place subsequent to the core's arrival at the Crary Laboratory in McMurdo Station, to judge by the following evidence: 1. Thin sections made and examined at McMurdo Station showed the same type of two-maximum fabric and the same lack of strain shadows as do thin sections made in Pasadena from the same core. 2. At McMurdo Station and in sea shipment of the ice to Port Hueneme, as well as in storage in Pasadena, the ice was kept at or below $-20°C$, which according to Gow (1994) is cold enough to prevent recrystallization (see also Section 2.3). It thus appears that if recrystallization occurred it was during the core drilling or during the two days involved in temporary storage and transport of

the core from the drill site to McMurdo Station. Without going into all the details, we estimate that the temperature range $-5°$ to $-10°$C applies to the surface transport and storage, with considerably lower temperatures during the flight to McMurdo Station. In the coring operation itself, done by hot-water drilling, the core was at or near the melting point for about 0.5 to 1 hour.

From the above time-temperature history we can attempt to judge the likelihood of annealing recrystallization on the basis of three sources of information:

1. Steinemann (1958, p. 33-40) studied post-kinematic recrystallization as a function of temperature and the compressive stress σ to which the ice was subjected prior to unloading. Table 2.3 is a compilation of data on the time for 50% recrystallization, extracted from his Figures 34, 35, and 36. Values for 0°C are extrapolated from his data for -1.9, -4.8, and -11.5°C. We take the stress $\sigma = 5 \times 10^5$ Pa as appropriate in relation to $\tau_M \approx 2.5 \times 10^5$ Pa. For the range $-5°$ to -10°C the 50% recrystallization time is $\sim$ 100 to 500 hours, somewhat longer than the actual time of about 50 hours that the ice was actually at this temperature. For 0°C the 50% recrystallization time is about 5 hours, somewhat longer than the actual 0.5 to 1 hour. These figures would suggest that the ice core did not have enough time (but not by a wide margin) to recrystallize during the coring operation or in transit to McMurdo Station. However, the problem is that in Steinemann's experiments, deformation and annealing recrystallization were at the same temperature, whereas in our core the ice was deformed at -24°C and then annealed at 0°C and $-5°$ to -10°C. Because of the slowness of synkinematic recrystallization at -24°C (Paterson, 1994, p. 86; Rigsby, 1960, p. 604), the ice deformed at that low temperature will probably be much more prone to recrystallize at or near 0°C. This might reduce the 50% recrystallization times to or below the actual times.

2. This problem is addressed by Wilson (1982, Fig. 5) who presents time-vs.-grain-size diagrams for recrystallization of ice that was deformed at -10°C and then unloaded and held at -1°C, resulting in what he terms thermal annealing recrystallization, which is qualitatively the type of recrystallization we are trying to assess. If we suppose that the 50% recrystallization time is the time for an increase in mean

Fig. No.	σ	Temperature			
	10^5 Pa	0°C	−1.9°C	−4.8°C	−11.5°C
36	20	0.2*	0.5	0.3	50
36	10	0.2*	4	10	90
35	5	5*	13	100	450
34	5	-	-	30	-
34	10	-	-	10	-

Table 2.3: Estimate of 50% recrystallization time (h) from Steinemann (1958), as a function of temperature and of compressive stress σ applied before unloading.
* Extrapolated from Steinemann's (1958) data.

grain size halfway from the starting level to the final plateau, then 50% recrystallization times of 1 day and 5 days are indicated for compressive strain rates 3.7×10^{-5} s^{-1} and 3.5×10^{-7} s^{-1}. (The total strains were 0.11 and 0.36 respectively.) Later, Wilson (1986, Fig. 8) presented a similar diagram (but without data points or specification of strain rate or total strain) indicating a 50% recrystallization time of 0.5 days. This again suggests that the ice did not have quite enough time to recrystallize. Deformation to a very large total strain at the lower temperature −24°C followed by thermal annealing at the higher temperature 0°C would presumably produce more rapid recrystallization, but whether it would reduce the recrystallization time scale from 0.5 or 1 day to 0.5 or 1 hour is not possible to say.

3. (Daley and Kirby, 1984, Fig. 2) reported that an ice specimen deformed to strain 0.046 at temperature −115°C and strain rate 3.5×10^{-6} s^{-1} partially recrystallized when a face of the specimen was melted so as to freeze it onto a glass slide. The time scale for temperatures near 0°C was not specified, but we estimate a few seconds — certainly not minutes — for the melting/freeze-on process. The deformation conditions are extreme in relation to what we are considering here (confining pressure 1200×10^5 Pa, yield strength 870×10^5 Pa) but this observation shows that very short recrystallization times can occur for deformation at low temperature followed by annealing at or near 0°C.

The above assessments do not provide us with a definite conclusion as to the likelihood for recrystallization of our core, but they make it a possibility.

There is, however, one piece of evidence that argues against post-kinematic annealing recrystallization of our core: the form of the observed *c*-axis fabric. If the fabric resulted from annealing recrystallization at or near 0°C from a sharp single-maximum fabric, as contemplated above, it would be expected to have the form observed by Gow (1994) in two ice samples from the sharp-single-maximum zone in the Byrd Station deep ice core; the two samples were allowed to anneal for one month at the melting point, resulting in a 3- to 5-fold enlargement of grain size. A similar experiment was carried out by Rigsby (1960, p. 604), with apparently similar results. The resulting fabrics (Gow, 1994, Fig. 5), although poorly defined because of the small number of grains (11 and 26) remaining in the samples after recrystallization and grain growth, show a large dispersal of c-axes into either a random pattern or a very diffuse small-circle girdle of approximate radius $35 - 50°$ centered on the position of the former sharp maximum. This pattern does not resemble the two-maximum fabric of Figure 2.4.

It would be quite surprising if post-kinematic recrystallization from an initial sharp single maximum pattern of apparent rotational symmetry would result in a pattern that is not rotationally symmetric and that fairly well resembles the two-maximum fabric produced experimentally by shear-induced recrystallization from an initially isotropic fabric (Kamb, 1972). The resemblance is good enough that the marginal-zone fabric can be used (Section 2.4) to identify the orientation of the shear plane and the sense of shear across it. The sense comes out consistently correct, which is a successful test of the interpretation based on the similarity to the experimental fabrics. (A more complete test is not possible, because the azimuthal orientation of the core is not known, other than from the fabric, as discussed in Section 2.4.)

Wilson (1982, Figs. 7, 8) gives *c*-axis fabrics as a function of thermal annealing time for the specimens discussed above. They start, before annealing, with a more or less well developed fabric with two broad, subequal maxima, which results from pure shear deformation, as can be expected (e.g., Kamb, 1972, Figs. 17a, 18). For thermal annealing times of up to 8 days the two maxima are retained but perhaps become somewhat broader, with much statistical fluctuation. For longer times the

fabric degrades to a more or less random one. These observations suggest that if our core underwent thermal annealing recrystallization, the in-situ fabric before recrystallization was a two-maximum fabric similar to the one we observe (Figure 2.4). In this case, since the enhancement factor is determined mainly by the c-axis fabric (Shoji and Langway, 1988, p. 150), the enhancement factor measured from the core should be representative of the marginal ice in situ, whether or not it recrystallized, and the inferred value of the marginal shear stress (Section 2.5) should be at least approximately correct. Why the in-situ fabric is not a sharp single maximum, according to this interpretation, is not explained.

If there was only partial recrystallization of the core, this would be observed as a variation in grain size in a horizontal section (one cut perpendicular to the long axis of the core), such as smaller grains around the perimeter of a section than in the center. No such variation in grain size is observed.

2.8 Conclusions

In case of no recrystallization the question is why strain shadows and kinks are absent in the core, and in either case the question is why a sharp single-maximum fabric is not present in the ice in situ, contrary to what is expected for a fabric developed at large shear strain. These and related questions raised in Section 2.7 need to be resolved by further research before we can reach a definitive conclusion as to the marginal shear stress of Ice Stream B and as to whether we have a fundamental problem in the discrepancy between the marginal shear stress values obtained by our method (Section 2.5) and by the ice-stream model of Echelmeyer and others (1994).

Chapter 3 Modelling of the Marginal Shear Zone

3.1 Introduction

Within the marginal shear zones (MSZs) of Ice Stream B, the flow velocity undergoes a large, steep increase inward over a short distance laterally. In conventional glaciological theory for flow of an ice sheet without lateral and longitudinal stress gradients, the flow velocity is controlled by the ice thickness and surface slope (Paterson, 1994, p. 240). However, thickness and surface slope are approximately constant across the ice stream and so are not the cause of the large, steep increase in velocity.

Enhancement of the ice flow due to strain softening has been proposed as the mechanism for this large, steep increase in velocity (Hughes, 1975; Echelmeyer *et al.*, 1994). Chapter 2 discusses an attempt to determine experimentally the magnitude of the flow enhancement. To investigate the results further and to estimate the magnitude of the enhancement from a theoretical point of view, a model of the velocity in the MSZ is here developed. The immediate objective is to obtain a flow model that gives a lateral profile of surface velocities matching the observed surface velocity profile, and to obtain such a model with the minimum assumption of flow enhancement, in view of the experimental results.

The ice-stream cross section is taken to be rectangular and constant along the length of the ice stream (cylindrical geometry), with constant surface slope and ice thickness. The width of the ice stream is taken to be 32 km and the ice thickness 1050 m. The cross-section used is shown in Figure 3.1. The actual thickness of the ice varies across the ice stream from about 890 m to 1140 m, the discrepancy being less than 16% from the constant thickness assumed in this study. Only half of the ice stream is modelled, as the flow geometry is assumed to be mirror-symmetrical about

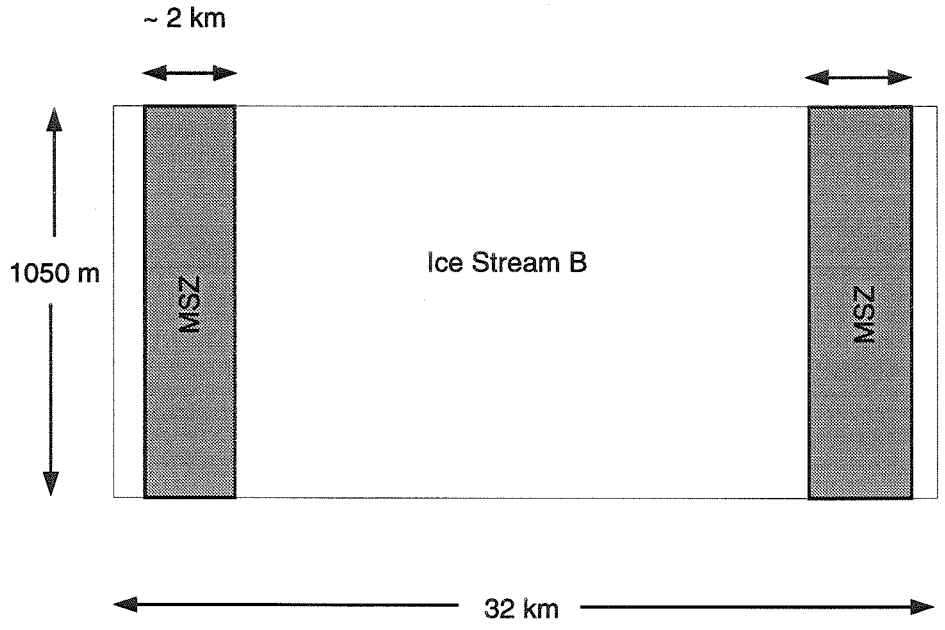

Figure 3.1: Cross-section taken perpendicular to flow of the model. The cross-section is taken to be constant along the ice stream. Only half of the ice-stream width is modelled, as it is assumed to be symmetrical about the center.

the center-line. Given the assumed cylindrical channel geometry and an assumed steady-state flow, the flow is necessarily rectilinear – i.e., in a fixed direction (parallel to the cylindrical axis and the centerline), with transverse and depth variation in flow but no variation of flow in the flow direction. Thus there is no divergence or convergence of flow. Velocity measurements on the ice stream by Echelmeyer and Harrison (1999) show that there is a small component of ice flow into the ice stream from the sides, but this amounts to only about 9.7 m a^{-1}, much less than the main ice-stream flow of 440 m a^{-1} parallel to the centerline.

The technique used to model the velocity is the finite element method. This method has become increasingly popular in the study of glacier flow (e.g., Hooke *et al.* (1979); Nixon *et al.* (1985); Fastook and Chapman (1989); Harbor (1992)). An advantage of the finite element method in this study (compared with the finite difference method) is ease of grid refinement. This is useful when there is more vertical and/or lateral variation in stresses and strain rates in one part of the domain than in another, as is the case in the MSZ. Hughes (1987) has written a thorough volume on

the finite element method and Lliboutry (1987) examines the particular case of the finite element method applied to glacier flow and other very slow flows of solids.

3.2 Physical Basis for the Finite Element Model

The physical basis for the finite element method used here is first described in general terms for three-dimensional flow, and is then specialized and simplified for two-dimensional rectilinear flow.

3.2.1 Three-dimensional quasi-viscous flow

According to Glen's flow law for isotropic ice (e.g., Paterson, 1994, p.91), the relationship between the effective strain rate, $\dot{\epsilon}$, and the effective stress, τ, is described by

$$\dot{\epsilon} = A\tau^n \tag{3.1}$$

where n is a constant, and $\dot{\epsilon}$ is the second invariant of the strain rate tensor:

$$\dot{\epsilon} = \left(\frac{1}{2}\dot{e}_{ij}^2\dot{e}_{ij}^2\right)^{\frac{1}{2}} \tag{3.2}$$

and τ is the second invariant of the stress-deviator tensor:

$$\tau^2 = \frac{1}{2}\tau'_{ij}\tau'_{ij} \tag{3.3}$$

The e_{ij} are the components of the strain rate tensor $\dot{e}_{ij} = \frac{1}{2}\left(\partial u_i/\partial x_j + \partial u_j/\partial x_i\right)$ for a flow velocity field $u_i(x_1, x_2, x_3)$, and the τ'_{ij} are the components of the stress-deviator tensor, which are related to the Cauchy stress tensor components τ_{ij} by

$$\tau'_{ij} = \tau_{ij} - \frac{1}{3}\delta_{ij}\tau_{kk} \tag{3.4}$$

In these tensor relations summation over repeated subscripts is understood. The flow law parameter A in equation (3.1) is temperature dependent, according to the

relation:

$$A = A_0 \exp\left(-Q/RT\right) \tag{3.5}$$

where A_0 is independent of temperature, R is the universal gas constant, Q is the activation energy for creep and T is absolute temperature. Values of A have been tabulated (Paterson, 1994, table 5.2). To take into account the possibility of flow-law enhancement due to ice recrystallization or other causes, an enhancement factor $E(y,z)$ is used. This is defined as the ratio of the actual strain rate to the strain rate of isotropic ice under the same stress and at the same temperature. It is incorporated into equation (3.1) by writing

$$\dot{\epsilon} = E(x,y,z)A\tau^n \tag{3.6}$$

A_0 can be spatially variable due to spatial variations in the chemical and physical state of the ice. A complete statement of Glen's law includes the relations between the individual strain-rate components $\dot{e}_{ij}$ and the deviatoric stress components τ'_{ij}:

$$\dot{e}_{ij} = A\tau^{n-1}\tau'_{ij} \tag{3.7}$$

which leads to (3.2).

The stress-equilibrium equations (e.g., Paterson, 1994, p. 259) in three dimensions are given by:

$$\frac{\partial \tau_{ij}}{\partial x_j} = -\rho g_i \tag{3.8}$$

$g_1 = g_x$, $g_2 = g_y$ and $g_3 = g_z$ are the components of gravity in x, y and z directions respectively and ρ is the (local) density of the ice.

The finite element method used here is based on a variational form for the solution of (3.7) and (3.8). A functional J is defined as an integral over the velocity and pressure fields $u(x,y,z)$ and $p(x,y,z)$ as follows:

$$J = \int_V (\Gamma - \vec{f}\cdot\vec{u} - p\vec{\nabla}\cdot\vec{u})dV - \int_{B_1} \vec{T}^*\cdot\vec{u}dS \tag{3.9}$$

where V is the volume of the flowing body with boundary surface B, $\vec{u}$ is the flow velocity, p is the mean compressive stress and $\vec{f}$ is the gravitational body force $\rho\vec{g}$ and dS is an increment of the boundary surface B. Γ incorporates the quasi-viscous flow law expressed in the form

$$\tau'_{ij} = \partial\Gamma/\partial\dot{e}_{ij} \tag{3.10}$$

as explained below. For the generalized Newtonian fluid, J has apparently no physical significance (Johnson, Jr., 1960, p.878).

The permissible boundary conditions are of two types: (1) parts of the boundary labelled collectively B_1 where the shear stress $\vec{T}^*$ across the boundary is specified; these parts make a contribution to J given by the last integral in equation (3.9); (2) parts of the boundary where the velocity is specified; these parts (which may be labelled collectively B_2, where $B = B_1 + B_2$) make no contribution to J.

The solution to the flow problem, u and p as functions of x, y and z, is obtained by minimizing J with respect to variations in u and p. This can be represented by

$$\delta J = 0 \tag{3.11}$$

where δ represents the variation operator. The variational principle (3.11) has been shown to be equivalent to the solution of the differential equations (3.8) governing creeping flow of an incompressible fluid with flow law described by (3.10) (Johnson, Jr., 1960; Oakberg, 1978).

The form of Γ needed to describe the standard quasi-viscous flow law of ice (3.7) is

$$\Gamma = \frac{4B\dot{\epsilon}^{\left(1+\frac{1}{n}\right)}}{1+\frac{1}{n}} \tag{3.12}$$

where n is the exponent appearing in (3.7) and B is a constant related to A in (3.7). The validity of (3.12) is shown by introducing it into (3.10). Carrying out the differentiation formally, we get

$$\tau'_{ij} = 2B\dot{\epsilon}^{-\left(1-\frac{1}{n}\right)}\dot{e}_{ij} \tag{3.13}$$

which is a restatement of (3.7), as the following shows. We calculate the effective shear stress τ from (3.3), (3.13) and (3.2):

$\tau^2 = \frac{1}{2}\tau'_{ij}\tau'_{ij} = (2B\dot{\epsilon}^{-(1-\frac{1}{n})})^2\frac{1}{2}\dot{e}_{ij}\dot{e}_{ij} = (2B\dot{\epsilon}^{\frac{1}{n}})^2$ so that

$$\tau = 2B\dot{\epsilon}^{\frac{1}{n}} \tag{3.14}$$

This is the same as Glen's law written in the standard form (3.1) with

$$B = A^{-1/n}/2 \tag{3.15}$$

If $\dot{\epsilon}$ from (3.1) and B from (3.15) are introduced into (3.13), we get (3.14) which is the detailed statement of Glen's law.

It will prove useful to define an effective viscosity function $\eta(\dot{\epsilon})$ using the standard relation

$$\tau'_{ij} = 2\eta(\dot{\epsilon})\dot{e}_{ij} \tag{3.16}$$

so that, from (3.13),

$$\eta(\dot{\epsilon}) = B\dot{\epsilon}^{-(1-1/n)} \tag{3.17}$$

When B from (3.17) is introduced into (3.12), Γ is expressed as

$$\Gamma = \frac{4\eta(\dot{\epsilon})\dot{\epsilon}^2}{1+\frac{1}{n}} \tag{3.18}$$

In the case of linearly viscous flow ($n = 1$), Γ has the simple form

$$\Gamma = 2\eta\dot{\epsilon}^2 \tag{3.19}$$

where η is independent of $\dot{\epsilon}$.

3.2.2 Simplification to two-dimensional rectilinear flow

For rectilinear flow, which occurs for steady flow in cylindrical channels with a free surface as noted in Section 3.1, the basic relationships simplify as follows. The channel

is taken to have uniform cross section and constant slope α (i.e., cylindrical). There is a single flow direction parallel to the cylindrical axis, with slope α. Choose a coordinate system with x axis along a cylindrical axis, positive in the direction of flow. The channel is assumed symmetrical, and the x axis is taken along the center line that bisects the channel symmetrically. The z axis is taken normal to the ice surface, positive downward. The y axis is then directed across the ice stream from an origin at the center line, and is a level line (strike line) on the ice surface (so that there is no driving force for transverse flow).

The only flow component is u_x, henceforth called simply u. It does not depend on x, so $\partial u/\partial x = 0$. The components u_y and u_z and all of their derivatives are 0. The only non-zero strain-rate and stress-deviator components are $\dot{e}_{xy}$, $\dot{e}_{xz}$, $\tau'_{xy} = \tau_{xy}$ and $\tau'_{xz} = \tau_{xz}$. All of their x derivatives are zero. From $\dot{e}_{xx} = \dot{e}_{yy} = \dot{e}_{zz} = 0$ it follows with use of (3.7) and (3.4) that $\tau_{xx} = \tau_{yy} = \tau_{zz}$.

The y and z stress equilibrium equations in (3.8) take on the specific forms:

$$\frac{\partial \tau_{yy}}{\partial y} = -\rho g_y \tag{3.20}$$

$$\frac{\partial \tau_{zz}}{\partial z} = -\rho g_z \tag{3.21}$$

In view of the condition $\tau_{xx} = \tau_{yy} = \tau_{zz}$, (3.20) and (3.21) are satisfied by

$$\tau_{xx} = \tau_{yy} = \tau_{zz} = -\rho g_z z \tag{3.22}$$

The x equilibrium equation in (3.8) reduces to

$$\frac{\partial \tau_{xy}}{\partial y} + \frac{\partial \tau_{xz}}{\partial z} = -\rho g_x \tag{3.23}$$

The flow relations (3.7) reduce to

$$2\dot{e}_{xy} = \frac{\partial u}{\partial y} = 2A\tau^{n-1}\tau_{xy} \tag{3.24}$$

$$2\dot{e}_{xz} = \frac{\partial u}{\partial z} = 2A\tau^{n-1}\tau_{xz} \tag{3.25}$$

The last three equations are sufficient to determine u, τ_{xy} and τ_{xz}.

The relations (3.9 – 3.12) underlying the finite element method are simplified somewhat for rectilinear flow as follows. The functional J from (3.9) reduces to

$$J = \int_A (\Gamma - \rho g_x u) dA - \int_{B_1} T^* u \; dl \tag{3.26}$$

in which the first integral is over the cross-sectional area A of the ice-flow domain in the y, z plane and the second integral is around that part of the perimeter, B_1, on which boundary conditions of type 1 (stress boundary conditions) are specified. The free-surface boundary condition is $\tau_{xz}(y, 0) = 0$. (The further condition $\tau_{yz}(y, 0) = 0$ is automatically satisfied, and $\tau_{zz}(y, 0) = 0$ is satisfied by (3.22).) In (3.26), $u = u_x(y, z)$ is the flow velocity in the flow direction (x axis), g_x is $g \sin \alpha$ and $\vec{T}^*$ is the specified boundary shear stress, which acts in the direction of the x axis. The $p\vec{\nabla} \cdot \vec{u}$ term in (3.9) has disappeared in (3.26) because $\vec{\nabla} \cdot \vec{u} = 0$ is automatically satisfied by a rectilinear velocity distribution, for which $\dot{e}_{xx} = \dot{e}_{yy} = \dot{e}_{zz} = 0$. Thus the variable p drops out of consideration. (From (3.22) it is given by $p = \rho g_z z$.) τ_{xx}, τ_{yy} and τ_{zz} are given by (3.22) and are not involved in the flow solution. Γ in (3.26) is given by (3.12), with the simplification that, because all strain rates except $\dot{e}_{xy}$ and $\dot{e}_{xy}$ are 0, $\dot{\epsilon}$ from (3.2) reduces to

$$\dot{\epsilon} = (\dot{e}_{xy}^2 + \dot{e}_{xz}^2)^{\frac{1}{2}} \tag{3.27}$$

and correspondingly

$$\tau = ({\tau_{xy}}^2 + {\tau_{xz}}^2)^{\frac{1}{2}} \tag{3.28}$$

The variational condition on the flow solution $u(y, z)$ remains $\delta J = 0$, where the variation δ operates on $u(y, z)$.

3.3 Finite Element Model

The finite element method discretizes the velocity field u and applies the variational condition $\delta J = 0$ to the corresponding quantity J calculated from a sum of discrete contributions.

The first step in the discretization is to choose a set of points (y, z), called nodes, at which the flow velocity will be calculated. Those nodes lying on the boundary of the deforming mass define the shape of the boundary. The interior nodes need to be distributed through the interior of the mass in a way such as to provide high spatial resolution in regions where the gradients of u and τ are steep; outside these regions the spatial resolution (i.e., the number of nodes per unit area) can be lower. The second step in the discretization is to connect adjacent nodes in such a way as to divide the mass into an array of polygons, here taken to be triangles. These triangles are called the *elements* of the finite-element array. Each element must have a reasonable shape, which requires a reasonable placement of nodes in relation to one another.

The velocity $u(y, z)$ within each element is taken to be determined by the velocity at its three nodes according to specified "shape functions," which are here taken to be linear functions of y and z. As a result, the non-zero strain-rate components $\dot{e}_{xy}$ and $\dot{e}_{xz}$ are taken to be constant within each element.

The detailed method by which nodes are chosen and the finite element calculation is carried out in the computer program are as follows. The program was developed by Charles Raymond, and the following information is from Raymond (1978).

An array of N nodes is chosen by first describing the cross section of the deforming mass in terms of the intercepts of the upper and lower surfaces with a set of parallel vertical grid lines (VGLs). Nodes on the boundary and in the interior are determined by specifying the number of nodes $I(y)$ on each VGL. These nodes are then spaced along each VGL according to the equation

$$z_i = S_U - (S_U - S_L)\left[\frac{(i-1)}{(I(y)-1)}\right]^{1/V} \tag{3.29}$$

where i runs from 1 to $I(y)$, S_U is the z co-ordinate of the upper surface, S_L is the z co-ordinate of the lower surface and V controls the spacing. (V is not related to the V in (3.9).) The ith node of one VGL is connected to the ith node of an adjacent VGL to form quadrilaterals. Each quadrilateral is then divided into two triangles by a diagonal as specified by the user. The recommended division is to alternate between diagonals running from top left to lower right and from top right to lower left, which lessens the propagation of errors. When two adjacent VGLs differ in their number of nodes by more than one, additional nodes are added. In this way, M triangular elements are formed.

The linear distribution of u in each triangular element is specified uniquely in terms of its values at the nodes. A continuous, piecewise linear distribution of velocity throughout the ice is thus determined by the nodal velocity values, which constitute the unknowns of the problem. Since from (3.24), (3.25) and (3.27) $\dot{\epsilon}$ is constant within each triangle, the contribution to J from each triangle is calculated analytically. J is found by summing these contributions and adding the contributions from B_1. Setting equal to zero the derivative of J with respect to each of the unknown nodal values of velocity, in accordance with (3.11), gives a set of equations which determine the nodal values of u and thus the distribution of velocity $u(y, z)$.

If the above set of finite-element equations is linear in the unknown nodal values of u, it can be solved for these unknowns by matrix methods. To have the necessary linearity, n must be taken equal to 1 so that $\dot{\epsilon}$ in (3.12) occurs to the power 2. Because the shape functions are linear in the unknown nodal u values, $\dot{e}_{xy}$ and $\dot{e}_{xy}$ are too, and thus $\dot{\epsilon}^2$ from (3.27) is quadratic in the unknown u's. Γ is integrated over each element with the summation giving J. Finally, differentiation of J with respect to each unknown u reduces it to an expression consisting of a sum of terms linear in the unknown u values. These expressions are set equal to 0, giving the set of linear finite-element equations. The coefficients matrix of these equations is symmetric and banded. The program automatically renumbers the nodes in order to minimize the bandwidth. This increases the efficiency of the solution. The equations are solved using an algorithm for Gaussian elimination coded for a symmetric, banded matrix.

In actuality n is not 1, so an iterative method is used to take into account the rheological nonlinearity while keeping the linear finite-element equations. At any particular stage i of the iteration, a trial solution u^i is taken as the output of the previous iteration stage. The value of $\dot{\epsilon}^i$ in each element is calculated from (3.27), $\eta^i(\dot{\epsilon})$ is calculated from (3.17) with $n = 3$, and Γ is then calculated from (3.19) which is based on $n = 1$. The resulting linear finite-element equations are then solved for an improved u^{i+1}. This approach substitutes a spatially varying $\eta(y, z)$ for the strain-rate dependent $\eta(\dot{\epsilon})$ in a self-consistent manner.

The initial trial solution is $u^i = 0$ at all nodes except the boundary nodes where u is specified as given boundary conditions. For the first few iterative steps, the simple successive approximation method described above is used. It almost always converges, but the convergence is slow. For later iterative steps the program switches to a more complicated iterative procedure based on Newton's method, which converges rapidly when it converges at all, but to do so requires a trial solution that is fairly close to the actual solution. The program is set up to switch to Newton's method after a certain number of iterations specified by the user (but > 3) Raymond (1978).

Two modifications were introduced into the program so it would more realistically model the conditions in the ice stream. Temperature dependence of A was added to the program, so that the rate of deformation is an increasing function of temperature (3.5). However, this is not a thermomechanical model: there is no feedback due to shear heating. An enhancement factor $E(y, z)$ is incorporated to take into account the possibility of flow-law enhancement due to ice recrystallization or other causes. E is defined as the ratio of the actual strain rate to the strain rate of isotropic ice under the same stress and at the same temperature. It is incorporated into equation (3.1) by writing

$$\dot{\epsilon} = E(y, z)A\tau^n \tag{3.30}$$

E here is generally taken to be a function of distance across the ice stream, but can vary with depth as well as distance.

3.4 Testing of the program

The program was initially tested by modelling classic problems in glaciology that have analytical solutions. The analytical solutions were first derived by Nye (1965). The solutions for an infinitely wide, rectangular channel, a semi-circular cross section and an infinitely deep channel will be presented here.

3.4.1 Infinitely wide channel

Consider an infinitely wide channel of uniform depth a and slope α. If the channel is infinitely wide, then there is no side shear, which means $\tau_{xy} = 0$. Equation (3.23) can now be integrated with respect to depth, z. Using the boundary condition $\tau_{xz} = 0$ at the surface, this gives

$$\tau_{xz} = -(\rho g a \sin\alpha)\frac{z}{a} \tag{3.31}$$

Substituting this result into equation (3.25), taking the velocity at the base of the glacier ($z = a$) to be zero, and integrating gives

$$u = \frac{2Aa(\rho g a \sin\alpha)^n}{n+1}\left\{1 - \left(\frac{z}{a}\right)^{n+1}\right\} \tag{3.32}$$

Figure 3.2 shows the velocity field $u(y, z)$ in an infinitely wide glacier calculated by the above equation with $n = 3$ and as calculated by the numerical model. The solutions are almost identical. The only noticeable difference is in the 2.5 m a^{-1} contour line. This contour shows a ripple effect which is related to the way in which the triangular elements are chosen (Section 3.3). The method used is chosen such that errors do not accumulate at one side of the domain, but what results is a series of alternating highs and lows. Another difference is that the 2.5 m a^{-1} contour line is at a shallower depth in the modelled result than in the analytical result, indicating that the ice flows more slowly in the modelled result, as shown also by the values $u(y, 0) = 2.535$ m a^{-1} in the analytical solution and $u(z = 0$, averaged over $y) \approx 2.521$ m a^{-1} in the finite-element model. This agrees with a comment by Nixon *et al.* (1985, p.11,309). The finite element method gives a numerical solution to the

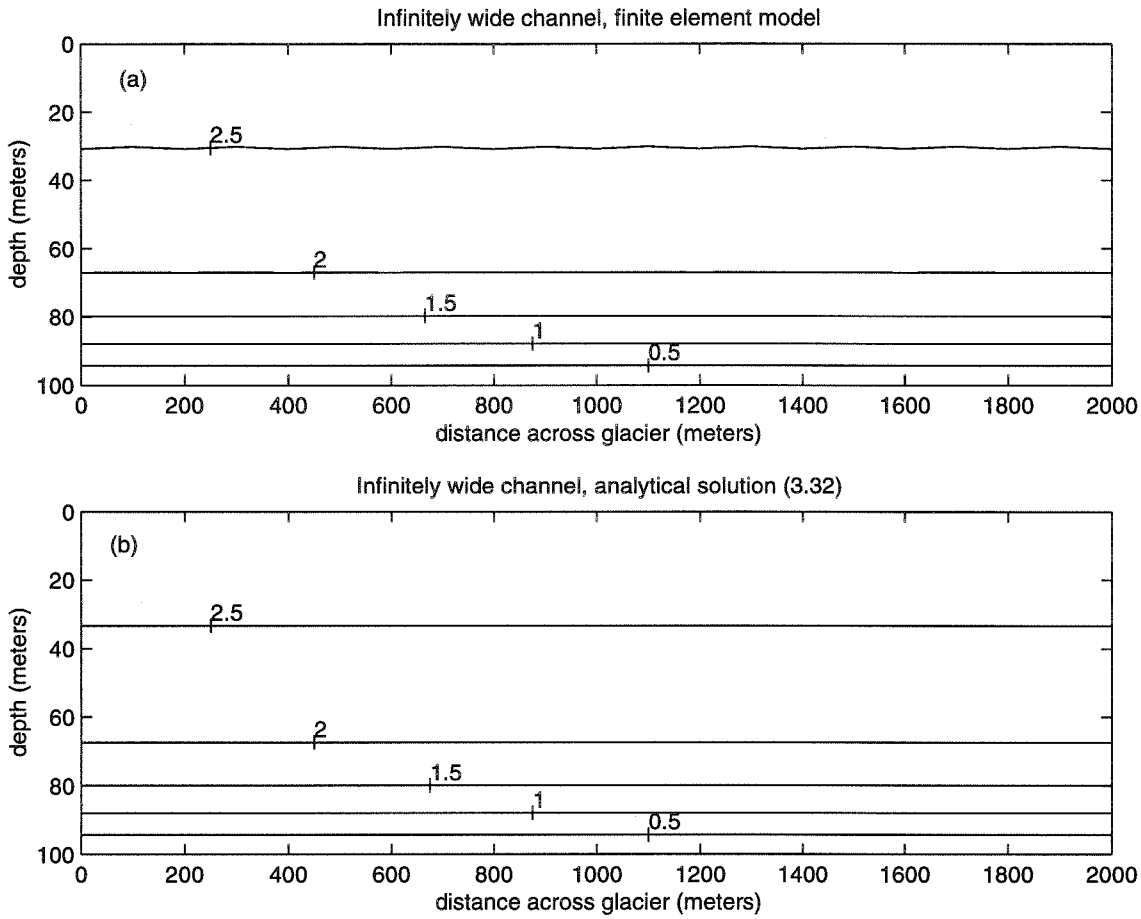

Figure 3.2: Flow in an infinitely wide channel, as calculated (a) by the finite-element model and (b) by the analytical solution 3.32. The channel shown, for which the finite-element calculation was done, is 2000 m wide and 100 m deep, a width-depth ratio of 20:1, but because of the lateral boundary condition $\tau_{xy} = 0$ on the sides ($y = 0, y = 2000$ m) it represents a 2000 m wide section of an infinitely wide channel. The vertical scale is exaggerated in both diagrams. The surface slope, α, is 4.55° and the flow law parameter, A, is 0.140 annum^{-1} bar^{-3}. Further boundary conditions are $u = 0$ at the base of the channel and $\tau_{xz} = 0$ on the free surface ($z = 0$). Velocity contours are labelled in metres year^{-1}. The ice surface ($z = 0$) is a velocity contour of value $u = 2.521$ m a^{-1} in (b) and approximately a contour of value $u = 2.535$ m a^{-1} in (a).

equations which is only an approximation caused by dividing the continuous mass into discrete elements. Nixon *et al.* suggest that because each element is assumed to deform uniformly and is connected to neighbouring elements only at certain nodal points, the finite element technique causes the ice in such models to be less responsive to deformation. The ice flows as though slightly stiffer, and hence slower, than in the analytical model.

3.4.2 Semi-circular channel

Consider a semi-circular channel of radius a, with the channel axis sloping at angle α. To derive the stresses, calculate the force balance equation on a cylindrical surface of radius r and of unit length parallel to the flow. τ_{xr} is a function or r only, so

$$\pi r \tau_{xr} = -\rho g_x \frac{\pi r^2}{2} \tag{3.33}$$

This can then be substituted into

$$\frac{\partial u}{\partial r} = 2A\tau_{xr}^{n-1}\tau_{xr} \tag{3.34}$$

and integrated. The boundary condition is that the velocity u is zero at $r = a$. This gives the velocity at any point at radius r in the glacier.

$$u = \frac{2Aa(\rho g a \sin\alpha)^n}{2^n(n+1)} \left\{ 1 - \left(\frac{r}{a}\right)^{n+1} \right\} \tag{3.35}$$

Figure 3.3 shows the velocity field $u(y, z)$ in a semi-circular channel calculated by the above equation for $n = 3$ and as calculated by the numerical model.

The differences between the two graphs are similar to the differences in the flow in the infinitely-wide-channel calculations (Figure 3.2). The highest contour, the 25 meter/year contour in this case, is nearer the surface in the finite element calculation than in the analytical solution. Again, it appears that the finite element calculation treats the ice in effect as slightly stiffer than in the analytical calculation. This is

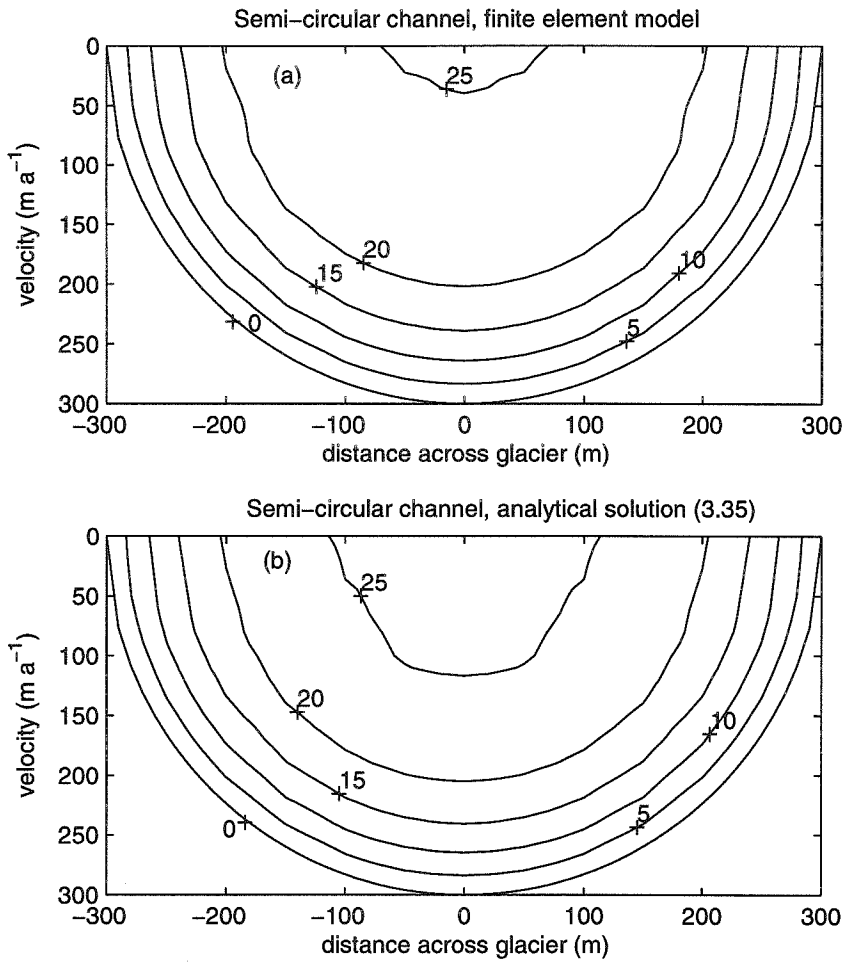

Figure 3.3: Flow in a semi-circular channel of radius $a = 300$ m, as calculated (a) by the finite- element model and (b) by the analytical solution 3.35. The surface slope, α, is 4.55° and the flow law parameter, A, is 0.140 year^{-1} bar^{-3}. Velocity contours are labelled in metres/year. The basal/lateral boundary condition is $u = 0$ at $r = a$, and the surface boundary condition is $\tau_{xz} = 0$ at $z = 0$.

also shown by the centerline velocity $u(r = 0)$, which is 27.4 m a^{-1} in the analytical solution and 25.2 m a^{-1} in the finite element model. However, agreement is generally good. The 5 meter/year contour is in the same place on each graph, although on first sight they may appear different because the scales in the two graphs are slightly different. The contour lines are not vertical at the surface as required by the surface boundary condition, shear stress $\tau_{xz} = 0$. This is an artifact of the plotting routine used by MATLAB rather than an error of the analytical calculation or the finite element model. The fact that the contours drawn in Figure 3.3 are not perfect semicircles is also due to the plotting routine.

3.4.3 Infinitely deep channel

Consider an infinitely deep channel of uniform width $2a$. This is very similar to the problem of the infinitely wide channel, but turned 90°. Because of the surface boundary condition and because the channel is infinitely deep, the shear stress $\tau_{xz} = 0$. Equation (3.23) can in this case be integrated with respect to distance across the glacier, y, with the boundary condition that there is no shear stress across the center plane of the glacier. The lateral shear stress is then

$$\tau_{xy} = -(\rho g a \sin\alpha)\frac{y}{a} \tag{3.36}$$

This is substituted into equation (3.24). Integrating with respect to y and fixing the integration constant from $u(y = a) = 0$ gives the velocity in the channel

$$u = \frac{2Aa(\rho g a \sin\alpha)^n}{n+1}\left\{1 - \left(\frac{y}{a}\right)^{n+1}\right\} \tag{3.37}$$

Figure 3.4 gives the graphs of $u(y, z)$ for $n = 3$. Both show identical flow at the surface. However, there is a very slight difference at the deepest part of the channel shown, although this is hard to see without measuring the graphs carefully. The numerical flow velocities are again slower than the analytical ones, although in

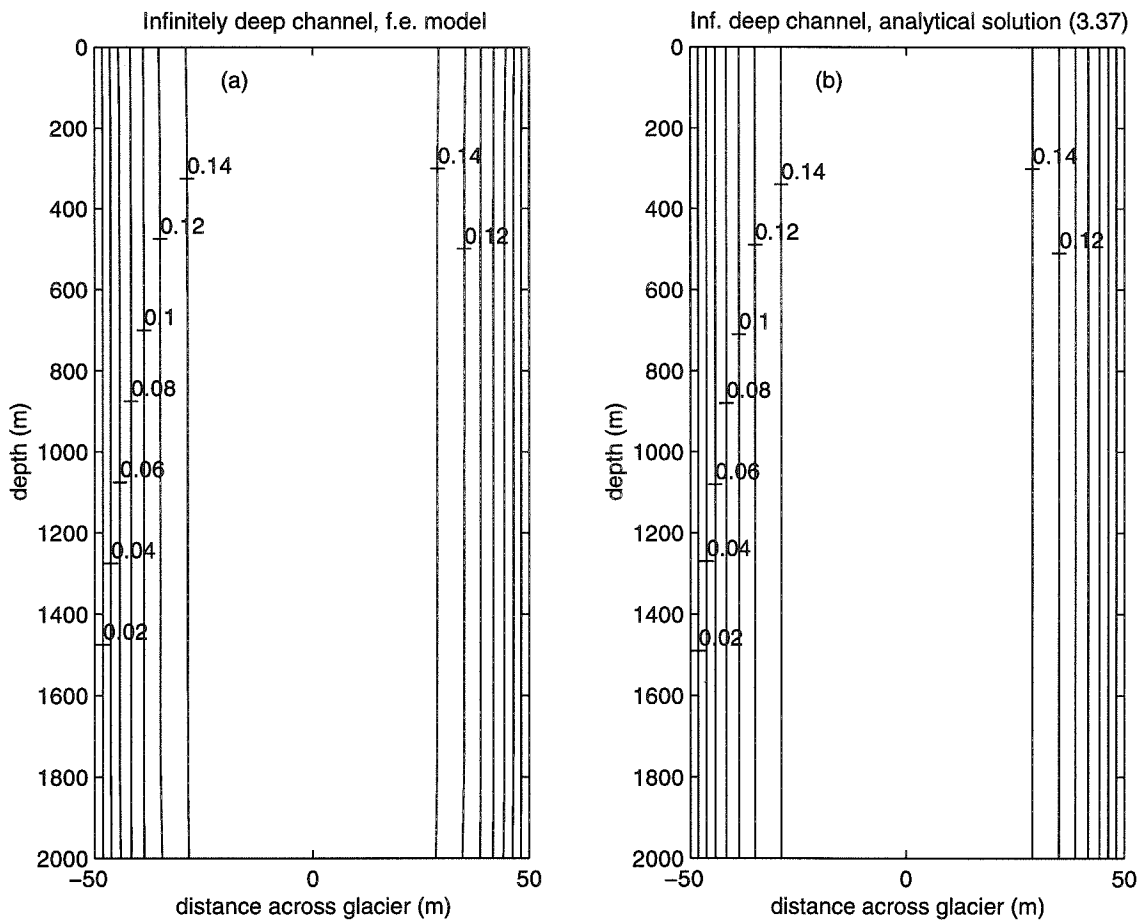

Figure 3.4: Flow in an infinitely deep channel, calculated (a) in the finite-element model and (b) from the analytical solution 3.37. In the finite element model, an infinitely deep channel is approximated by a channel 100 m wide and 2000 m deep, a width-depth ratio of 1:20. Because of the basal boundary condition $\tau_{xz} = 0$ this is effectively a finite-depth piece of an infinitely deep channel. The horizontal scale is exaggerated on both figures. The surface slope, α, is 4.55° and the flow law parameter, A, is 0.140 year^{-1} bar^{-3}. The velocity at the sides is zero. Velocity contours are labelled.

this case by a very small amount. The centerline velocities are 0.158 m a^{-1} in the analytical solution and 0.154 m a^{-1} in the finite element model.

3.5 Flow Model for an Ice Stream with Marginal Shear Zone

The velocity profile across the ice stream and MSZ will now be modelled. The immediate objective is to find a flow model that gives surface velocities matching the observed surface velocity profile, and that involves the assumption of little or no flow enhancement, in view of the experimental results in Chapter 2. The ultimate goal is to understand and if possible correct the discrepancy between the experimental work in Chapter 2 and the previous numerical model results of Echelmeyer *et al.* (1994), as discussed in Section 3.5.7.

Several different approaches were used in searching for a model giving surface velocities that match the observed profile. The first was to vary the basal shear stress $\tau_{xz}(y, 0)$ across the ice stream and MSZ. Next, the enhancement factor found in the experimental work (Chapter 2) was used as a depth-independent enhancement factor $E(y)$ in the MSZ model. Finally, several models were tried in which $E(y)$ was varied while trying to keep its peak value as low as possible. Only the last approach was successful in matching the observed surface velocity profile. In the following sections the observational constraints on the flow modelling are first discussed, followed by the actual model results and their comparison with the observed surface velocity profile.

3.5.1 Measured surface velocity profile

The velocity data available to constrain the models or to provide tests of their success are as follows. A surface velocity profile was measured in a transect across the ice stream by Echelmeyer *et al.* (1994). Twenty markers were placed in a transect across the shear margin and into the middle of the ice stream. The markers were surveyed three times over about 8 day intervals using a theodolite and an electronic

distance meter. For those markers in the crevassed region, a retro-reflecting prism was mounted on each marker so these sites did not have to be re-occupied after the installation. The estimated error limits on these velocity measurements are ± 3 to 5 m a^{-1}. Velocities calculated over the two different time intervals between surveys agree within these error limits. The present study has the advantage of 20 additional velocity measurements made by Echelmeyer's group in December 1993, January 1994 and January 1995, which were not included in their original report (Echelmeyer and Harrison (1999)). These measurements (which will subsequently be called the "additional data") were made over the outer 2 km of the shear margin at an average spacing of 110 m. This newer transect crosses the arcuate crevasses on the outer edge of the shear margin, and extends into, but not completely across, the chaotic sub-zone of the shear margin (Figure 2.2). These markers were surveyed three times, first at a six-week interval, then at a one-year interval. Markers were surveyed using a theodolite and an electronic distance meter, with retro-reflecting prisms on most of the poles. The velocities used here are the average over the whole fifty-eight week period. The probable error in these velocity measurements is 3.5 m a^{-1}. Both the original measurements across the southern half of the ice stream (including the MSZ) as well as the more closely spaced measurements over the outer two km of the MSZ are shown in Figure 3.5.

In this figure and all subsequent figures, the co-ordinate system is changed somewhat from that used previously, as follows. The x-axis is as before in the ice surface along the center-line, positive in the direction of flow. The z-axis is normal to the surface as before, but positive upward with origin at the base of the ice stream. The y-axis is directed across the ice stream with the origin at the outer edge of the marginal shear zone. The origin is approximately at the fairly abrupt boundary at the outer limit of the large, widely spaced, arcuate crevasses that mark the outer edge of the shear margin (Echelmeyer *et al.*, 1994, p. 529). This origin is about 11 km south of the Upstream B camp (Figure 2.2).

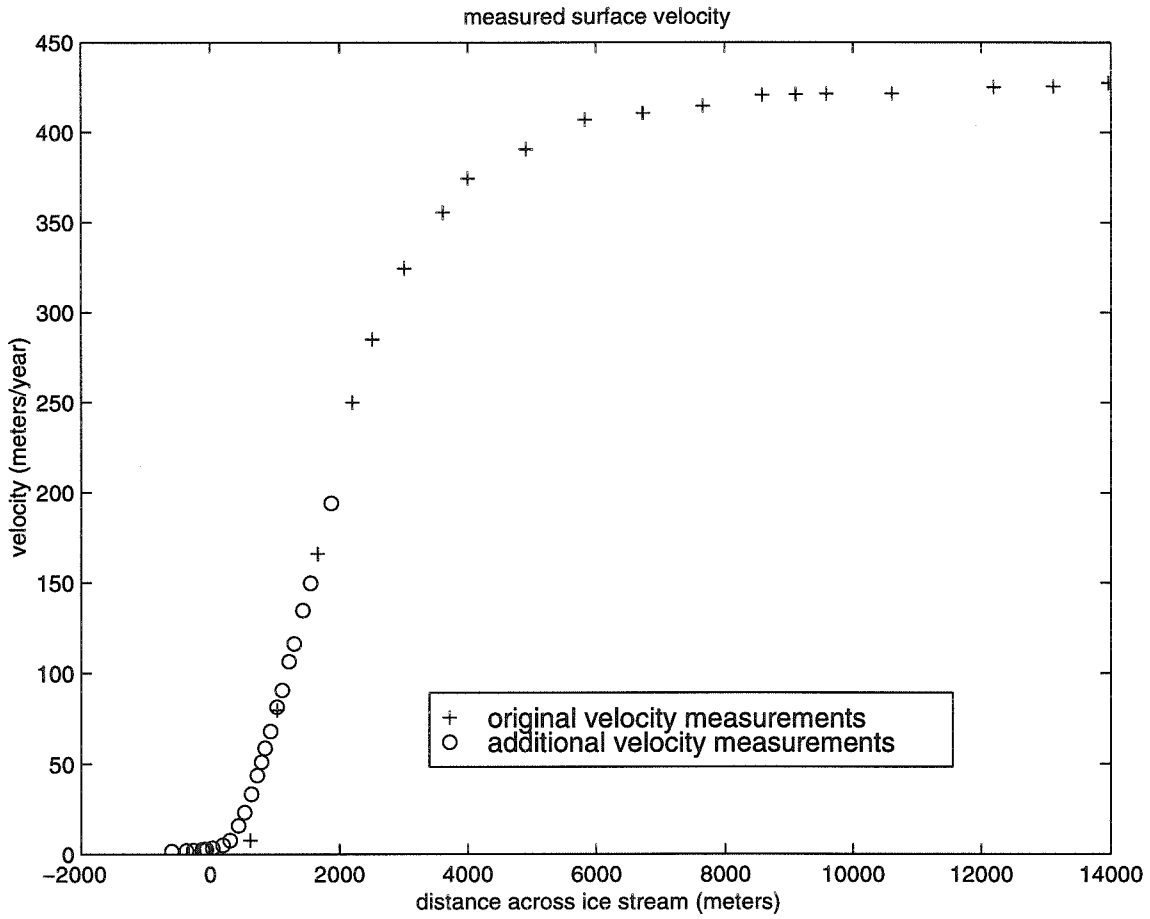

Figure 3.5: Surface velocity measurements. Original data used in Echelemeyer model are marked by crosses; more recent data (see text) are marked by open circles. The origin is at the outer edge of the MSZ (see text). The centre-line of the ice stream is at y co-ordinate 16000 m.

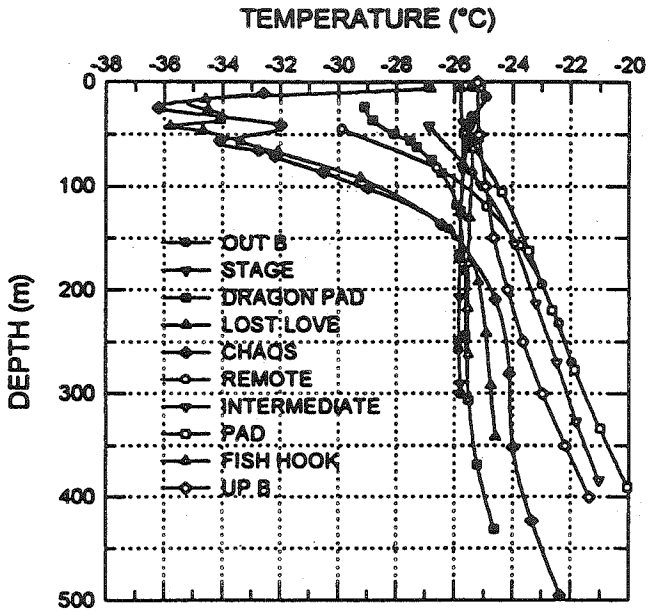

Figure 3.6: Temperature in the ice stream from Harrison *et al.* (1998). Some of the different sites in which temperatures were measured are shown in Figure 3.7.

3.5.2 Temperature field

The same temperature field is used as in Echelmeyer *et al.* (1994). The temperature field consists of four layers. The bottom 50 m is at the melting point, the next 250 m are at $-9°C$, the next 400 m are at $-20°C$ and the top 380 m are at $-24°C$. Within each layer, the model uses the appropriate flow law parameter A as given by equation (3.5).

Temperature profiles measured through the ice by Harrison *et al.* (1998) (Figure 3.6) show that in the outermost part of the MSZ there is near-surface (upper 150 m) cooling of 2°C to 10°C due to a heat pump effect in the bridged crevasses there (average mid-winter temperatures are -35 to $-40°$ and cold winter air becomes ponded in the crevasses). The top layer in the model is 380 m thick so this cooling effect is averaged over the whole layer to give 3.6°C of cooling in the outermost 400 m of the MSZ (from y co-ordinate 0 to y co-ordinate 400 m), and 2.9°C of cooling in the next 600 m (from y co-ordinate 400 to y co-ordinate 1000 m). The temperature field is

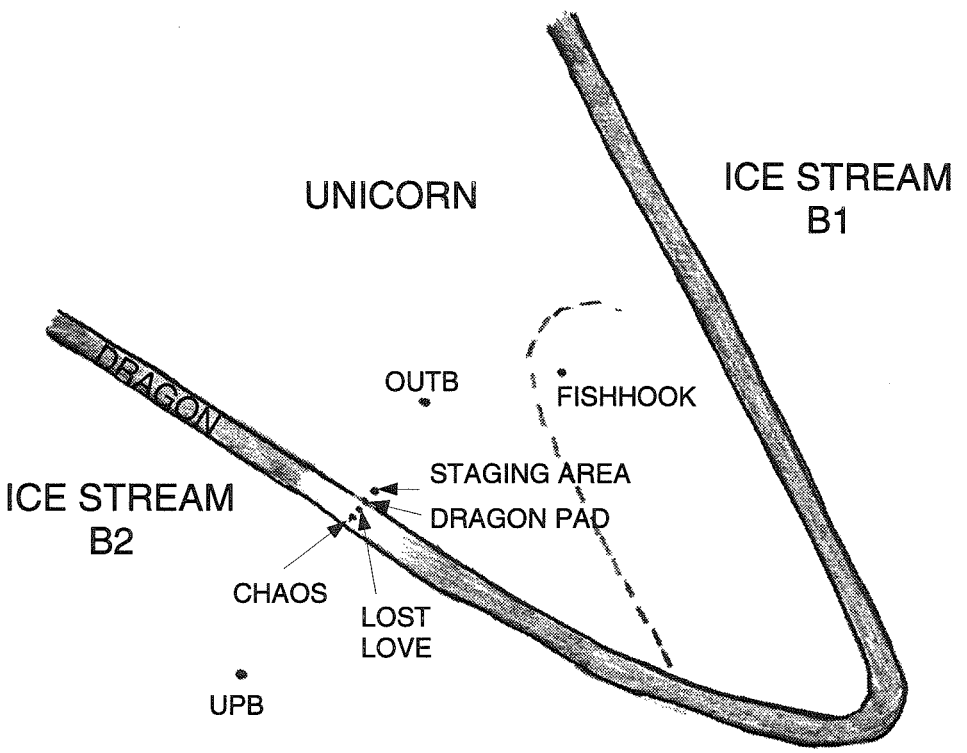

Figure 3.7: Location map for different sites from which cores were taken and some of the sites where temperatures were measured. The shaded area marks the MSZ. For scale, the distance between the Out B site and the Staging Area site is 5 km.

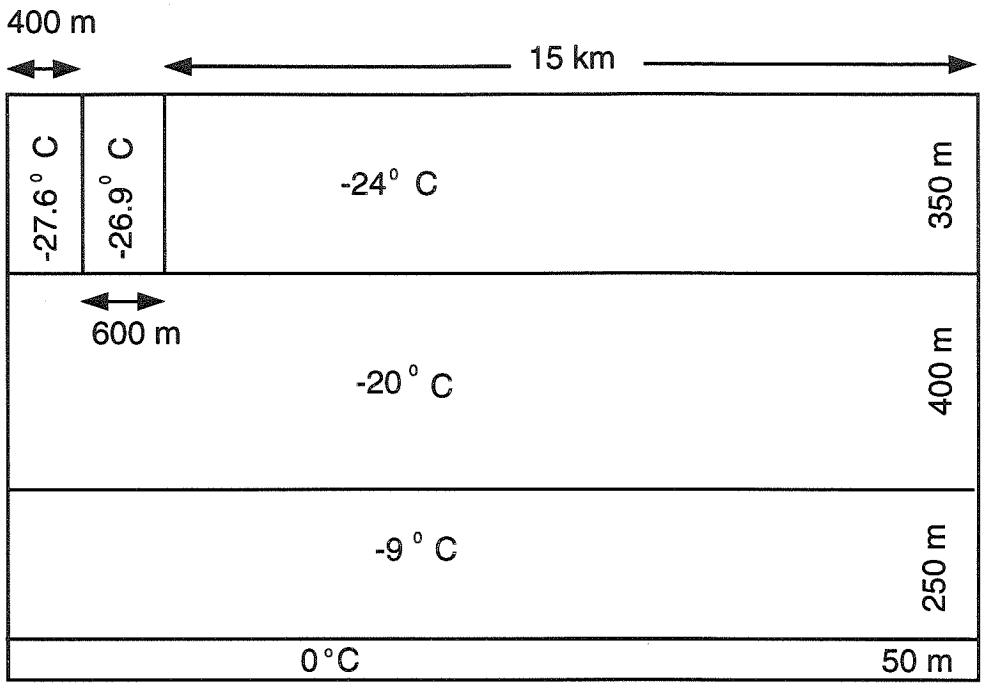

Figure 3.8: Temperature field showing the different temperature layers and the cooling in the outer part of the shear margin due to the crevasses.

shown in Figure 3.8.

3.5.3 Extent of frozen bed in models

Using measured values for the temperature shown in Figure 3.6 (e. g. , Stage curve or Dragon Pad curve) and other known parameters for the ice, the surface velocity tends to be too high over the outer 1000 m of the velocity profile (the additional data) unless the basal velocity is fixed at zero by assuming this part of the MSZ is frozen to the bed. This is a reasonable assumption, because it is known that the ice on the Unicorn (Fig. 2.1) is frozen to the base (Engelhardt, pers. comm.), and it is not known precisely where the demarcation is at the base of the ice between a frozen and unfrozen base.

Figure 3.9 shows two examples of surface velocity over the outer 2500 m. One model has enhancement of ice flow of either 1 or 1.17 over these 2500 m and is up to 60% faster than the measured surface velocity. The second model has $u = 0$ at the bed from $y = 0$ m to $y = 1000$ m, and shows good agreement with the surface

velocity. Hence, a model incorporating the outer 1000 m of the MSZ frozen to the bed is the simplest way to reproduce the surface velocity in this part of the MSZ. In order to get a similar profile without assuming a frozen bed, it would be necessary to assume either hardening of the ice here or temperatures much lower than have been measured and modelled by Harrison *et al.* (1998).

3.5.4 Models based on adjustment of the basal shear stress

Initially, an effort was made to develop a model of the ice stream by adjusting the basal shear stress $\tau_{xz}(y, 0)$. The constraints on $\tau_{xz}(y, 0)$ are as follows. Directly beneath the ice of the ice stream is a meters-thick layer of water-saturated till (Blankenship *et al.*, 1987; Engelhardt *et al.*, 1990), which is thought to be weak and to "lubricate" the bed, allowing the rapid ice streaming motion at low $\tau_{xz}(y, 0)$ (Alley *et al.*, 1987). The till layer is not continuous or uniformly thick everywhere (Rooney *et al.*, 1987) and presumably in places where there is no till and the ice is in contact with bedrock, the basal stress is higher than elsewhere. The shear stress at the base of Ice Stream B has not been measured directly and the only observational value related to it is from shear strength tests on the till (Kamb, 1991). These tests gave a value for the shear strength of 0.02×10^5 Pa. If there is water between the till and the ice, this would further lubricate the bed, and the basal shear stress in such places would probably be lower than elsewhere. It is hard to detect the presence of such a water layer directly, but in a study of the hydraulic system of Ice Stream B based on hot-water drilling, Engelhardt and Kamb (1997) found evidence for a water layer, 2 mm or thinner, that is present discontinously at the ice/till interface. They also postulated the presence of broad, shallow canals on the uppermost surface of the till.

As examples of the search for a satisfactory model, Figure 3.10 shows the surface velocity profiles from two models. The first has a constant basal shear stress of 0.054×10^5 Pa across the ice stream. The second has zero basal shear stress between $y = 1000$ m and 3400 m, and 0.06×10^5 Pa basal stress elsewhere. Between 1000 m and 3400 m is where the gradient in surface velocity is steepest, and where conditions,

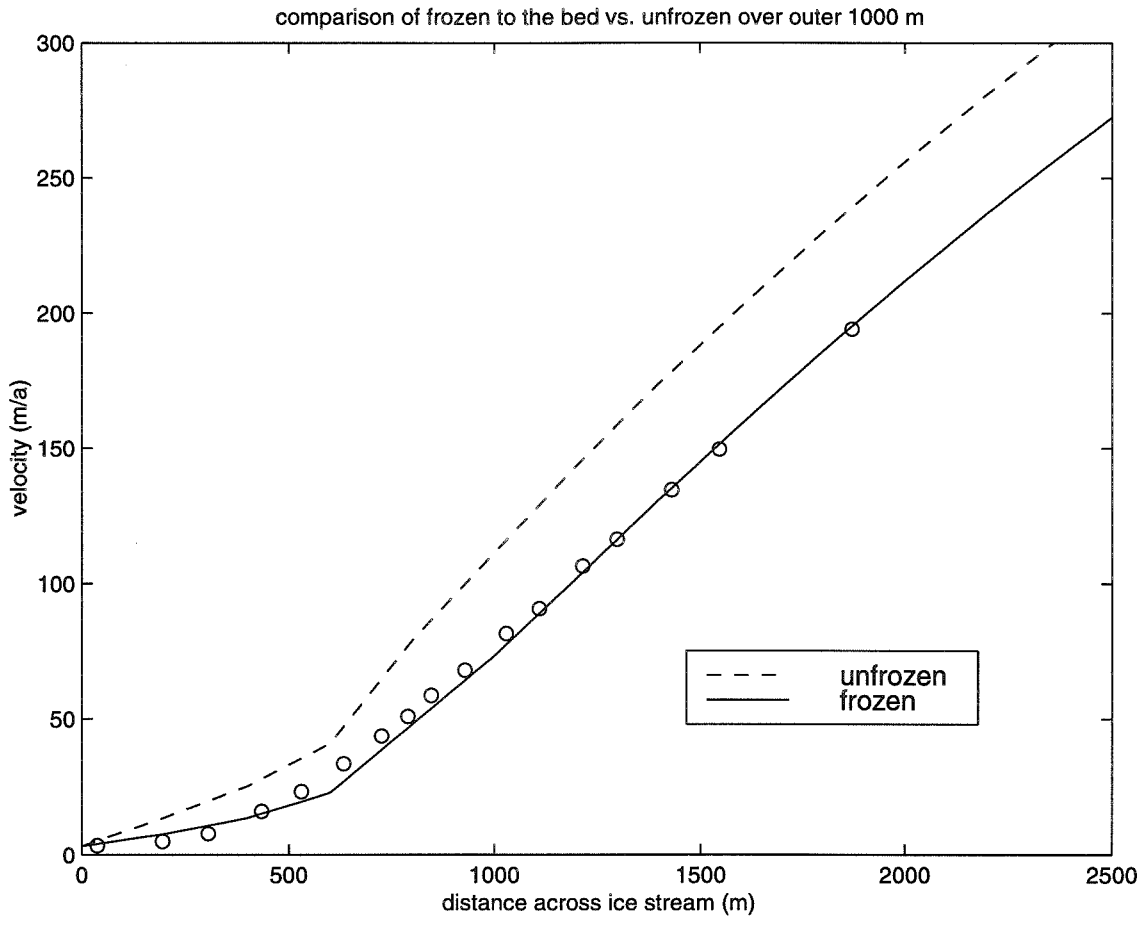

Figure 3.9: Surface velocity profile using the value for the enhancement factor from the experimental work in Chapter 2. The ○ are the additional velocity measurements not available in the original study by Echelmeyer *et al.* (1994) (see text). The dashed line represents a model where the outer 400 m of ice has no enhancement, and the rest has enhancement of 1.17, the value found in the experimental work. Temperatures are as described in the text. Even with such conservative values for enhancement, the ice is much too fast. The solid line respresents a model where the outer 1000 m of ice is frozen to the bed. This model shows good agreement with the measured velocities.

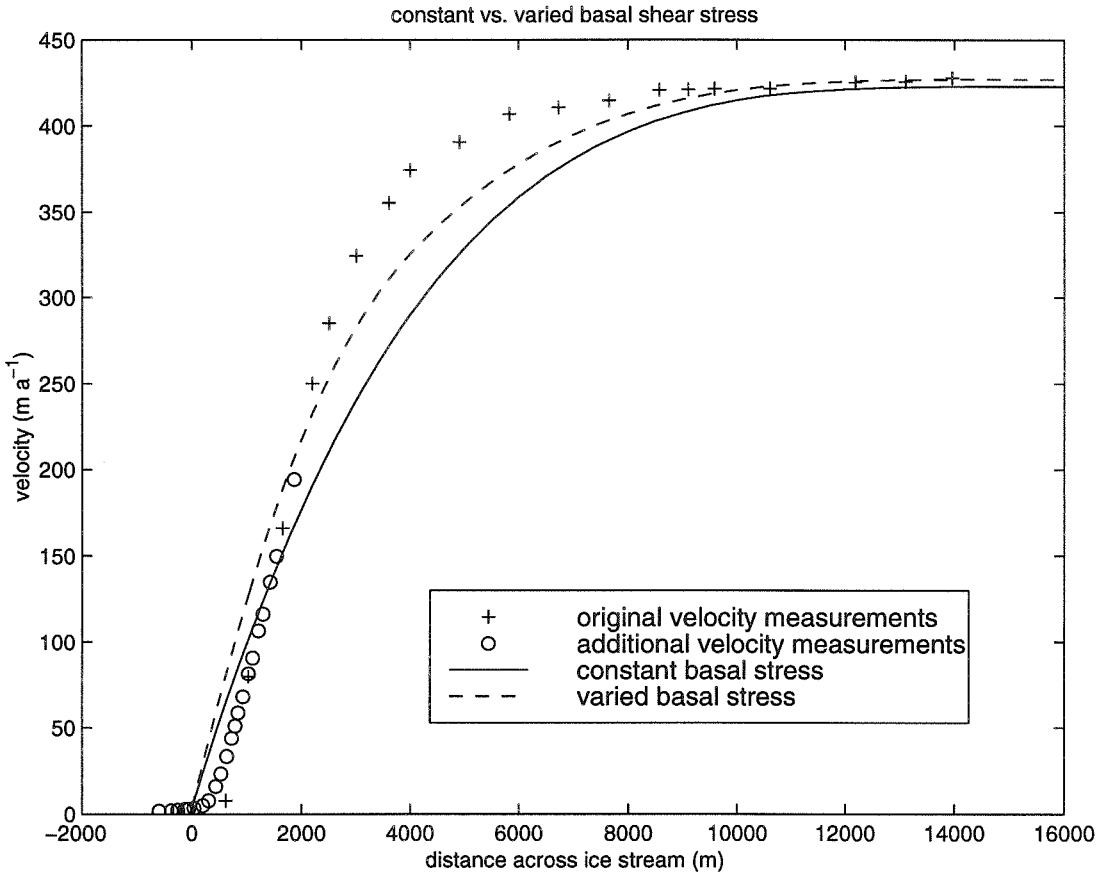

Figure 3.10: Surface velocity profile for laterally constant basal shear stress compared with the velocity profile for laterally varying basal shear stress. The constant basal shear stress is 0.054×10^5 Pa while the laterally varying basal stress is 0.06×10^5 Pa between 0 and 1000 m and between 3600 and 16000 m and is zero elsewhere, as discussed in the text. Ice thickness is 1050 m and surface slope, α, is 1.3×10^{-3}.

either in the ice or at the base, must be different from elsewhere. This is done to test whether the increase in velocity over a short lateral distance is because the basal conditions change over a short distance, and the ice is moving faster because there is less drag. Putting zero basal stress in this region will give the sharpest possible gradient in velocity due to a variation in basal conditions, while keeping the basal shear stress within reasonable limits. Because negative basal shear stress is excluded (see below), zero is the lowest possible stress. 0.06×10^5 Pa is chosen as the basal shear stress over the rest of the ice stream based on the discussion in Echelmeyer *et al.* (1994, p. 532). The two distributions of basal shear stress give approximately the same surface velocity in the middle of the ice stream, although they represent two extreme models in terms of basal shear stress distribution - constant basal shear stress vs. two distinct shear stress values, one the minimum possible value and the other three times the value measured experimentally. This example shows that even when the variation in the basal shear stress is at the limit of what is physically reasonable, the surface velocity profiles are still very similar and do not show the sharp velocity gradient between $y \approx 0$ and $y \approx 4000$ m, which is seen in the graph of measured surface velocities (Figure 3.5).

In the attempt to develop a satisfactory ice-stream model by adjusting the basal shear stress distribution $\tau_{xz}(y, 0)$ it is found that the effect of changing the basal stress at one node tends to spread laterally as it propagates through the thickness of the ice stream, resulting in a broad, low-amplitude effect on the calculated surface velocity profile. It is thus not possible to replicate the steep marginal gradient in the observed surface velocity profile by adjusting only the basal shear stress in the model.

It may be possible to match the observed surface velocity profile by using negative values for the basal shear stress over certain intervals of the y co-ordinate near $y = 0$. Negative basal stress implies that the bed of the ice stream is dragging forward the ice above it, which is not physically realistic.

A further comparison of two models with different basal conditions but with the other parameters identical is described in Section 3.5.6.

In most of the subsequent models, the basal shear stress is taken to be almost

uniform across the ice stream with a value of 0.01×10^5 Pa. Given the preceding discussion in this section about the basal conditions and the till strength, this is a reasonable value. Because of the spreading effect of the basal shear stress applied at any one node, allowing the basal stress to vary across the ice stream has only a minor effect on the detailed shape of the resulting velocity profile. But adjusting the general level of the basal shear stress for $y > 1000$ m does affect significantly the attempt to make the model fit the observed centerline velocity of 430 m a^{-1}. The models in Figure 3.10 are far from satisfying this constraint. It can, however, be satisfied by a constant basal shear stress of about 0.026×10^5 Pa. This stress level would be different if the flow parameter A were different, which is possible since the actual value of A for the ice of Ice Stream B is not known.

3.5.5 Model based on experimentally derived enhancement factor

A velocity model, model A, for the ice stream is calculated using the quantity derived experimentally in Chapter 2, $E(2000 \text{ m}, 300 \text{ m}) = 1.17$. This value is used where the velocity gradient is steepest, between 400 m and 2800 m. The enhancement factor is taken to be 1 (i.e., no enhancement) elsewhere. The outer 1000 m of the bed are assumed to be frozen and the basal shear stress is 0 between 1000 m and 16000 m. It is highly unrealistic that the basal shear stress is zero over this much of the ice stream, but it is used here as an extreme condition in order to force a match, if possible, between the model and the measured profile. The flow parameter A was adjusted so that there is agreement with the surface velocity in the center of the ice stream.

The boundary condition at the outer edge of the shear margin of the ice stream, at $y = 0$, is chosen as a condition on the velocity $u(0, z)$ as follows. The velocity at the surface ($z = 1050$ m) is taken to be the observed value $u(0, h) = 3$ m a^{-1}

Table 3.1: Different velocity models A - F across the ice stream and shear margin, showing the basal conditions for each model, either frozen ("frzn") or specified basal shear stress in bars, and the enhancement factor $E(y)$. Each column gives values for the range of y co-ordinate indicated (in m).

	basal conditions			enhancement factor $E(y)$				
	0-1000m	1000-3600m	3600-16000m	0-400m	400-1000m	1000-2800m	2800-4000m	4000-16000m
A	frzn	0.0	0.0	1.0	1.17	1.17	1.0	1.0
B	frzn	0.01	0.01	1.4	5.0	4.3	2.6	1.0
C	frzn	0.0	0–0.04	1.4	5.0	4.3	2.6	1.0
D	frzn	0.0	0–0.04	1.7	5.9	4.8	3.5	1.0
E	0.06	0.06	0.06	3.0	3.0	12.5	12.5/5[1]	5/1.0[2]
F	frzn	0.01	0.01	1.4	1.7/17.9[3]	1.7/16.4[4]	2.9	1.0

1. 12.5 between 2800 m and 3500 m; 5.0 between 3500 m and 4000 m.
2. 5.0 between 4000 m and 6000 m; 1.0 between 6000 m and 16000 m.
3. 1.7 in the upper 350 m; 17.9 in the lower 700 m.
4. 1.7 in the upper 350 m; 16.4 in the lower 700 m.

(Echelmeyer and Harrison, 1999), and the variation with depth is given by

$$u(0,h) - u(0,z) = u(0,h)\left(1 - \frac{z}{h}\right)^{n+1} \tag{3.38}$$

where $u(0,h)$ is the surface velocity at $y = 0$, z is the height above the base, h is the thickness of the ice, n is taken as 3 and $u(0,z)$ is the velocity at height z above the base. The form (3.38) is chosen to represent the vertical profile of velocity expected from (3.32) in the ice sheet outside the ice stream, where the ice is frozen to the bed.

Figure 3.11 shows the resulting velocity profile.

The profile is much too broadly rounded from about $y = 1000$ m to 10,000 m. Varying the basal shear stress has little effect on the shape of the profile, but instead simply increases or decreases the velocity all across the ice stream, and does not make it possible to match the observed velocity profile.

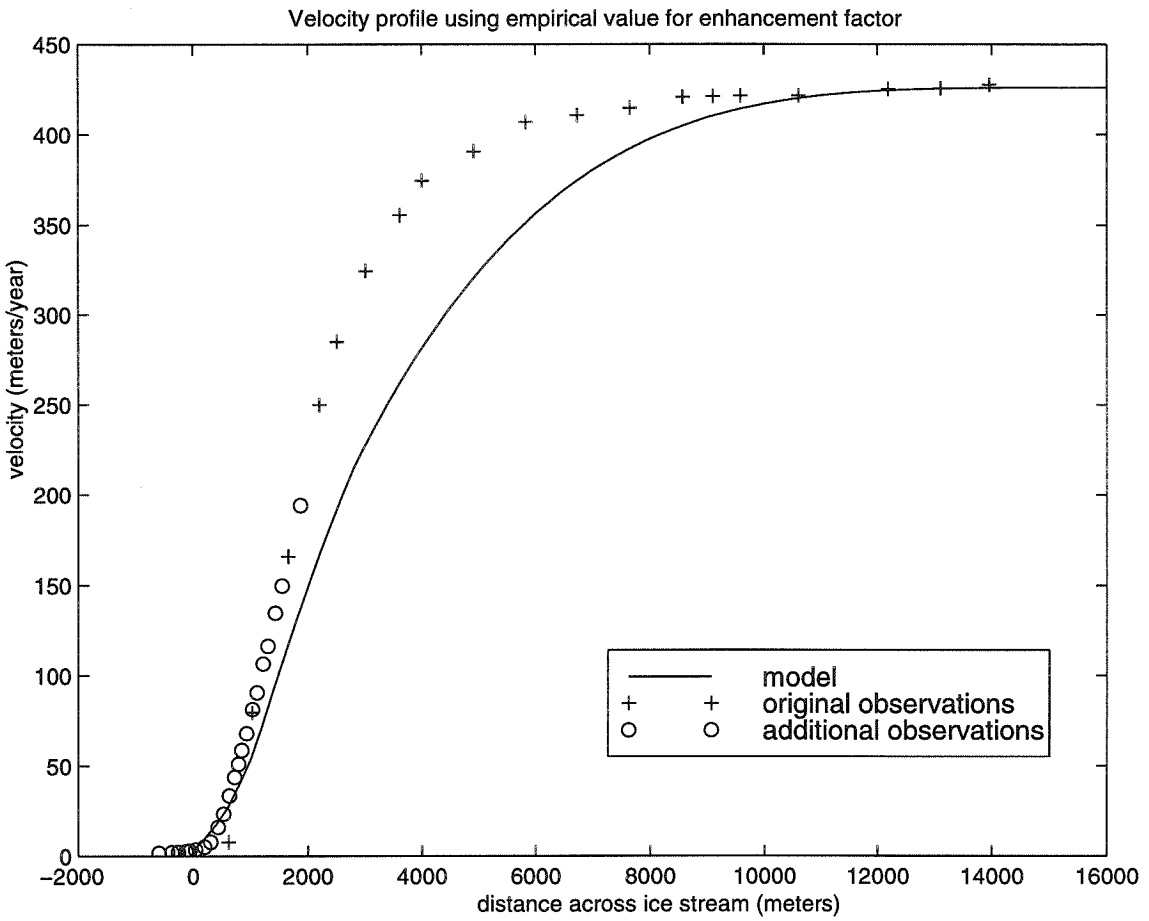

Figure 3.11: Surface velocity profile using the value for the enhancement factor from the experimental work in Chapter 2. The ∘ are additional velocity measurements not available in the original study by Echelmeyer *et al.* (1994) (see Section 3.5.1. The outer 1000 m of the ice stream ($0 < y < 1000$ m) are assumed to be frozen to the bed, and the basal shear stress is taken as zero over the rest of the ice stream.

3.5.6 Velocity model for Ice Stream B and the Dragon

Several models were found that successfully matched the surface velocity profile. These models have the same temperature field and the same velocity boundary condition as described in previous sections, but with the rheology varying laterally across the ice stream. (The model of Section 3.5.5 is a model of this type, but with a much smaller lateral variation of $E(y)$ than that considered here.) Although the rheology probably varies gradually, it is modelled here as though the ice stream has five discrete rheological zones laterally, arrayed parallel to the margin as suggested in Figure 3.12. Thus in the model, the outermost part of the ice stream, from y co-ordinate 0 to 400 m, has a different rheology at all depths from the adjacent part from y co-ordinate 400 m to 1000 m, and so on to the innermost zone from $y = 4000$ m to $y = 16{,}000$ m (see Figure 3.12). The rheology of the ice in each zone is represented by a corresponding enhancement factor (Figure 3.12 and Table 3.1). In most models the flow parameter A (equation 3.5) is adjusted to give the observed surface velocity at the centerline of the ice stream.

All the successful models tended to show similar lateral variation in rheology. The first successful model to be presented, model B, has the following characteristics (Table 3.1). The outer 1000 m of the ice stream are frozen at the bed and the specified basal shear stress over the rest of the base is 0.01×10^5 Pa. The velocity along the outer edge of the ice stream is as described in Section 3.5.5 and the temperature field is as described in Section 3.5.2. The enhancement in the middle of the MSZ is as high as 5, ranges between 1.4 and 4.3 over the rest of the MSZ and is 1 outside of the MSZ. The enhancement factor of 5 is the lowest peak E value found to give a good match between the observed and calculated surface velocity profiles. The observed and modelled surface velocity profiles, and the different enhancement factors used for each zone, are shown in Figure 3.12.

A very similar result, called model C, is found using the same enhancement factors and flow law parameter A but different basal conditions. In model C, the outer 1000 m of the ice stream is frozen to the bed (as in the previous two models), the basal

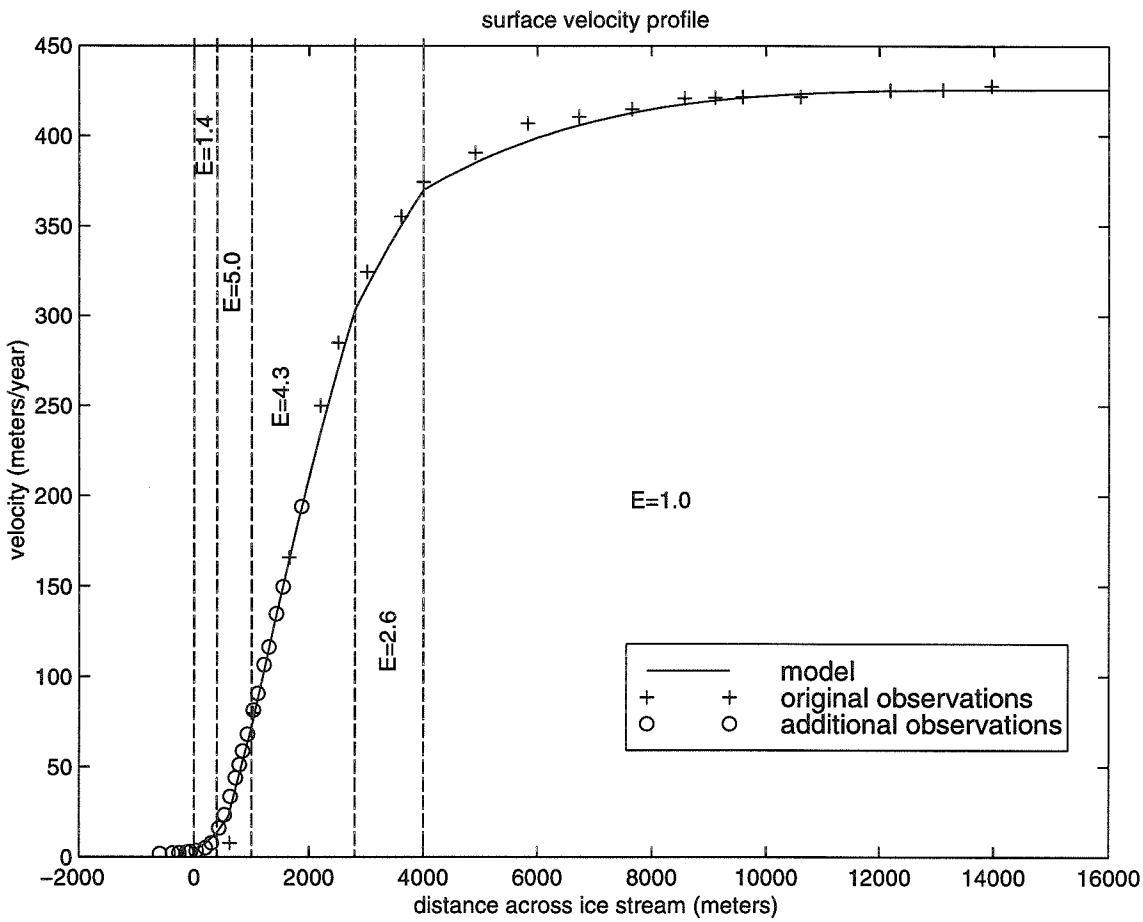

Figure 3.12: Surface velocity profile calculated from model B, in which the enhancement factor varies across the ice stream as follows. The enhancement factor is 1 between 4000 m and 16000 m. The enhancement factor is 1.4 between 0 and 400 m; 2.6 between 2800 m and 4000 m; 4.3 between 1000 m and 2800 m and 5.0 between 400 m and 1000 m. Vertical dashed lines separate zones of different rheology.

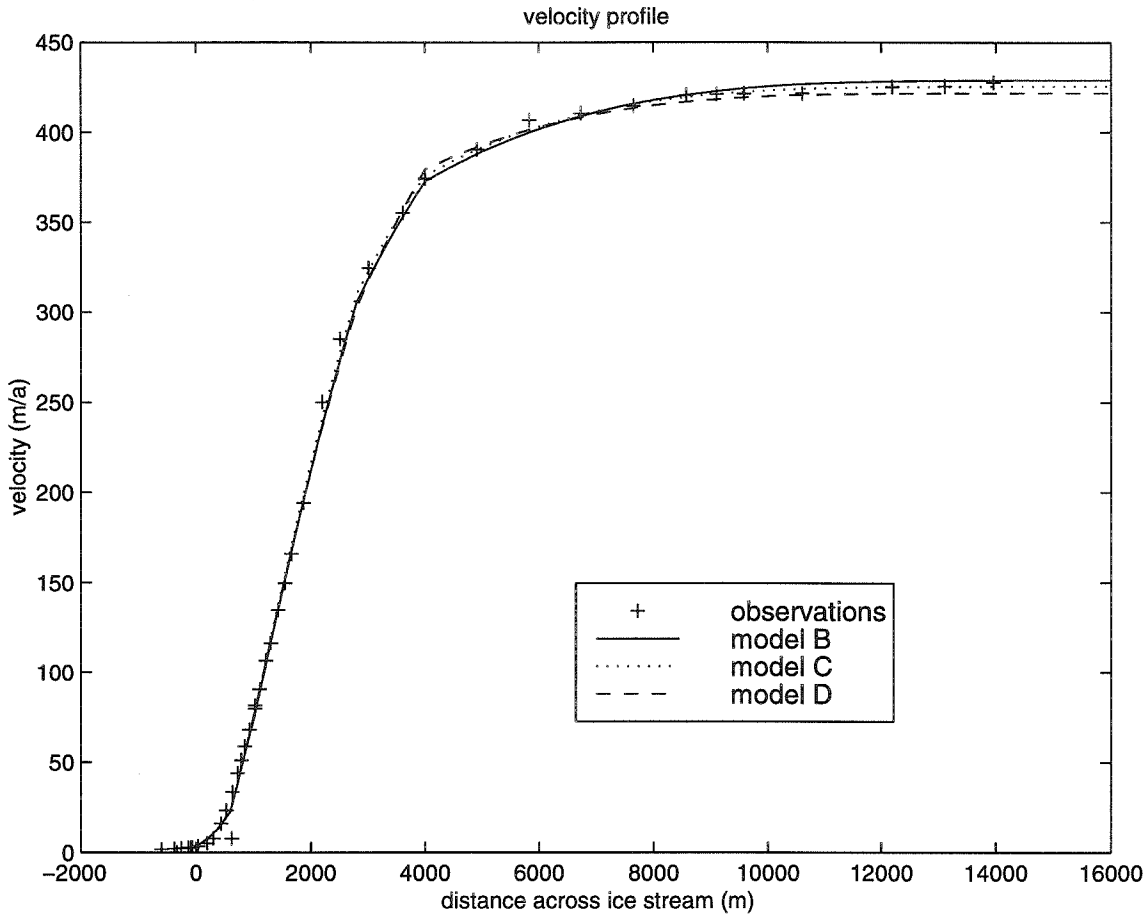

Figure 3.13: Comparison of velocity profiles calculated by models B, C and D, which have different basal conditions and different enhancement factors as described in the text and in Table 3.1.

shear stress is 0 between 1000 m and 10500 m; 0.02×10^5 Pa between 10500 m and 14500 m and is 0.04×10^5 Pa between 14500 m and 16000 m.

Model D has the same basal shear stress distribution as model C but slighly different lateral variation in rheology. The enhancement factor is as given in Table 3.1. The surface velocity profiles for models B, C and D are shown together in Figure 3.13.

The lowest peak enhancement factor in any of the above models is 5. This is more than four times the experimentally indicated value 1.17 (Chapter 2). As the same time it is less than half the enhancement factor of 12.5 that Echelmeyer *et al.* (1994) found necessary to match the observed surface velocity by modelling. Possible reasons

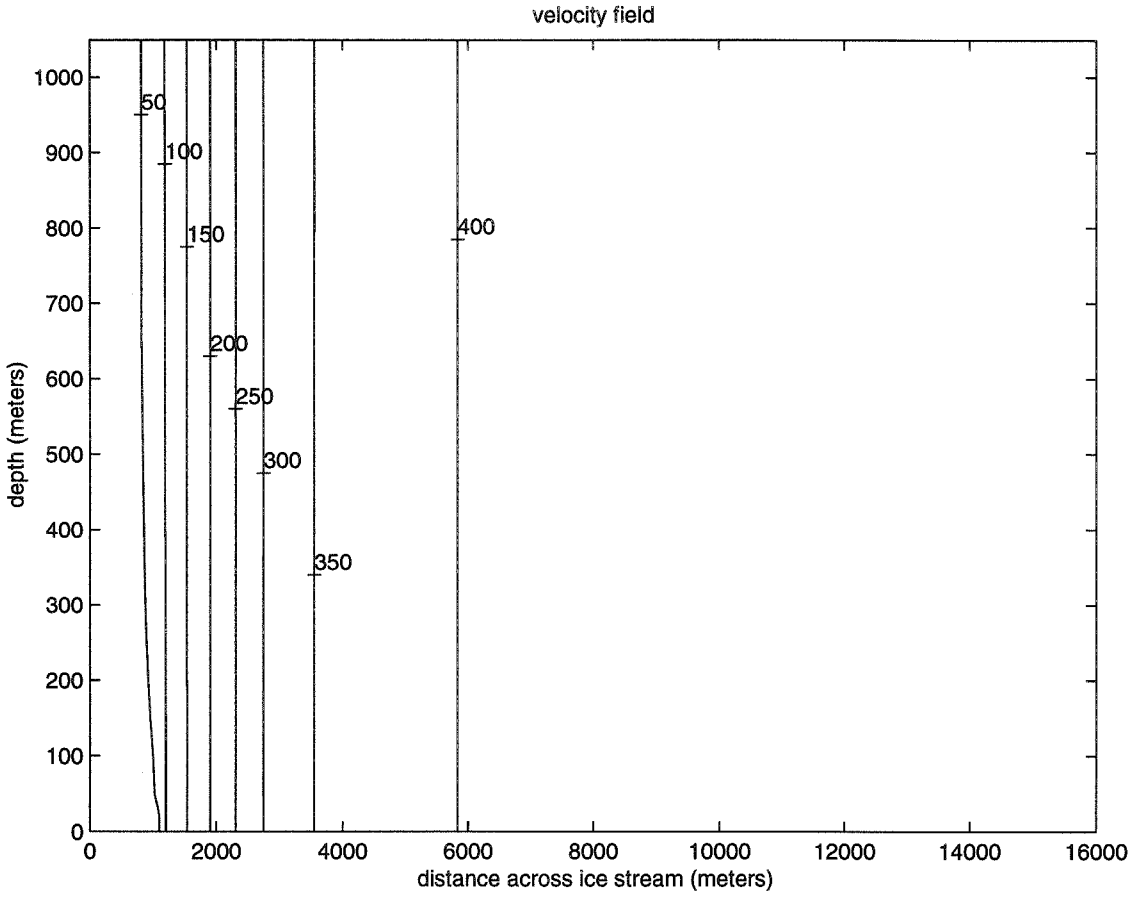

Figure 3.14: Velocity field calculated for model B. Contours lines are labelled in meters/year.

for these discrepancies are discussed in Section 3.6. They used four rheological zones whereas all the models in this study use five zones. The main reason for the fifth zone is that the extra detail provided by the additional observations that were not available to Echelmeyer *et al.* (1994) suggest a change in rheology in the outermost kilometer of the MSZ.

The full velocity field for model B is shown in Figure 3.14. Except for the lower part of the 50 m a^{-1} contour line, the contour lines are almost vertical, indicating that the lateral shear stress is dominant over the basal shear stress as discussed further in Section 3.5.9.

3.5.7 Echelmeyer model

An additional test of the program was made by trying to reproduce modelling results given by Echelmeyer *et al.* (1994, Fig. 4). The purpose of this was to find out if the two quite different finite-element modelling programs would produce the same model results when applied to the same flow problem with the same boundary conditions. The test involves modelling the flow in a rectangular channel 32 km wide (mirror symmetric about the center) and 1100 m deep. This 1100 m thickness includs a 50 m thick layer at the base that is assumed to be a layer of deformable till. The till is assumed to follow the same type of power-law as ice, with $n = 3$. No-slip conditions are imposed between the ice and the till, and at the base of the till. To represent the very different rheology (low strength) of the till, a very large enhancement factor is used in the basal layer. This enhancement factor, which is taken to be constant across the bed, is adjusted so that the calculated velocity matches the measured velocity in the center of the ice stream. The value of E used in the basal layer in this test was about 120,000, which agrees with the value used by Echelmeyer (pers. comm.).

The enhancement factors used in the test model are $E = 3$ over the outer 1 km of the ice stream, $E = 12.5$ between 1,000 m and 3,500 m, $E = 5$ between 3,500 m and 6,000 m and $E = 1$ (i.e., no enhancement) over the rest of the ice stream. This model is designated model E in Table 3.1

The temperature distribution in the ice stream is represented by a four-layer model, with different layers at the following temperatures: 700 – 1100 m at $-24°C$; 300 – 700 m at $-20°C$; 50 – 300 m at $-9°C$ and the basal layer at the melting point. These are the same as the temperature layers used in the models presented here (Section 3.5.2), except that the uppermost layer is 50 m thicker. The outer margin of the ice stream is at a fixed velocity to approximate the no-slip interface with the slow moving ice outside the ice stream.

The results of this test model are shown in Figure 3.15, the dashed curve as calculated by Echelmeyer *et al.* (1994, Fig. 4) and the solid curve as calculated here. There is good agreement. The curves are approximately the same shape, but the

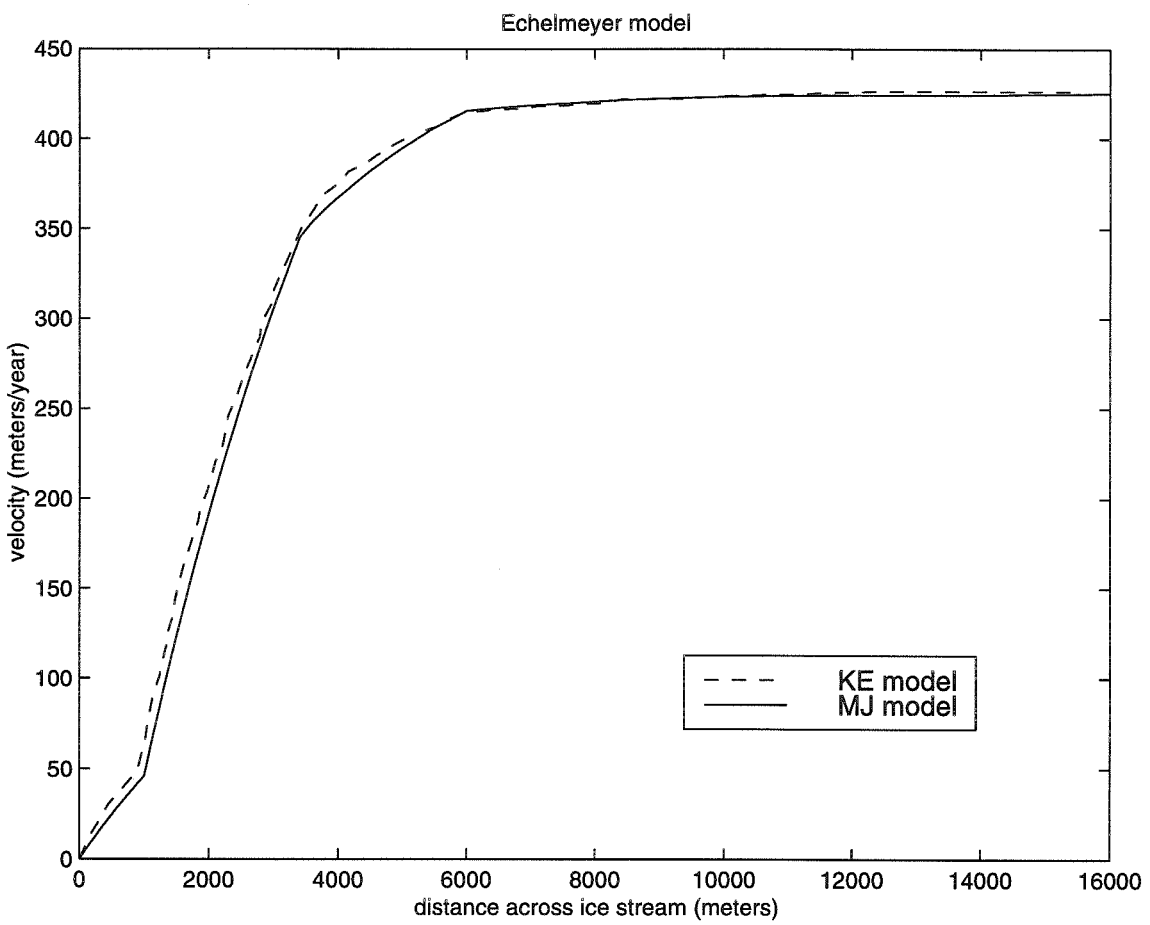

Figure 3.15: Comparison of Echelmeyer *et al.* (1994) model calculated by their finite element program and the same model calculated by the finite element program used here. The two results are labelled KE model and MJ model respectively. For model parameters see text.

outer 5 km of the model as calculated by Echelmeyer *et al.* has slightly higher surface velocity values. The velocity gradients $\partial u/\partial y$ in the different rheological zones are the same, except for the zone between 3,500 m and 6,000 m. The values for the Echelmeyer model were read from a copy of the graph of $u_s(y)$ in their Figure 4. This is rather small in the published form of the paper, which is probably the main reason for the slight differences observed between the profiles in Figure 3.15 here. To this level of accuracy the agreement of the two profiles in Figure 3.15 constitutes a verification of the reliability of the two different methods of modelling. This shows that the further adjustments of $E(y, z)$ tried here in the search for satisfactory models with smaller enhancement factors are meaningful.

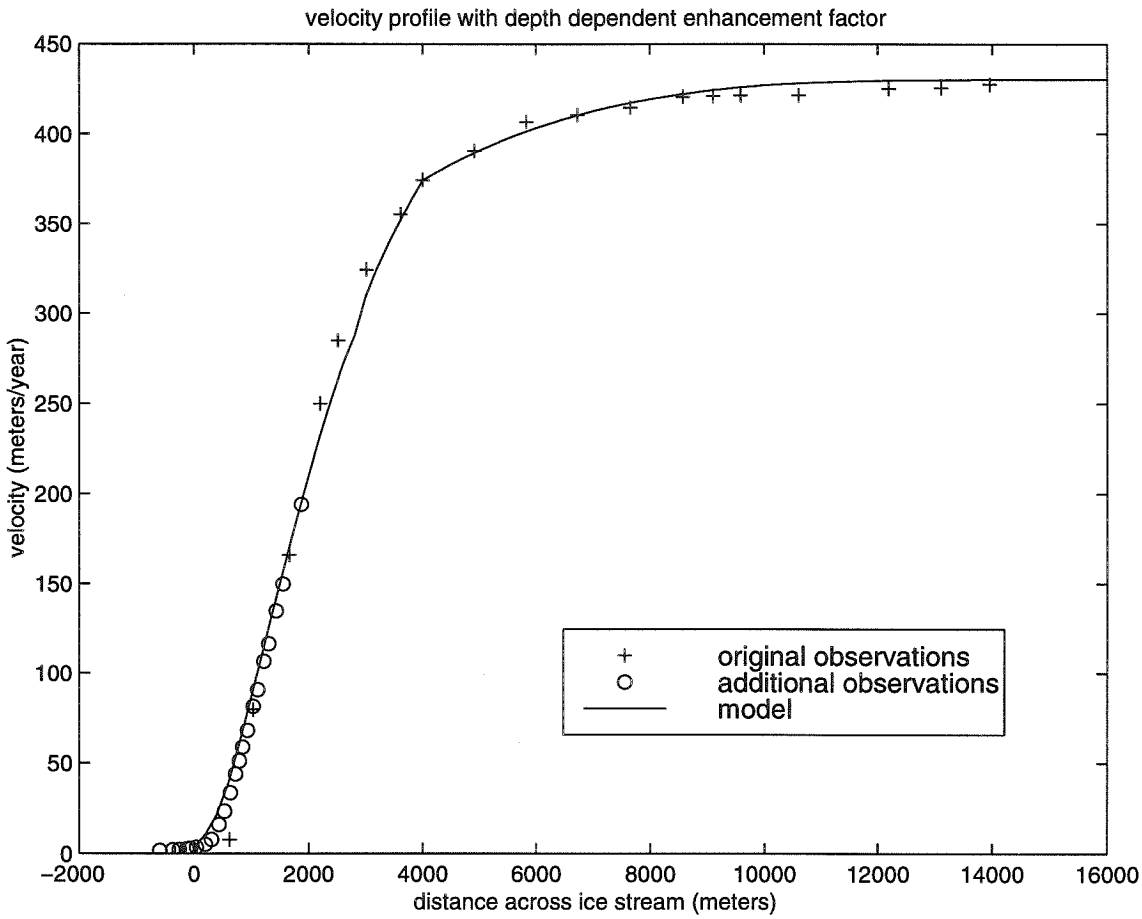

Figure 3.16: Surface velocity profile calculated from model F, in which the enhancement factor varies with depth as well as with distance across the ice stream. The enhancement factors used are shown in Figure 3.17.

To use the same flow relation (3.1) for till as for ice, as is done in the above test, is not realistic. Experimental testing of this till shows that it cannot be reasonably modelled as a quasi-viscous materical, and that it is more accurate to use a plastic rheology (Tulaczyk, submitted). However, Echelmeyer *et al.* (1994) report that the model results did not depend strongly on the assumed constitutive relation for the till.

3.5.8 Depth dependent enhancement factor

It is probable that the enhancement factor is not constant with depth. There should be less enhancement in the ice nearer the surface, where it has not been under enough

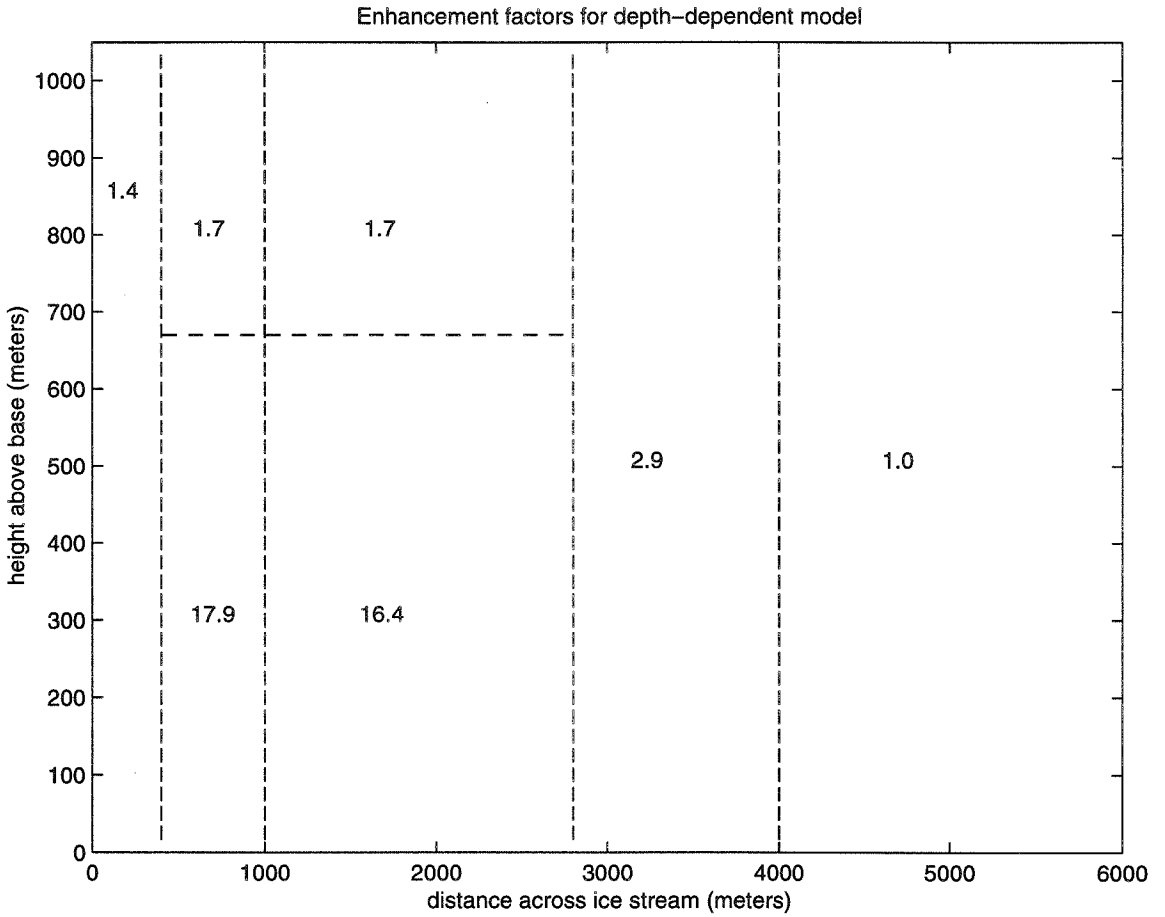

Figure 3.17: Enhancement factors for Model F. There is variation in the enhancement factor with depth between $y = 400$ m and $y = 2800$ m. The enhancement factor is 1.0 between $y = 4000$ m and the middle of the ice stream ($y = 16000$ m).

stress for there to be much alignment of the grains. In the chaotic part of the MSZ the jumbling effect of the crevasses will lessen the alignment, also.

Figure 3.16 shows a velocity profile for model F which was calculated using an enhancement factor that varies with depth. The enhancement factors used are shown in Figure 3.17.

The enhancement factor in the top 380 m is taken to be 1.7 near Camp Chaos, i.e., between $y = 400$ m and $y = 2800$ m. This is of the order of the experimental value. Other enhancement factors were adjusted to give a model that has the same surface velocity profile as the measured profile. The enhancement factors at depth in the Camp Chaos region must show a sudden increase to more than 16 in order

to show the steep increase in velocity seen in the profile. Such a sudden jump is not intended to be realistic but is rather a modelling tool. However, it should be noted that fabrics from deep ice cores sometimes show a sudden change in fabric (e.g. Herron and Langway, Jr. (1982) show a sudden and pronounced change in fabric at a depth of about 1140 m). This implies that the rheology of the ice can change fairly suddenly and hence that the enhancement factor could change suddenly. If the increase in enhancement is more gradual, that means the enhancement factor at depth would need to be even greater than 17 and, according to Shoji and Langway, Jr. (1988), 17 is approximately the highest enhancement factor possible. Hence, a depth dependent enhancement factor can correctly reproduce the measured velocity profile using the enhancement factor found in the experimental work in the upper portion of the ice stream, and would entail a sudden jump in rheology as possibly observed on (need refs.).

3.5.9 Derived stresses and strain rates

The lateral shear strain rate, $\dot{e}_{xy}$, which is here equal to half the transverse derivative of the longitudinal velocity, is shown in Figure 3.18, calculated at depth 130 m from the velocity field of Model B. The maximum value of $\dot{e}_{xy}$, at $y = 1250$ m, is 0.072, which corresponds well with the strain rate value used in the experimental work in Chapter 2. The value shown in Figure 3.18 is at a depth of 130 m, but the graph $\dot{e}_{xy}(y)$ is very similar for all depths in the top 500 m or more of the ice stream. In the lower half of the ice stream, the maximum strain rate is higher and is shifted slightly more to the outside of the MSZ.

According to Echelmeyer *et al.* (1994), the width of the $\dot{e}_{xy}(y)$ peak is related to the width of the crevassed region in the MSZ, with heavy crevassing occurring for shear-strain rates greater than 0.005 a^{-1}. In Figure 3.18 the width of this peak (and hence of the zone of heavy crevassing) is just less than 4 km.

The marginal shear stress τ_{xy} and base parallel shear stress τ_{xz} in the ice stream

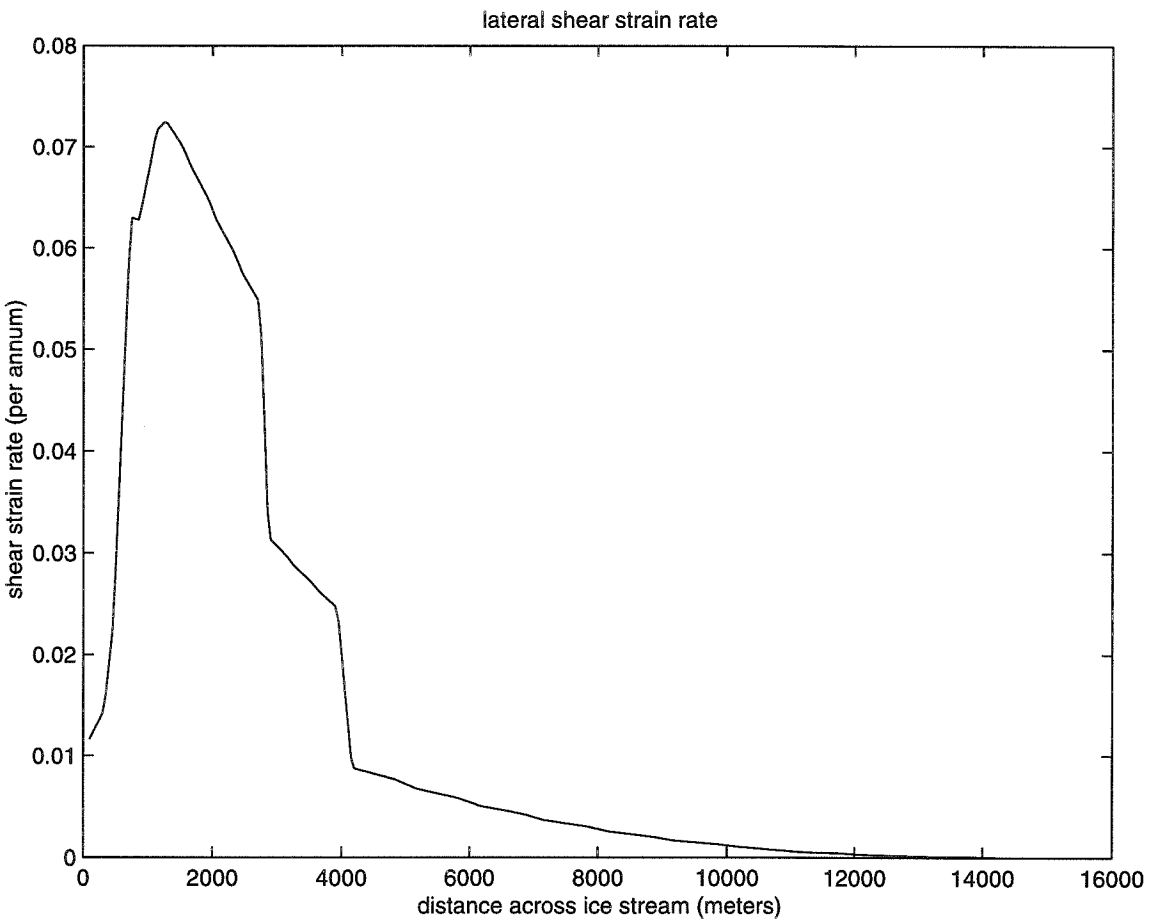

Figure 3.18: Margin-parallel shear strain rate $\dot{e}_{xy}$ at depth 130 m (z = 920 m) in model B.

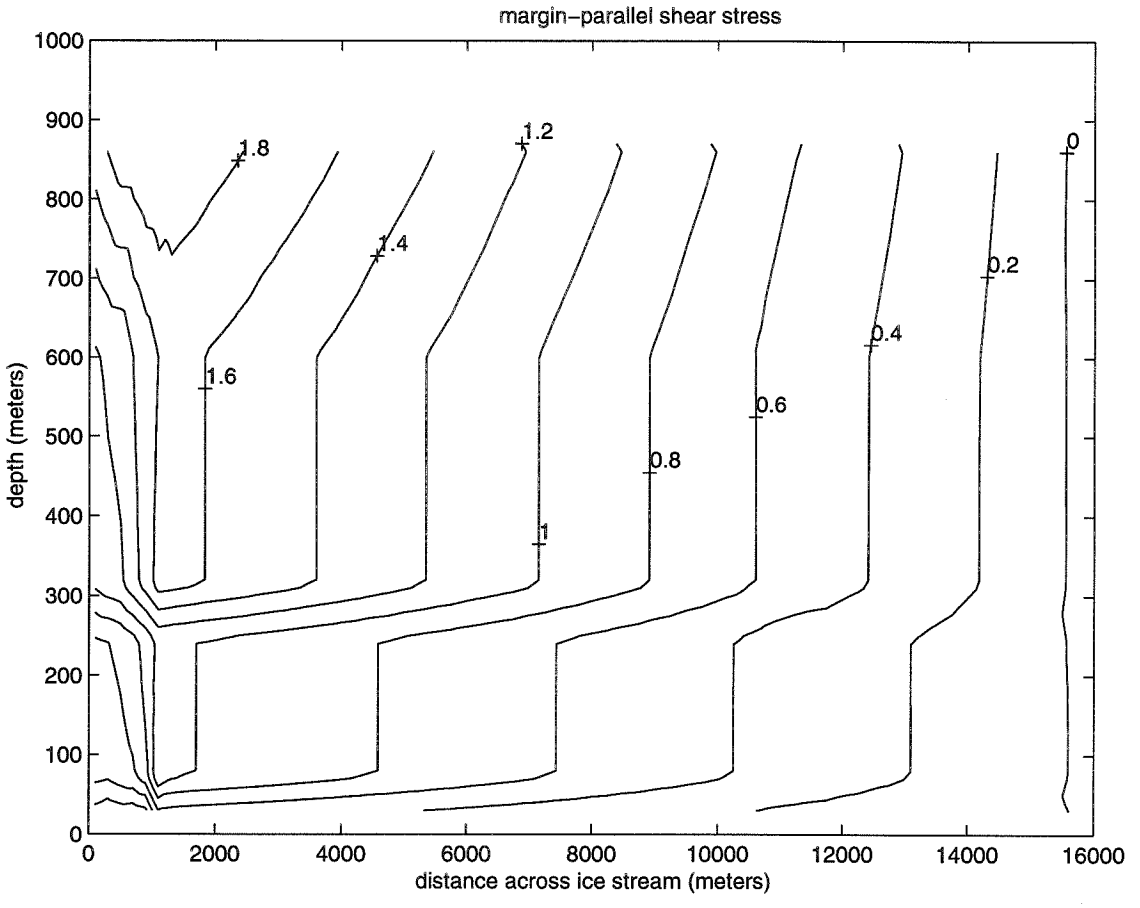

Figure 3.19: Lateral shear stress $\tau_{xy}(y, z)$ for model B. Contours are marked in 10^5 Pa. The lateral shear stress is calculated by taking a partial derivative of the velocity and is smoothed, so contours are calculated only up to 860 m above the base of the ice, not all the way up to the surface.

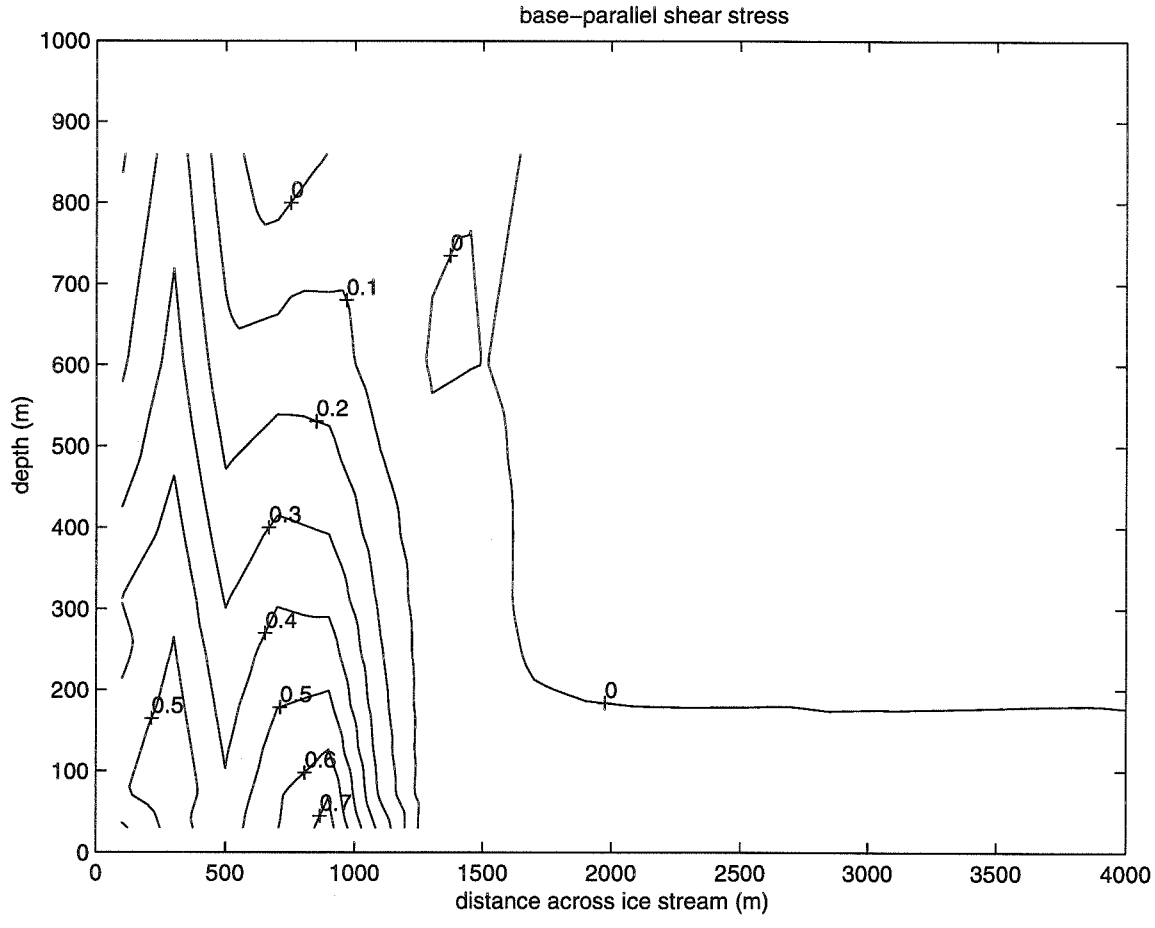

Figure 3.20: Base-parallel shear stress τ_{xz} calculated for model B. Contours are labelled in 10^5 Pa. Only that part of the ice stream from $y = 0$ to $y = 4000$ m is shown, because the basal shear stress is close to zero outside of the shear margin.

can be derived from the calculated flow field at depth. These quantities are given by:

$$\tau_{xy} = 2\eta\dot{e}_{xy} \tag{3.39}$$

$$\tau_{xz} = 2\eta\dot{e}_{xz} \tag{3.40}$$

where η is the effective viscosity given by (3.17), and τ_{xy} and τ_{xz} are the same quantities given by (3.24) and (3.25). The margin-parallel or "lateral" shear stress $\tau_{xy}(y, z)$ and base-parallel shear stress $\tau_{xz}(y, z)$ are shown in Figures 3.19 and 3.20 respectively.

The marginal shear stress ranges from zero in the center to 1.8×10^5 Pa in the middle of the MSZ. This quantity is not calculated for the top 190 m of ice, but inspection of the graph indicates that the marginal shear stress probably reaches a maximum of 2.2×10^5 Pa in the middle of the MSZ (i.e., in the region of Camp Chaos) at the surface, as calculated in Chapter 2. The stress is lower at depth in the ice due to the higher temperatures there. The effects of the temperature stratification used in the models (Section 3.5.2) is clearly shown in Figure 3.19. There are pronounced "steps" in the graph at each thermal boundary, especially at 300 m above the base where this layer is 9°C colder than the layer below and 11°C warmer than the layer above.

The base-parallel shear stress reaches a maximum of 0.7×10^5 Pa (Figure 3.20). There is an apparent trough at $y = 500$ m. This is due to a peak in the effective viscosity in the outer part of the ice stream ($y < 400$ m) and a peak in the effective strain rate at $y = 1000$ m, especially near the base. The peak in effective strain rate is mainly due to the change in conditions at the base of the ice stream from the ice being frozen to the bed to it being unfrozen.

The difference between the lateral shear stress and the basal shear stress (or strictly, the base-parallel shear stress) is shown clearly in Figure 3.21. Lateral shear stress dominates over nearly all the ice stream except for a small region at the outside part of the MSZ near the base of the ice. This confirms that the ice stream is generally controlled by its margins rather than the base.

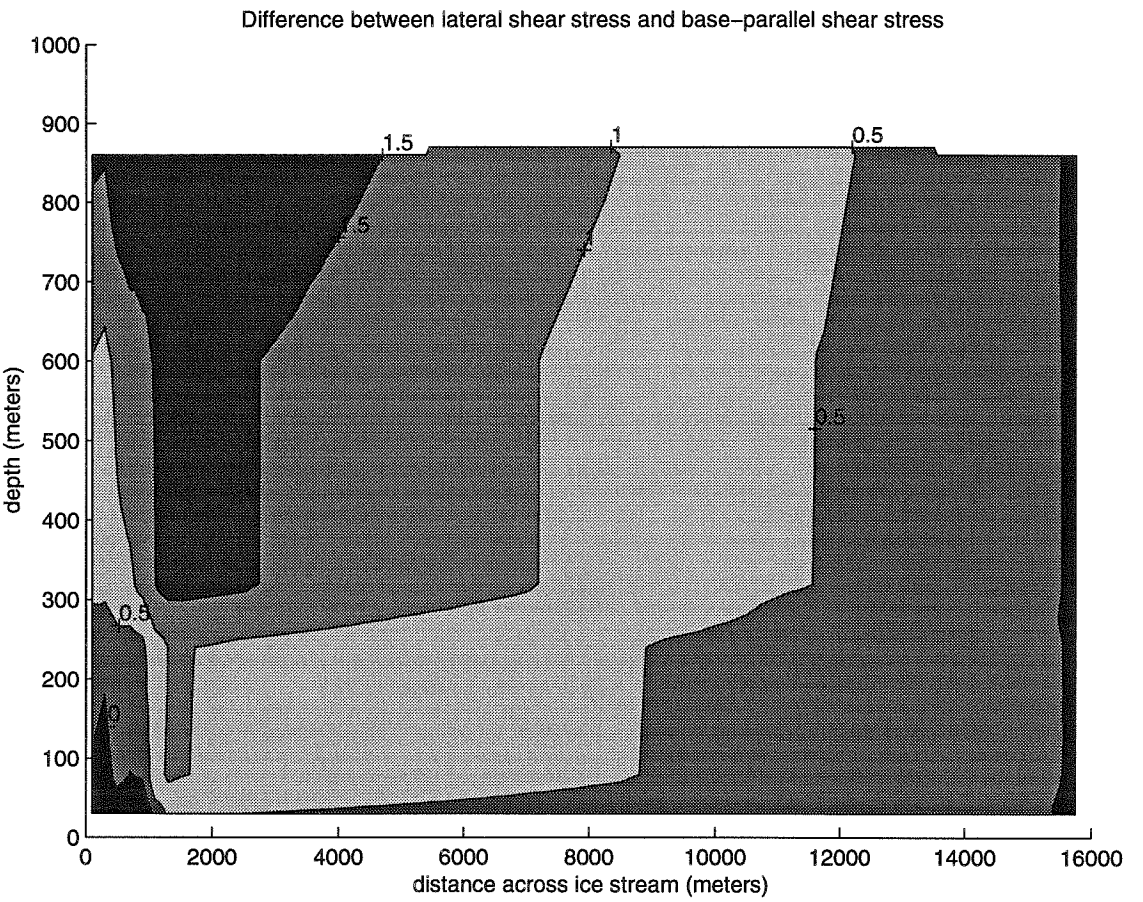

Figure 3.21: Difference between lateral shear stress and basal shear stress, $\tau_{xy} - \tau_{xz}$. Contours are marked in 10^5 Pa. This quantity is calculated by taking a partial derivative of the velocity and is smoothed, so contours are calculated only up to 860 m above the base of the ice, not all the way up to the surface.

3.6 Interpretation of the Modelling Results

Several efforts were made to model the velocity field within the ice stream in such a way as to get the same surface velocity profile as is observed. This study shows that it is not possible to successfully model the measured surface velocity profile using the enhancement factor E that was found experimentally. Possible reasons why the results of the experimental work may not be correct, in spite of their consistency, have already been discussed in Chapter 2 and are discussed further in Chapter 5.

It is possible to get the same surface velocity profile as was measured without having to resort to the high enhancement factors used by Echelmeyer *et al.* (1994). One possibility that was only briefly explored here was variation of enhancent with depth. However, if the value of enhancement in the top 380 m of the ice is $E = 1.7$, then the enhancement in the lower 700 m must be more than 16. Such a large, sudden jump in enhancement is physically unrealistic. The main source of enhancement is assumed to be softening due to the effects of cumulative strain, which would almost certainly increase with depth in the ice stream, but not quite so dramatically.

The source of enhancement may be higher ice temperatures or impurities in the ice. Increase of temperature with depth and its effects on the velocity are incorporated into the models presented here, as well as some cooling of the ice at the outer edge of the ice stream due to the heat pump effect in bridged crevasses, but otherwise the temperature was assumed to be constant laterally across the ice stream.

It is possible to model the velocity profile without having to use a laterally changing enhancement factor at all. Fastook (pers. comm.) was able to model the profile by incorporating the effects of strain heating within the shear margin. Fastook's model assumed rectlinear flow, but although this simplification appears to have little effect on the results presented here, in the Fastook model it meant the ice appeared to spend more time in the shear margin than it actually does. This ice would then be subject to a larger total strain heating, temperatures would be higher and this would cause a sharper increase in strain rate in the center of the shear margin, thus mimicking the observed surface velocity profile. However, the large (5°C or more)

temperature increases that Fastook used in his model are not observed in the ice stream (Figure 3.6). At a strain rate of 0.14 a^{-1} and a residence time of 8-40 years (Echelmeyer *et al.*, 1994), strain heating is only about one or two degrees per year for the ice in the middle of the shear margin compared to the ice outside the ice stream. It appears, then, that the effects of strain heating are small.

3.6.1 Variation in n or E

The adjustment of E rather than n in equation (3.1) is standard convention in glaciology. Equation (3.1) is essentially an empirical law. It is based on laboratory experiments and field data. n depends on the creep mechanism operating in the ice and A in equation (3.1) is a measure of the viscosity of the ice (e.g. Hooke, 1980, p.41).

There is much experimental data on laboratory ice and natural ice that suggests that n has a value of 3. However, very different values of n as well as A have been obtained by different researchers. Measured strain rates at the same stress and temperature differ by a factor of about 10 (Weertman, 1973, Fig. 4) and values of n vary from at least 1.5 to 4.2 (Weertman, 1973, Table 2) and, according to some researchers, the variation could be even greater. It is possible that n is approximately 3 in temperature glaciers but could be less than 3 in ice sheets where the temperature is lower. The experimental work in Chapter 2 supports a value of approximately 3, hence that value was used in the modelling.

3.6.2 Longitudinal variation in rheology

In the modelling results presented here, the goal was to successfully reproduce a single measured surface velocity profile across the ice stream. However, the velocity field changes longitudinally. Other surface velocity profiles measured across the ice stream have a different form (Jackson, 1991, Fig. 8). Velocity measurements were made using repeat aerial photogrammetry. Three profiles are shown that are spaced 11 km apart, the downstream profile being in approximately the same position as the profile in this study. The velocity profile becomes more rounded further upstream,

at least on the "Dragon" side of the ice stream. This may indicate that as the ice passes through the MSZ it changes fairly rapidly from an almost random fabric with little or no resulting enhancement in flow, to a pronounced fabric with the c-axes aligned that has significant flow enhancement. Much of this metamorphism will take place at depth, and it is possible that the 300 m depth from which the cores were extracted is too shallow to have undergone enough metamorphism to show much flow enhancement.

3.6.3 Marginal shear stress and ice-sheet models

The primary motivation for much of the glaciological research undertaken in West Antarctica is to understand the possibility of collapse of the West Antarctic Ice Sheet and the nature and timescale of this collapse. Many models of the Antarctic ice sheet do not consider the ice streams (Huybrechts, 1990; Fastook and Prentice, 1994, e.g.). Such models can be very informative but do not help us understand the stability of the ice streams, and how ice stream stability affects the overall stability of the ice sheet.

Other models (Payne and Dongelmans, 1997, e.g.) include ice streams but generally do not consider the dynamics of the shear margin. Payne and Dongelmans (1997), for example, consider the basal thermal regime to be the switch between ice streams and ice sheet ice. They do not consider the importance of the primary retarding force on the ice streams, the marginal shear stress.

Marginal shear stress in the ice streams provides between half and all of the support of the gravitational force driving ice flow. Any decrease in the marginal shear stress would lead to faster ice flow and hence to net outflow of ice, and negative mass balance. The pattern of mass balance is not uniform over the ice streams in West Antarctica and may be positive or negative depending not only on which ice stream is being considered but also on which part of the ice stream (Bindschadler, 1994, Fig. 5). If we are to understand fully the stability of the West Antarctic ice sheet then the ice streams, and especially their shear margins, need to be incorporated

realistically into any future models.

Chapter 4 Fabrics in the Marginal Shear Zone

4.1 Introduction to Fabrics

When ice first forms from snow, it is isotropic. If the ice deforms, the size and orientation of the grains gradually change. If one stress component is dominant, this will be reflected in the orientation of the *c*-axes of the grains, as they will align themselves in response. The orientation distribution of the *c*-axes is the fabric of the ice. The texture of the ice (the size and shape of the ice crystals) is also of significance.

Measurement of the orientation of the *c*-axes is described in Appendix A. The *c*-axis orientations can be contoured, to give a contoured density or fabric diagram. Normally, the contours are drawn of the percentage of points per 1% of area. The fabric diagrams shown here are contoured following the methods of Kamb (1959). Only that portion of the hemisphere where *c*-axes occur is considered in choosing the area of the counter used in the contouring procedure. Using this method, it is possible to get a fabric diagram that is smoother than those prepared using conventional contouring methods and shows variations which are statistically meaningful.

The fabric diagram is the product of the stress and strain history of the ice. A fabric from a core that was taken from a dome where the ice is spreading out will be different from a fabric from ice from the base of a glacier where the ice is under shear. Figure 4.1 shows the basic *c*-axis fabrics produced by the most common stress regimes in an ice mass.

Unconfined compression commonly occurs at an ice dome, such as Siple Dome, and at the summit of ice sheets, and produces a single maximum fabric. In the laboratory it is not possible to get the strains seen in ice sheets by deforming the ice at the same stresses and temperatures because the amount of strain that has typically

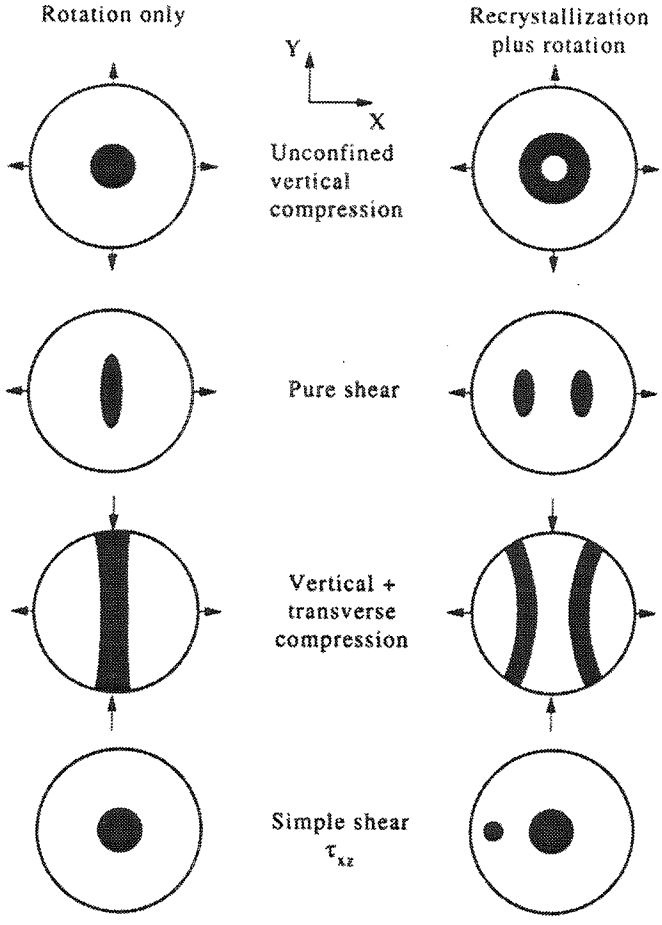

Figure 4.1: *c*-axis fabrics produced by the basic stress systems that may be present in an ice mass. From Paterson (1994).

occurred in ice has accumulated over many years. Hence, to reach the same strain in the laboratory, the ice is deformed at higher stresses and temperatures and this causes dynamic recrystallization to occur. Ice fabrics observed in laboratory ice thus tend to differ from those observed in ice sheets because the fabric is formed not only by rotation of the grains, but by rotation and recrystallisation. In the laboratory, then, unconfined compression results in a small-circle girdle fabric (Figure 4.1).

Pure shear, which is the dominant state of stress in ice shelves, produces a symmetric double maximum fabric, when recrystallization as well as rotation has occurred. Theoretically, an elongated single maximum should be seen in glacier ice where there has been rotation only, but in practice, fabrics from ice shelves have a double maximum fabric (Budd, 1972; Wakahama, 1974, e.g.). Presumably, temperatures in an ice shelf tend to be higher than in an ice sheet, so there is more likelihood of fabrics from an ice shelf showing evidence of recrystallization.

Vertical compression occurs in the basal ice of domes where there is no lateral shear taking place. A girdle fabric may be formed, or, commonly, the *c*-axes are clustered into several maxima (e.g., Thwaites *et al.*, 1986).

Simple shear occurs at the base of many glaciers and ice sheets, and in the margins of glaciers and ice streams. According to Paterson (1994), a single maximum is produced in ice under simple shear when there is rotation only. However, in the laboratory, when recrystallization also is taking place, an asymmetrical double maxima is produced. The principal maximum will be normal to the shear plane and the secondary maximum will be inclined at about 20° to the shear plane (Kamb, 1972). Budd and Jacka (1989) suggest that once the shear strain reaches 2, the secondary maximum, which is not stable to shear, will disappear.

Wilson (1982) performed laboratory experiments in pure and simple shear. He suggests that the primary maximum is due to the simple shear component and the secondary maximum is due to the pure shear component (which will almost always exist in an ice mass, to some extent).

Hudleston and Hooke (1980) examined the development of foliation and fabric at the base of the Barnes Ice Cap. They state that ice needs to have reached a strain of

1 for the initial development of a marked preferred orientation of c-axes in ice with little or no original preferred orientation. However, Budd and Jacka (1989, Fig. 3c) show a clear example of an asymmetrical double maxima developed under simple shear in the laboratory after a strain of 0.95 (although they give it as an example of a single maximum). It is possible that the double maximum fabric persists at higher strains in the colder temperatures of Barnes Ice Cap and the shallower depths of Ice Stream B, but is destroyed by rotation and the usual temperatures in the laboratory.

Because of the difficulties of replicating in the laboratory what is observed in nature, at the same time scales and stresses, relating fabrics to stress/strain history can be an inexact science. The change of fabric with depth in an ice sheet, especially under an ice dome, is generally well understood. Several deep cores have now been drilled and the results, although not always consistent, generally show the same pattern. However, ice that has been under simple shear has not been as well studied. This study is the first instance in which the ice fabric in a major shear zone has been studied by means of core samples from a sequence of boreholes across the zone.

4.2 Fabrics within the Marginal Shear Zone

Fabrics from the MSZ were first studied in order to orient the ice correctly for the ice deformation experiments as described in Chapter 2. The fabrics are also inherently interesting for what they tell us about the stress and strain history of the shear margin (Section 4.1).

A study of the surface velocity by Echelmeyer *et al.* (1994) shows that the dominant strain in the shear margin is simple shear in a left lateral sense. Previous experimental results (Kamb, 1972) suggest that ice that has recrystallized under simple shear would have an asymmetrical double maximum fabric This is seen as two distinct maxima with one maximum, considered the primary maximum, containing more c-axis orientations and also showing more scatter in these orientations so that the primary maximum takes up more area on the fabric diagram than the secondary maximum. (Ice that has been under pure shear (biaxial compression) shows two

maxima also (e.g., Budd and Matsuda, 1974), but in this case the maxima are approximately equal.) The primary maximum is at the pole of the shear plane and a smaller, secondary maximum is about 20° away from the shear direction. Other experimental work (Bouchez and Duval, 1982), indicates that when the accumulated strain exceeds 200% the second maximum disappears. Those crystals (in the main maximum) with their basal planes parallel to the shear direction are able to shear without crystal lattice rotation occurring, but the other crystals (those in the secondary maximum) are thought to rotate with the deformation until they are all aligned with the principal maximum. The paucity of observations of asymmetrical double maximum fabrics may indicate that this is sometimes correct. However, another possibility may be that those crystals that are oriented in the secondary maximum are discounted as "outliers" or even as errors. To do so could lead to an unrepresentative depiction of the fabric, particularly because the crystals in the secondary maximum may be the bigger grains.

4.2.1 Camp Chaos

Camp Chaos is in the most intensely crevassed part of the MSZ and is one of the sites from which a core was taken (see Figure 3.7 for the location of all coring sites). At Camp Chaos (2.2) the longitudinal flow velocity is 150 m a^{-1} (Echelmeyer and Harrison, 1999) and the transverse derivative of the longitudinal velocity, $\partial u/\partial y$, which is the lateral shear rate, is about 0.14 a^{-1} (Harrison *et al.*, 1998), almost the maximum value for this quantity in the shear margin.

Two ice cores were retrieved from the Camp Chaos site at a depth of 300 m and 302 m. Total ice thickness at this site is approximately 940 m (Echelmeyer and Harrison, 1999). The lengths of the cores were 2.07 m and 2.00 m. Maximum core diameter is 9.5 cm. The cores are not azimuthally oriented when retrieved and the orientation is determined from *c*-axis fabric diagrams (Chapter 2, page 12).

The texture of the ice from this site is non-tessellate and interlocking. The average areal grain size is 15 mm^2. It was measured by counting all the grains within a certain

area of a thin section cut vertically from the core (i.e., parallel to the core axis). Grains up to 70 mm^2 in area are present. Photographs of three sections are shown in Figure 4.2.

Figures 4.3, 4.4 and 4.5 show the point diagrams and fabrics (Chaos-2, Chaos-1 and Chaos-3) that were measured from ice slabs that were cut vertically. These three fabrics are consistent - that is, they are all in the same orientation and so the fabrics are in the same orientation and are similar. Figure 4.6 shows a point diagram. Figures 4.4 and 4.5 clearly show two maxima, both centered approximately in the horizontal plane (which is vertical in these figures). Figure 4.3 shows what looks like three maxima. However, this section had only 72 grains measured, compared to 139 and 85 respectively for the other two. With more grains measured, the weak third maximum would probably prove to be part of the greater maximum.

The fabrics show simple shear in the left-lateral sense, as expected from the measured velocity field. If M_1 denotes the principal maximum and M_2 denotes the seconday maximum, the shear plane is perpendicular to M_1 and the sense of shear across it is the same as the sense of rotation of M_2 away from the direction of shear Kamb (1972).

4.2.2 Lost Love

Lost Love is in the MSZ where the crevassing is almost as intense as at Camp Chaos. It is 621 m from Camp Chaos and is between Camp Chaos and the outside edge of the MSZ. At Lost Love the longitudinal ice surface velocity is about 70 m a^{-1} (Echelmeyer and Harrison, 1999) and the lateral shear rate, $\partial u/\partial y$, is 0.12 a^{-1} (Harrison *et al.*, 1998).

One core was obtained from Lost Love at 300 m depth. Figure 4.7 shows a fabric from this core. This digram shows an asymmetrical double maximum, with the asymmetry being stronger than seen in the Camp Chaos fabrics (Figures 4.4, 4.3 and 4.5). This section was cut horizontally from the core, rather than vertically as the previous ones were, so the *c*-axes maxima appear on the equator of the hemisphere,

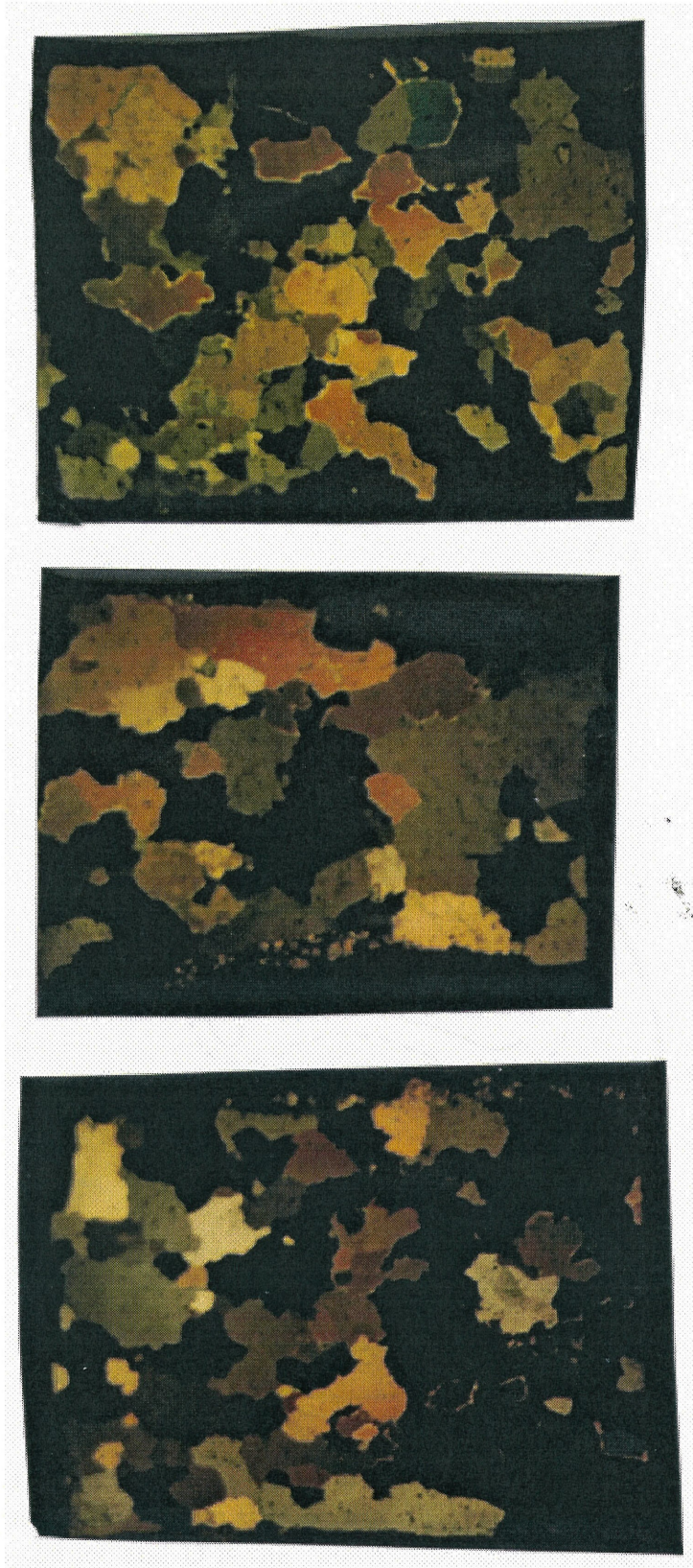

Figure 4.2: Photographs of the sections Chaos-2, Chaos-3 and Chaos-4.

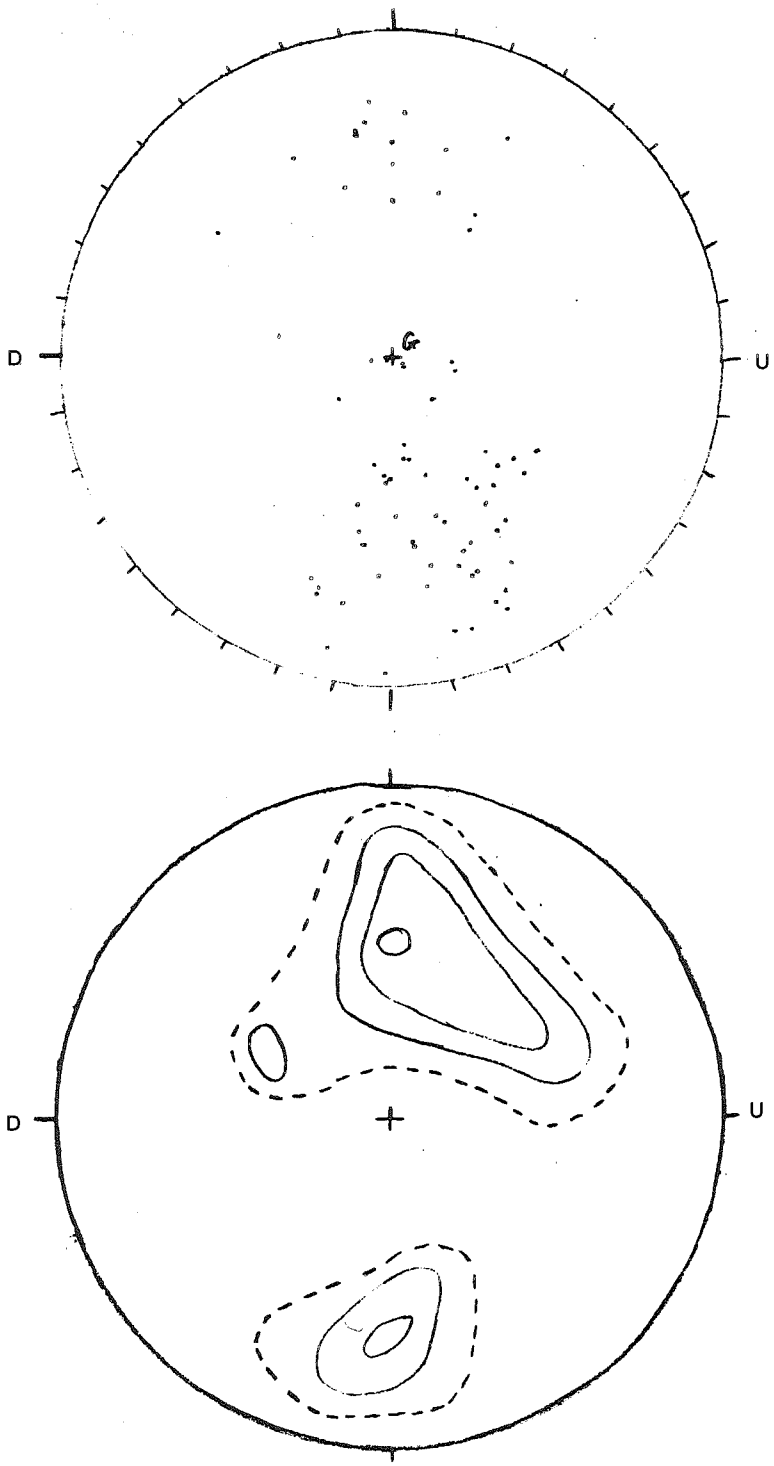

Figure 4.3: *c*-axis fabric "Chaos-1" from a depth of 300 m at Camp Chaos in the middle of the shear margin. This section was cut vertically from the core. U is the "up" direction in the ice and D is the "down" direction; G is an arbitrarily chosen reference in the azimuthal plane. The orientations of the *c*-axes of 72 grains were measured.

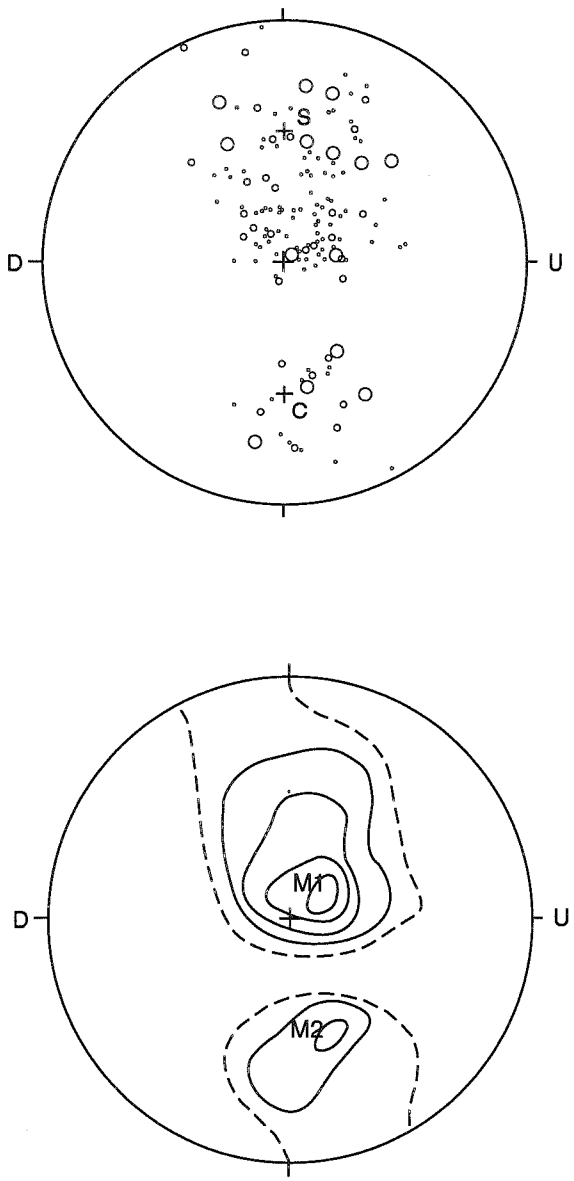

Figure 4.4: *c*-axis fabric "Chaos-2" from 300 m depth at Camp Chaos. This section was cut vertically from the core. The orientations of 139 c-axes were measured. The points were counted with a counter area of 2.4% of the area of the hemisphere. (2.4% was used rather than the usual 1% to give a better representation of the fabric, following the methods of Kamb (1959)). Solid contours are at 1, 2, 3, 4% per 1% of area, dashed contour at 0.3% per 1%. This diagram is the same as Figure 2.3. M_1 and M_2 mark the principle and secondary maxima; their positions are not exactly defined.

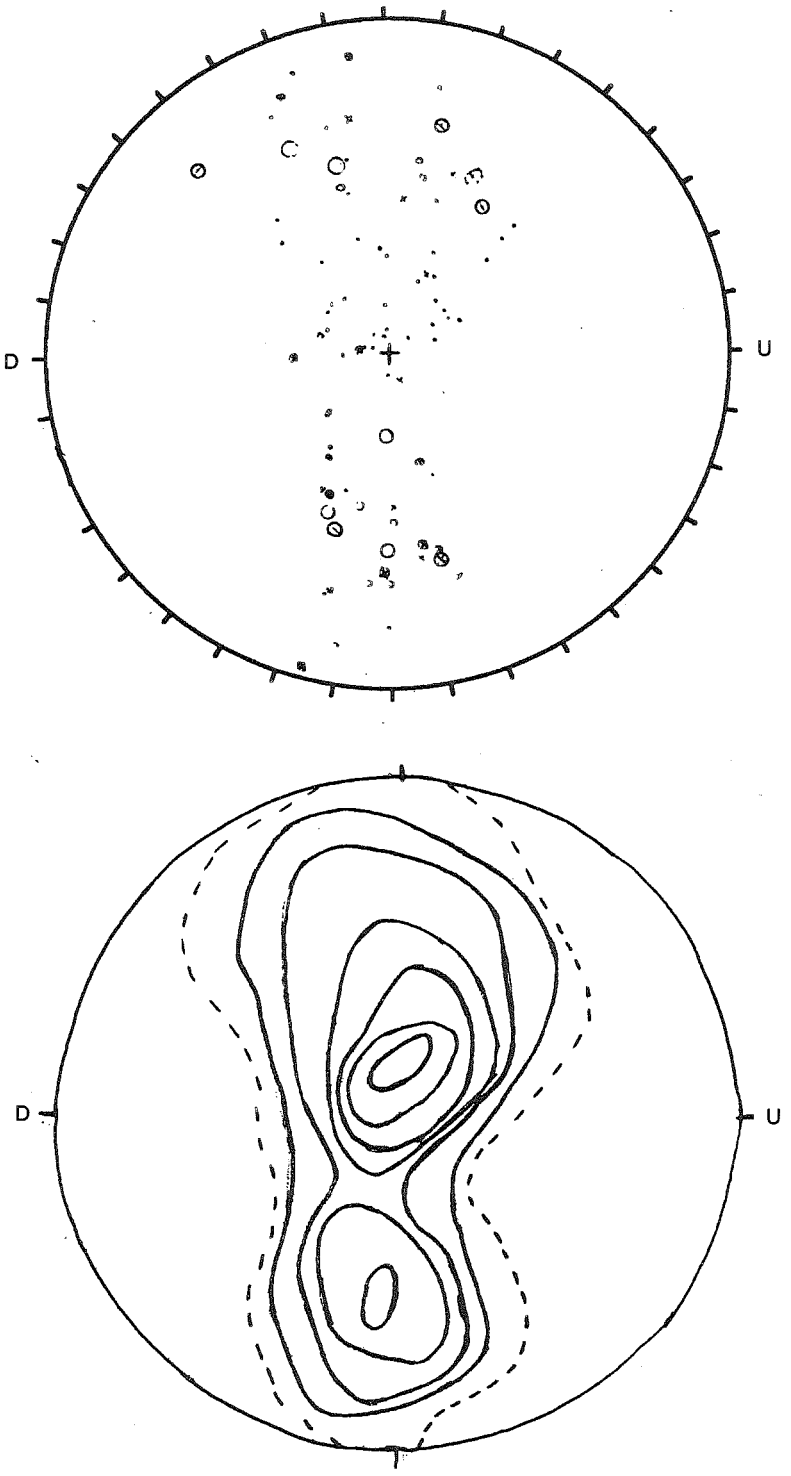

Figure 4.5: *c*-axis fabric Chaos-3 from Camp Chaos. This section was cut vertically from the core. The orientations of 85 *c*-axes were measured. The points were counted with a counter area of 3.5% of the area of the hemisphere. Solid contours are at 1, 2, 3, 4 ... % per 1% of area, dashed contour encloses that area of the figure where *c*-axes are present.

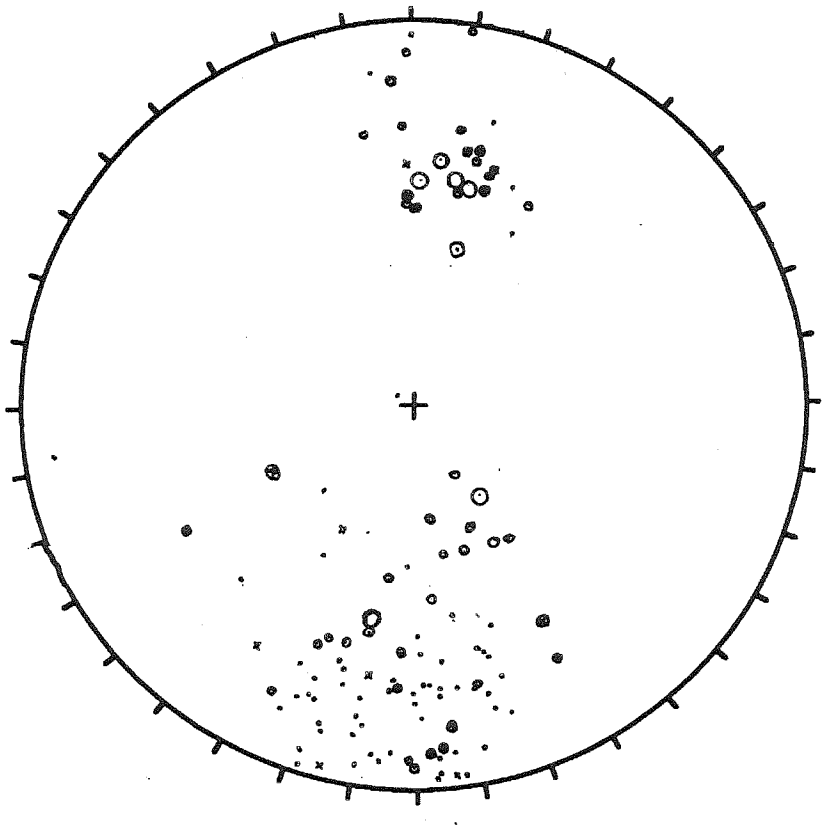

Figure 4.6: *c*-axis orientations for Chaos-4 from Camp Chaos. This section was cut vertically from the core. The orientations of 43 *c*-axes were measured.

rather than on the north-south great circle as the previous maxima did. If the c-axis orientations in Figure 4.7 were rotated 90°, then the maxima would be in a similar position to those of the Camp Chaos fabrics (Figs. 4.4, 4.3 and 4.5).

4.2.3 Dragon Pad

Dragon Pad is 469 m from Lost Love, and is just a few hundred meters inside the edge of the MSZ where the arcuate crevasses end. The longitudinal velocity at Dragon Pad is 16 m a^{-1} and the lateral velocity directed into the ice stream is 1 m a^{-1} (Echelmeyer and Harrison, 1999). Lateral shearing, $\partial u/\partial y$, is 0.07 a^{-1} (Harrison *et al.*, 1998).

Figure 4.8 shows a fabric from a depth of 300 m at the Dragon Pad site. This shows a fairly diffuse single maximum (Although this figure shows three maxima, there is only one that is within one standard deviation, and is thus statistically significant.) and may be a pure shear fabric. It is interesting that there is a single maximum at this site, but a double maxima fabric at the sites further into the ice stream where the ice has undergone much more strain. According to conventional thinking regarding the development of the double maxima fabric under simple shear, and the disappearance of the secondary maximum at higher strains, it should be the other way around. This is an interesting anomaly that is worthy of further investigation.

4.3 Fabrics outside but near the Marginal Shear Zone

4.3.1 Staging Area

The Staging Area was the site used during the drilling operations as the closest point to the MSZ where it was safe to go without using the special precautions such as roping up that were used in the crevassed areas. It is about 790 m from Dragon Pad (Echelmeyer and Harrison, 1999). The longitudinal velocity here is only 3 m a^{-1}, and the lateral velocity into the ice stream is 1 m a^{-1} (Echelmeyer and Harrison, 1999).

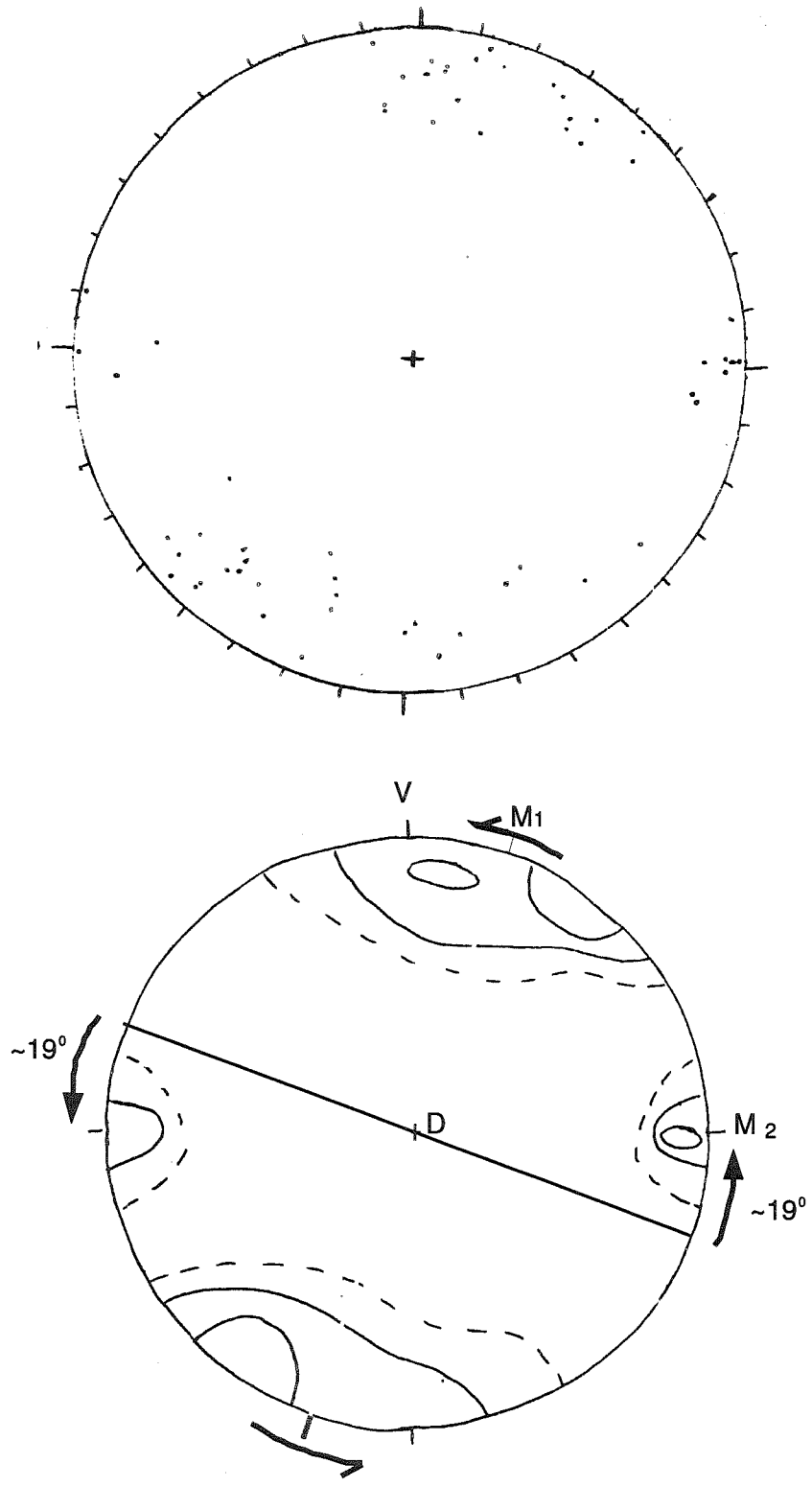

Figure 4.7: *c*-axis fabric from Lost Love in the shear margin. This section was cut horizontally from the core. The orientations of 59 *c*-axes were measured. The half-arrows indicate the sense of shear.

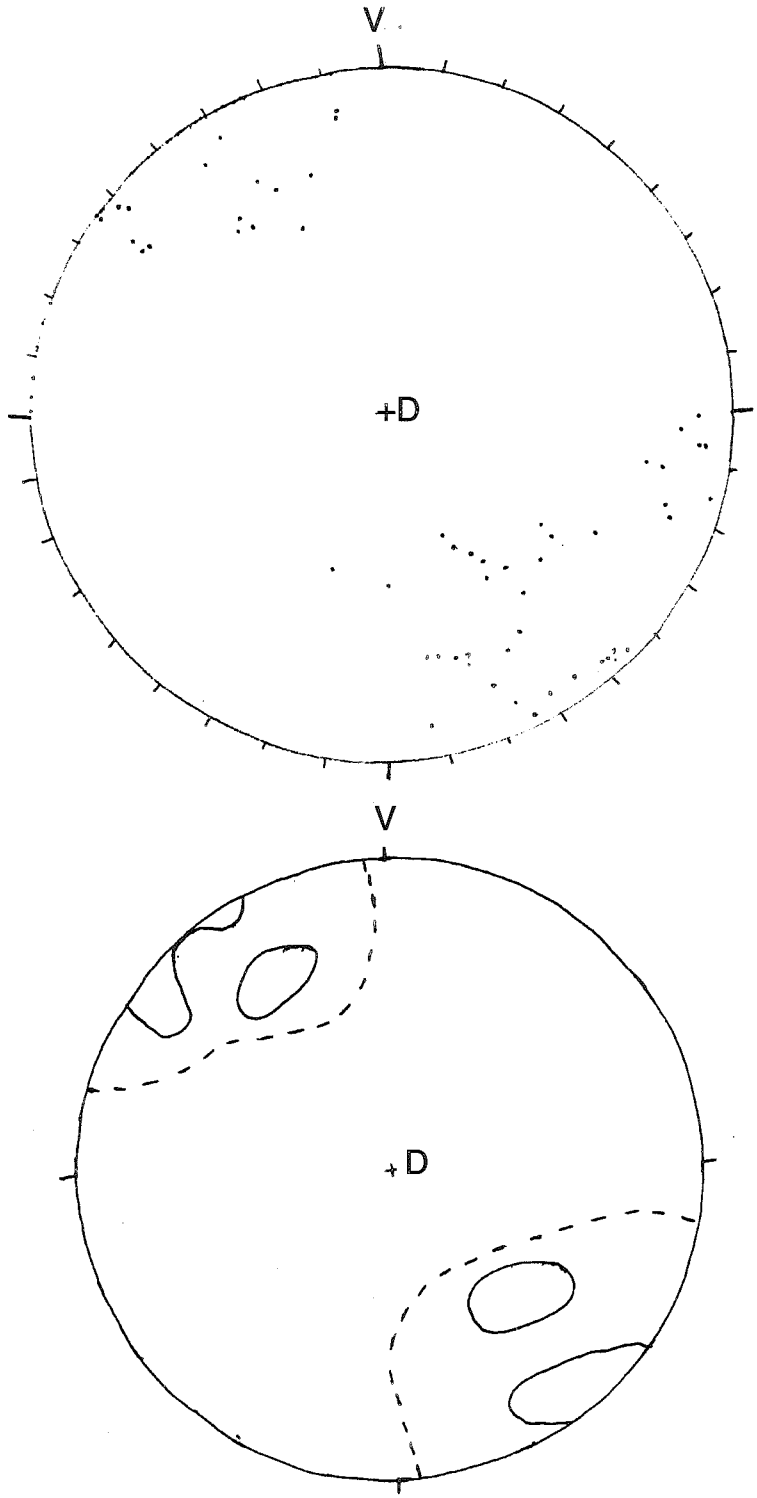

Figure 4.8: *c*-axis fabric from Dragon Pad on the edge of the shear margin. This section was cut horizontally from the core. The orientations of 54 *c*-axes were measured. D indicates the "down" direction in the ice and V is an arbitrarily chosen reference in the azimuthal plane.

The lateral shearing here, $\partial u/\partial y$, is 0.013 a^{-1} (Harrison *et al.*, 1998).

The fabric from a depth of 300 m at the Staging Area drill site is shown in Figure 4.9. It shows a moderatly strong peak with a broad diffuse "apron" extending asymmetrically on one side of the peak. As discussed in subsection 4.2.3, this is too shallow for this fabric to be from vertical compression of the ice. Also, the *c*-axes are horizontal so this is also a fabric due to simple shear.

4.3.2 Unicorn Camp

The Unicorn Camp (also called Out B) was in the middle of an area known as the Unicorn, which is a region of ice between the two branches B1 and B2 of Ice Stream B (Figure 2.1). On the Unicorn the ice is moving at low speeds which are indicative of ice-sheet ice and at the Unicorn Camp, the measured velocity is about 0.5 m a^{-1} (Echelmeyer and Harrison, 1999). There is little or no lateral shearing. This site is 5 km from the Staging Area.

The fabric from the Unicorn Camp is shown in Figure 4.10. It is a weak, diffuse fabric. Only 22 *c*-axes were measured, which may be why the fabric is so weak, although it is probable that because the stresses are not high in this area, even with many orientations measured, it would still be a fairly diffuse fabric.

4.3.3 Fishhook

The Fishhook drill site is also on the Unicorn and has a velocity of 1.6 m a^{-1}. The Fishhook is 7.9 km from the Unicorn Camp (Echelmeyer and Harrison, 1999, Table1).

The term "Fishhook" refers to a hook-shaped surface lineation observed in satellite imagery (Merry and Whillans, 1993) that is slightly brighter than the surrounding ice. Clarke et al. (in preparation) and Whillans and Hamilton (submitted) suggest that the feature is related to recent changes on and around the Unicorn inter-ice stream ridge, and that it may be an abandoned ice stream margin based on the observation of buried crevasses with an ice-penetrating radar system by Clarke et al.

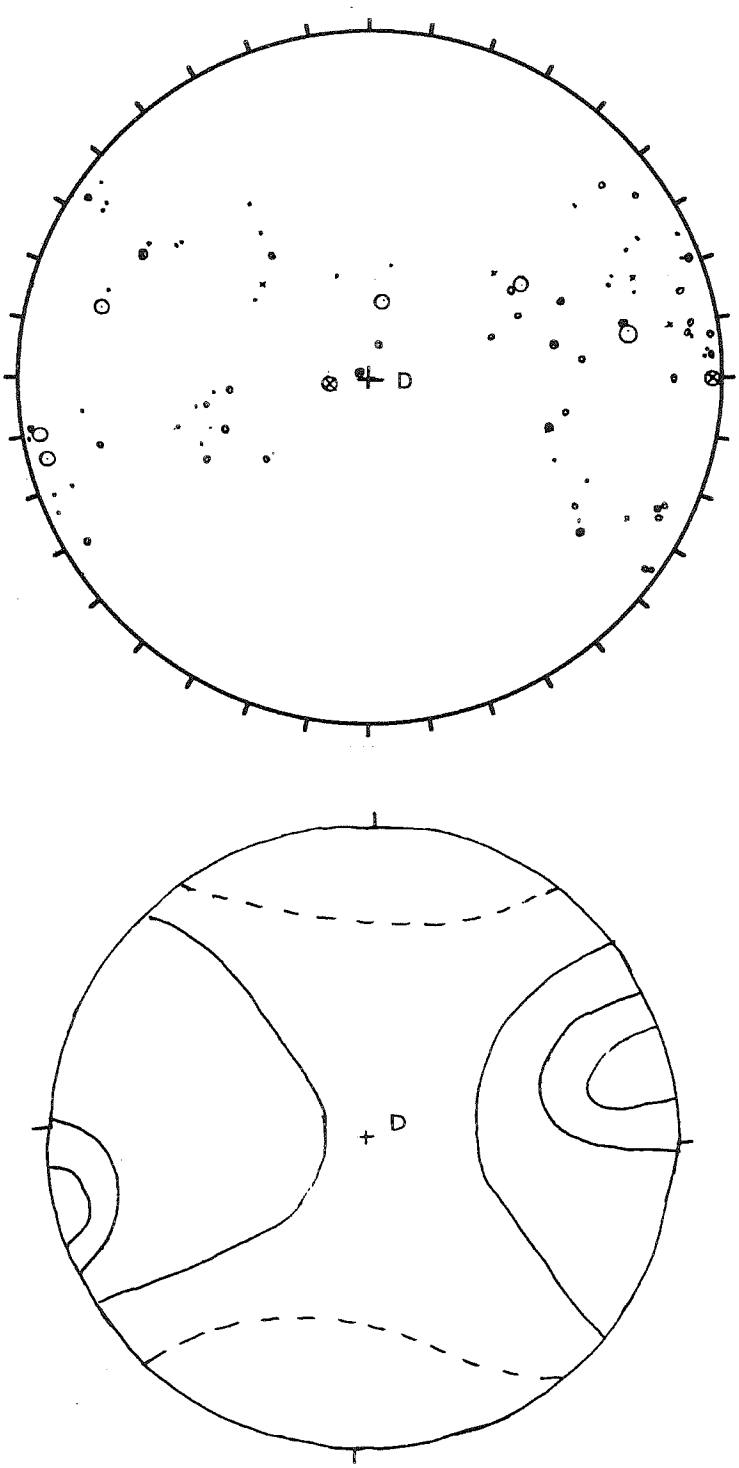

Figure 4.9: *c*-axis fabric from Staging Area just outside the shear margin. This section was cut horizontally from the core. The orientations of 87 *c*-axes were measured.

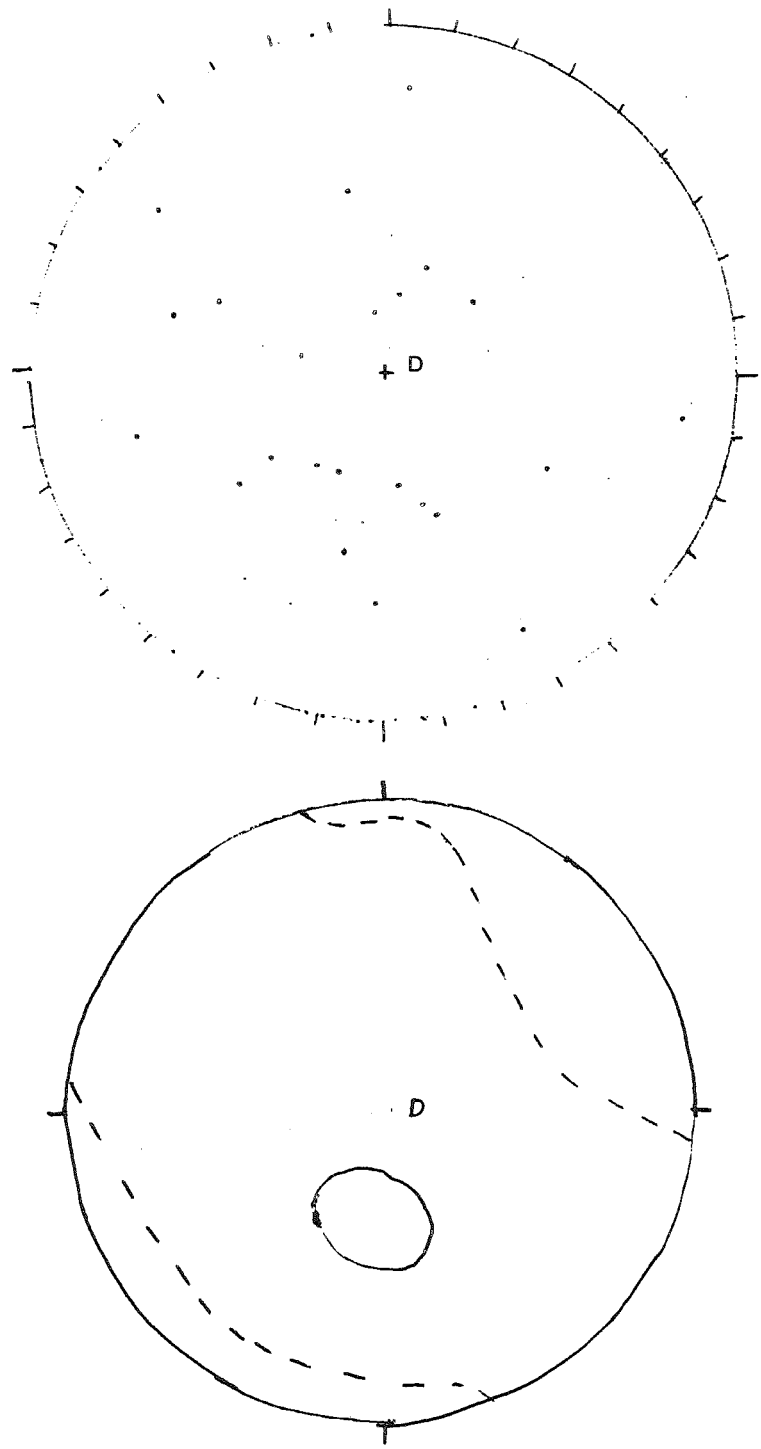

Figure 4.10: Fabric from Unicorn Camp. The orientations of only 22 c-axes were measured. This section was cut horizontally from the core.

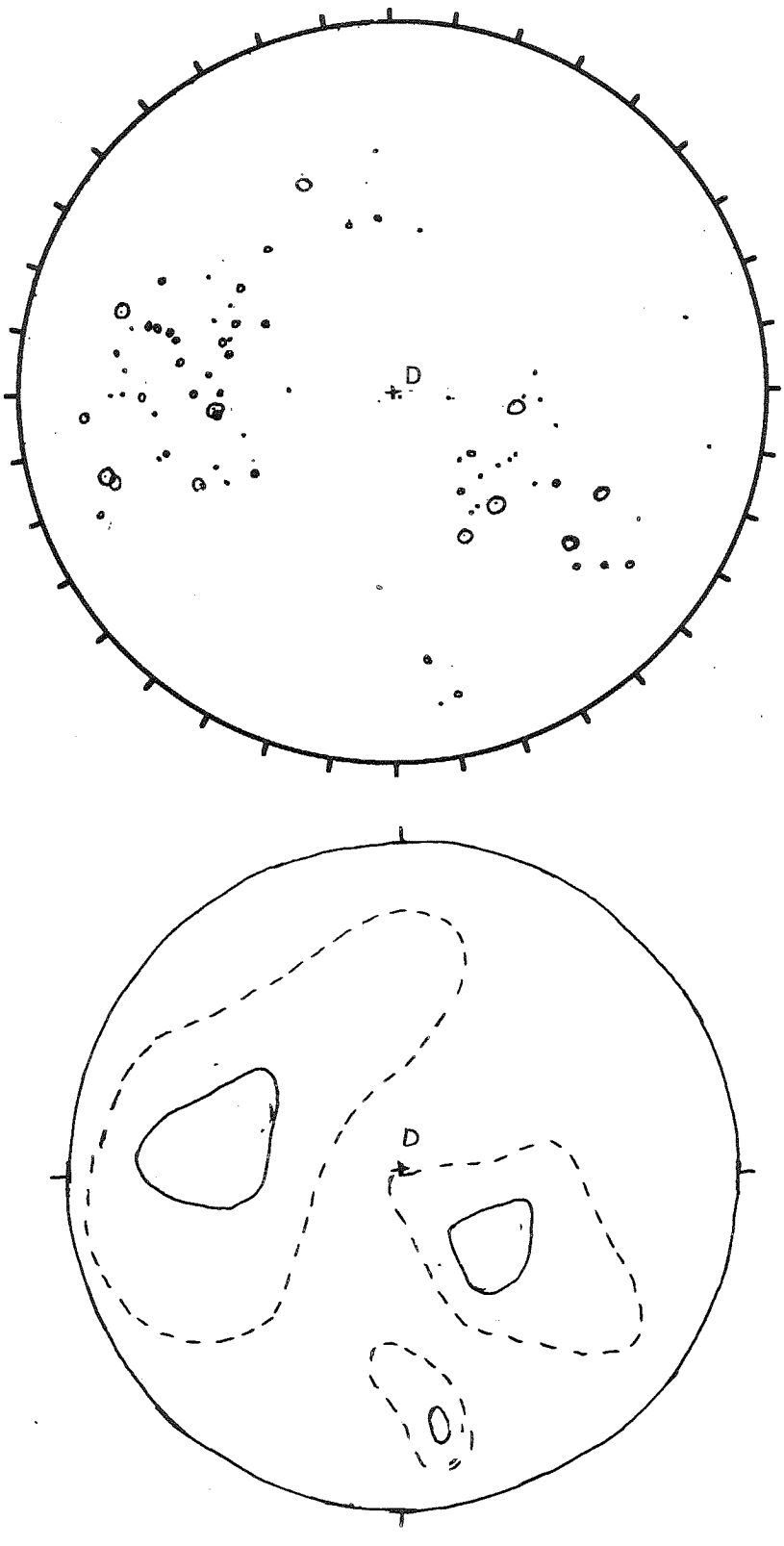

Figure 4.11: Fabric from Fishhook. This section was cut horizontally from the core. The orientations of 78 *c*-axes were measured.

The fabric for the Fishhook site is shown in Figure 4.11. This is a fairly complex fabric. There appear to be several maxima — three or four — but the maxima are of unequal size. This could even be a double maximum, with the two maxima being fairly broad. A multiple maxima fabric suggests that the ice was under vertical unconfined compression. According to the above interpretation of the Fishhook feature, the ice from the Fishhook site was never in an ice stream. In this case, the only stress that would have acted on the ice is vertical compressive stress. However, the observation by Clarke et al. (in preparation) of isolated diffractors that are probably buried crevasses offset about 2.5 km from the surface lineation would indicate that the surface lineation does not correspond with the buried shear margin. It is possible that the Caltech drill site was above or fairly close to this buried shear margin. This means the ice was probably in a fairly complex stress environment, and the multi-maxima fabric could indicate a change in stress at some point rather than being a representative pattern of a particular state of stress.

4.4 Comparison with other Ice Sheet Fabrics

Gow and Williamson (1976) studied the variations in texture and fabric in the Byrd ice core, from West Antarctica. Similar studies were done on cores from Greenland (Herron and Langway, Jr., 1982; Herron *et al.*, 1985) and East Antarctica (Lipenkov *et al.*, 1989; Fujita *et al.*, 1987). More recently, Thorsteinsson *et al.* (1997) and Gow *et al.* (1997) studied the textures and fabrics in two deep cores from the central Greenland summit site. These studies showed that generally grain size increases with depth (although not always in a simple way) and that there is a change in fabric from a random fabric near the surface to a single-maximum or four-maximum fabric with depth. However, apart from some evidence of folding near the bottom in the Greenland cores, the overall stress regime generally indicates increasing vertically compressive stress with depth, and in some case, some base-parallel shear in cores towards the bottom of the ice sheet.

Hudleston (1977) examined ice fabrics across a shear zone in the margin of Barnes

Ice Cap. He related the fabric to the amount of shear strain the ice had undergone which he calculated from bubble shape and changes in vertical bubble trains. From the margin of a shear zone to the center of a shear zone, the fabric changes from a random fabric with no preferred orientation of *c*-axes to a very strong single maximum fabric in the center of the shear zone where the strain is 5-8. The total width of the shear zone was 11 cm. Some of the intermediate fabrics show a secondary maximum, as expected for simple shear. This work shows the progressive change in fabric with increasing shear strain, at a site where the strain was fairly well known. The work by Hudleston has some similarities to this present work, but in the MSZ of Ice Stream B, the strains and even the present stress are a lot less well understood than in the small shear zone that Hudleston studied.

4.5 Fabric Maps

In order to analyze the fabrics in more detail the *c*-axis orientation of each crystal was related to the location of the crystal in a given section. This is called mapping the fabric or "A.V.A." (Achsenverteilungsanalyze or axial distribution analysis) (Sander, 1970).

Each of the fabrics for Camp Chaos (Figures 4.3, 4.4 and 4.5) shows two maxima — a principal maximum and a secondary maximum. Those grains whose *c*-axis orientation falls in the principal maximum are colored pink on the fabric maps (Figures 4.12 and 4.13), and those grains whose *c*-axis orientation falls into the secondary maximum are colored green.

c-axes orientations were mapped for three of the fabrics from the Chaos core. Figure 4.12, the mapped fabric for Chaos-3, shows two interesting features. The grains in the secondary maximum tend to be larger grains. If those grains are ignored because there are only a few of them and they do not fall in the main maximum, an inaccurate picture of the fabric is obtained. Another feature revealed by fabric mapping is that, at least in this example, the grains in the secondary maximum are in a rudimentary "stripe".

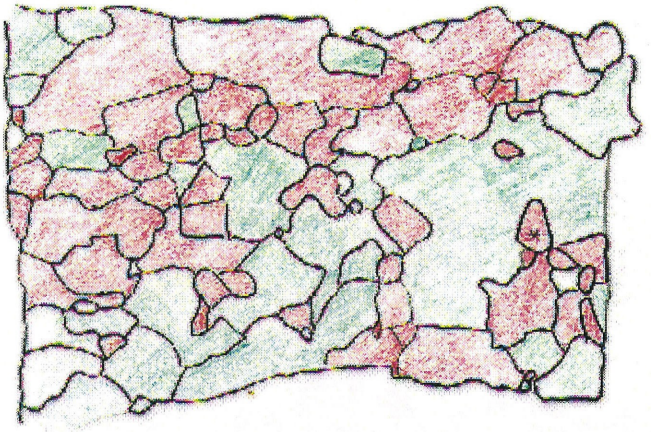

Figure 4.12: Mapped fabric for Chaos-3 section. The pink color identifies grains in the main maximum and green identifies grains in the secondary maximum. This is a vertical section. It is 8 cm wide.

Figure 4.13 shows two more fabric maps for sections Chaos-2 and Chaos-4. These fabrics do not show the pronounced stripe that was seen in Figure 4.12, but do show that the pattern of the grains in the two different orientations is not random. Figure 4.13a and to a lesser extent Figure 4.13b show that the larger grains tend again to be those in the secondary maximum, and that although there are far fewer grains in this orientation than in the principal maximum, almost half of the ice volume must consist of grains in this orientation.

An example of "crystal striping" is seen in the GISP2 core from central Greenland (Gow *et al.*, 1997). Those stripes are seen in vertical thin sections, and occur at much greater depths, below 2000 m. They respresent planar layers of grains with their *c*-axes oriented approximately in the dip direction of the layers. They are related to folding that eventually becomes overturned and can be of significance because they can affect ice viscosity which could produce larger scale deformation features and loss of stratigraphic order.

Figure 4.13: Fabric map for (a) Chaos-2 and (b) Chaos-4 sections. The pink identifies grains in the main maximum and green identifies grains in the secondary maximum. White identifies grains that did not have their *c*-axes measured and yellow identifies grains whose *c*-axis orientations fall outside both of the two maxima. These are both vertical sections. They are both 8.5 cm wide.

4.6 Interpretation

It is thought that ice that recrystallizes under simple shear has an asymmetrical double maxima fabric. As the strain increases, those grains with c-axes in the secondary maximum, which is not stable to shear, will rotate until there is only one maximum. As many of the grains in the secondary maximum tend to be the larger grains in the section, this raises a couple of interesting possibilities. One is that larger grains are more resistant to rotation, so that whereas smaller grains will become aligned with the grains in the principal maximum, the larger ones stay in their original orientation. Another possibility is that as stress is applied, the grains in the orientation of the secondary maximum will combine with other grains in that orientation, rather than rotate. This could also account for these grains being grouped together.

It is possible that the reason asymmtrical double maxima are not seen for ice that has undergone a certain amount of strain ($\gamma \approx 2$, according to Budd and Jacka (1989)) is that the grains were not of the correct size to resist the rotation. The ice in the MSZ of ice stream B has probably had a very different history (deformation and otherwise) than the ice in valley glaciers, ice domes and ice shelves that is usually studied, and may have the optimum grain size to retain its original double maximum fabric. Further deformation experiments on cores in conjunction with fabric studies would resolve questions concerning the relationship, if any, between grain size and double maximum fabrics.

Another possibility is that the fabric is somehow reset due to recrystallisation. The lack of strain shadows observed in the sections support this idea. The strain that the ice would have undergone would then be less than suggested by the measured velocity field.

Chapter 5 Conclusions

In laboratory tests, ice from the shear margin of Ice Stream B requires a shear stress of $(2.4 \pm 0.2) \times 10^5$ Pa to deform at the observed marginal shear strain rate $\dot{\gamma} = 0.14$ a^{-1}. The corresponding flow enhancement factor is 1.2. On this basis the average marginal shear stress, corrected for the vertical variation of ice temperature and (roughly) for crevassing, is $(2.2 \pm 0.3) \times 10^5$ Pa. Using this value in a force-balance model of the ice stream shows that the main resistive drag that opposes the driving stress comes from the shear margins. What surface slope to use in this model is equivocal, but all reasonable values give a predominating role to the margins, which provide 63-100% of the drag that resists the gravitational driving force.

The marginal shear stress 2.2×10^5 Pa is roughly twice as large as the value indicated by the ice-stream model of Echelmeyer *et al.* (1994).

Numerical modelling was performed to determine whether the enhancement factor $E = 1.2$ could correctly reproduce the measured surface velocity profile in the MSZ. Using reasonable values for conditions in the ice stream, it was not possible to obtain a model that reproduces the observed velocity profile using an E value of 1.2. The lowest value that gave an adequate velocity profile was 5. In actuality, the enhancement is probably lower than this near the surface and greater at depth. It was possible to get a model that used a value of the order of the experimentally measured value in the upper few hundred meters, although it requires a sharp contrast in enhancement between the upper and lower depths of the ice stream. There is some discrepancy, then, between the experimental work of Chapter 2 and the numerical modelling described in Chapter 3, which is roughly in agreement with the ice stream model of Echelmeyer *et al.* (1994).

At first the possibility of recrystallization of the ice samples prior to testing, causing a change in enhancement factor for them, was considered as the reason for the discrepancy. It was considered that annealing recrystallization of the ice could

have occurred during or after core sampling. However, ice *c*-axis fabrics from the center of the MSZ, especially the Camp Chaos site, are of the asymmetrical double maxima type. This fabric is an indication that the core has not recrystallized post-kinematically or that, if it did recrystallize, this would not have substantially changed the fabric, as experimental data from Wilson (1982) suggest. In this case the measured flow law, which is mainly affected by flow enhancement due to the fabric, should be applicable to the marginal ice in situ and the resulting marginal shear stress (Section 2.5) should be correct.

It is possible that the shear tests did not correctly measure the enhancement factor in the ice. Jacka (pers. comm) suggests that to successfully perform a shear test by applying a compressive force to the ice is very much dependent on having the correct initial orientation. The only way to do this experiment successfully would be to perform several tests and take that test in which the ice deformed at the rate as being correct. Even this approach may be flawed because as soon as stress is applied to the ice, the grains start to change orientation slowly and the ice gradually becomes no longer in the correct orientation. However, these comments are probably not relevant at the very low strains ($< 1\%$) that were used here.

A study of the ice fabrics across the MSZ shows a progressive change from an asymmetric double maximum fabric in the center of the shear margin to unoriented ice in the middle of the Unicorn, an inter-ice stream area. The double maximum fabric persists even in regions where the strain is thought to be too high for such a fabric and where conventional thinking dictates a single maximum fabric. This may be due to one or both of the following factors. In the MSZ temperatures are colder than generally observed in laboratory experiments on simple shear and even than in many ice masses where simple shear is taking place, and cores have been taken. However, temperature shouldn't have much effect on the secondary maximum as these grains should change by rotation Secondly, the grains in the secondary maximum tend to be larger than those in the primary maximum, and may indicate slightly different conditions than observed elsewhere, such that the ice in the MSZ is not favorable to destruction of the secondary maximum by increasing simple shear.

The fabrics observed are compatible with simple shear, but are not compatible with the large strains measured This is the first time that fabrics have been measured in a major shear zone.

The MSZ of Ice Stream B is a complex environment. The rapid increase over a short distance in the measured surface velocity cannot be explained by lateral variations in temperature or basal shear stress and must be due to enhanced flow within the ice. However, it has not been possible to give a definitive value for this enhancement. The measured *c*-axis orientations indicate that the ice in the shear margins is under simple shear (as the measured velocity field also shows) although the asymmetrical double maximum fabric indicative of simple shear at low strains is retained in the MSZ even at relatively high strains.

Appendix A Measurement of the *c*-axes

Orientations of the *c*-axes are measured using a universal stage. This is a device that enables an ice thin section to be rotated about horizontal and vertical axes, with four axes of rotation. The ice section to be measured is placed between two polaroid sheets. These are oriented at 90°, so that the two polaroids are crossed. If the upper polaroid sheet (the analyzer) is oriented to transmit light vibrating in a north-south direction, for example, the lower polaroid sheet (the polarizer) must be oriented to transmit light in an east-west direction. A grain to be measured is selected, and the section is rotated about the inner vertical axis until the grain is at extinction (no light is transmitted). The grain is tested for extinction by rotating on the north-south axis. If the grain becomes light, rotate the stage 90°. The grain should be at extinction in this position also. Rotate the stage again about the north-south axis to see if the grain becomes light. In the position in which the grain remains dark, this shows that the east-west plane contains the *c*-axis. The stage is now rotated about the east-west axis a few degress until the grain becomes light, and then rotated about the north-south axis until the grain is dark again. The section is again rotated about the east-west axis to the initial (zero) position, then rotated about 45° on the outer vertical axis. If the grain stays in extinction, then the *c*-axis is vertical. If the grain becomes light, then the *c*-axis is in the plane of the section and east-west. By manipulating the section about three different axes, as above, it is possible to measure the orientation of each crystal in the section. The *c*-axis orientations of the crystals are then plotted on the lower hemisphere of a Schmidt equal area projection, giving a Schmidt diagram.

Bibliography

Alley, R. B., Flow-law hypotheses for ice-sheet modelling, *J. Glaciology*, *38*(128), 245–256, 1992.

Alley, R. B., In search of ice-stream sticky spots, *J. Glaciology*, *39*(133), 447–454, 1993.

Alley, R. B., and I. M. Whillans, Changes in the West Antarctic Ice Sheet, *Science*, *254*, 959–963, 1991.

Alley, R. B., D. D. Blankenship, C. R. Bentley, and S. T. Rooney, Deformation of till beneath Ice Stream B, West Antarctica, *Nature*, *322*(6074), 57–59, 1986.

Alley, R. B., D. D. Blankenship, C. R. Bentley, and S. T. Rooney, Till beneath Ice Stream B. 3. till deformation: evidence and implications, *J. Geophys. Res.*, *92*, 8921–8929, 1987.

Bindschadler, R. A., WAIS illustrated summary, http://igloo.gsfc.nasa.gov/wais, 1994.

Blankenship, D. D., C. R. Bentley, S. T. Rooney, and R. B. Alley, Till beneath Ice Stream B. 1. properties derived from seismic travel times., *J. Geophys. Res.*, *92*, 8903–8911, 1987.

Bouchez, J. L., and P. Duval, The fabric of polycrystalline ice deformed in simple shear: experiments in torsion, natural deformation and geometrical interpretation, *Textures and Microstructures*, *5*, 171–190, 1982.

Budd, W. F., The development of crystal orientation fabrics in moving ice, *Zeitschrift für Gletscherkunde und Glazialgeologie, VIII (1-2)*, pp. 65–105, 1972, Series A.

Budd, W. F., and T. H. Jacka, A review of ice rheology for ice sheet modelling, *Cold Regions Science and Technology*, *16*, 107–144, 1989.

Budd, W. F., and M. Matsuda, Short report: On preferred orientation of polycrystalline ice by bi-axial creep test, *Low Temperature Science*, *32*, 261–265, 1974.

Daley, M. A., and S. H. Kirby, Thin sectioning and surface replication of ice at low temperature, *J. Glaciology*, *30*(105), 248–250, 1984.

Duval, P., and O. Castelnau, Dynamic recrystallization of ice in polar ice sheets, *Journal de Physique IV*, *5*, 197–205, 1995, Supplément au 3.

Echelmeyer, K. A., and W. D. Harrison, Ongoing margin migration of Ice Stream B, Antarctica, 1999, submitted.

Echelmeyer, K. A., W. D. Harrison, C. Larsen, and J. E. Mitchell, The role of the margins in the dynamics of an active ice stream, *J. Glaciology*, *40*(136), 527–538, 1994.

Engelhardt, H., and W. B. Kamb, Vertical temperature profile of Ice Stream B, *Antarctic Journal of the U.S.*, *28*(5), 63–66, 1994, Review 1993.

Engelhardt, H., and W. B. Kamb, Basal hydraulic system of a West Antarctic ice stream: constraints from borehole observations, *J. Glaciology*, *43*(144), 207–230, 1997.

Engelhardt, H., and W. B. Kamb, Basal sliding of Ice Stream B, *J. Glaciology*, *44*(146), 1, 1998.

Engelhardt, H., N. Humphrey, W. B. Kamb, and M. Fahnestock, Physical conditions at the base of a fast moving Antarctic ice stream, *Science*, *248*(4951), 57–59, 1990.

Fastook, J. L., and J. E. Chapman, A map-plane finite-element model: three modelling experiments, *J. Glaciology*, *35*(119), 48–52, 1989.

Fastook, J. L., and M. A. Prentice, A finite-element model of Antarctica: sensitivity test for meteorolgical mass-balance relationship, *J. Glaciology*, *40*(134), 167–175, 1994.

Fujita, S., M. Nakawo, and S. Mae, Orientation of the 700 m Mizuho core and its strain history, in *Proceedings of the NIPR Symposium on Polar Meteorology and Glaciology, 1*, pp. 122–131, Natl. Inst. of Polar Res., Tokyo, Japan, 1987.

Gow, A. J., Post-drilling recrystallization of the Byrd Station deep ice core and its relevance to current and future deep-core drilling on polar ice sheets, *Annals of Glaciology*, *20*, 231–236, 1994.

Gow, A. J., and T. Williamson, Rheological implications of the internal structure and crystal fabrics of the West Antarctic ice sheet as revealed by deep core drilling at Byrd Station, *Geol. Soc. Am. Bull.*, *87*(12), 1665–1677, 1976.

Gow, A. J., D. A. Meese, R. B. Alley, J. J. F. k, S. Anandakrishnan, G. A. Woods, and B. C. Elder, Physical and structural properties of the Greenland Ice Sheet Project 2 ice core: A review, *J. Geophys. Res.*, *102*, 26559–26575, 1997.

Harbor, J. M., Application of a general sliding law to simulating flow in a glacier cross section, *J. Glaciology*, *38*(128), 182–190, 1992.

Harrison, W., and K. Echelmeyer, Temperature measurements in the margin of Ice Stream B, 1993-1994, *Antarctic Journal of the U.S.*, *29*(5), 60, 1994, Review 1994.

Harrison, W. D., K. A. Echelmeyer, and C. F. Larsen, Measurement of temperature in a margin of Ice Stream B, Antarctica: implications for margin migration and lateral drag, *J. Glaciology*, *44*(148), 569–578, 1998, in press.

Herron, S. L., and C. C. Langway, Jr., A comparison of ice fabrics and textures at Camp Century, Greenland and Byrd Station, Antarctica, *Annals of Glaciology*, *3*, 118–124, 1982.

Herron, S. L., C. C. Langway, Jr., and K. Brugger, Ultrasonic velocities and crystalline anisotropy in the ice core from Dye 3, Greenland, in *Greenland Ice Core: Geophysics, Geochemistry and the Environment*, edited by C. C. Langway, Jr., H. Oeschger, and W. Dansgaard, vol. 33, pp. 49–56, AGU, Washington, D.C., 1985, Geophys. Monogr. Ser.

Hooke, R. L., *Principles of glacier mechanics*, Prentice-Hall, New Jersey, 1980.

Hooke, R. L., C. F. Raymond, R. L. Hotchkiss, and R. J. Gustafson, Calculations of velocity and temperature in a polar glacier using the finite element method, *J. Glaciology*, *24*(90), 131–146, 1979.

Hudleston, P. J., Progressive deformation and development of fabric across zones of shear in glacial ice, in *Engergetics of geological processes*, edited by S. Saxena and S. Bhattarchaji, pp. 121–150, Springer Verlag, Amsterdam, 1977.

Hudleston, P. J., and R. L. Hooke, Cumulative deformation in the Barnes Ice Cap and implications for the development of foliation, *Tectonophysics*, *66*, 127–146, 1980.

Hughes, T., The West Antarctic ice sheet: instability, disintegration, and initiation of ice ages, *Rev. Geophys. Space Phys.*, *13*(4), 502–526, 1975.

Hughes, T. J. R., *The finite element method*, Prentice-Hall, New Jersey, 1987.

Huybrechts, P., The Antarctic ice sheet during the last glacial-interglacial cycle: a three-dimensional experiment, *Annals of Glaciology*, *14*, 115–119, 1990.

Jacka, T. H., and W. F. Budd, Isotropic and anisotropic flow relations for ice dynamics, *Annals of Glaciology*, *12*, 81–84, 1989.

Jackson, M., Repeat aerial photogrammetry of ice stream B, West Antarctica, Master's thesis, Ohio State University, 1991.

Johnson, A. F., Creep characterization of transversely-isotropic metallic materical, *Journal of the Mechanics and Physics of Solids*, *25*, 117–126, 1977.

Johnson, Jr., M. W., Some variational theorems for non-Newtonian flow, *Physics of Fluids*, *3*(6), 871–878, 1960.

Kamb, W. B., Ice petrofabric observations from Blue Glacier, Washington, in relation to theory and experiment, *J. Geophys. Res.*, *64*, 1891–1909, 1959.

Kamb, W. B., Experimental recrystallization of ice under stress, *American Geophysical Union, Geophysical Monograph Series*, *16*, 211–241, 1972.

Kamb, W. B., Rheological nonlinearity and flow instability in the deforming bed mechanism of ice stream motion, *J. Geophys. Res.*, *96*, 16585–16595, 1991.

Kamb, W. B., and H. Engelhardt, Antarctic Ice Stream B: conditions controlling its motion and interactions with the climate system, *International Association of Hydrological Sciences Publication 208*, pp. 145–154, 1991, (Symposium at St. Petersburg 1990 — Glaciers–Ocean–Atmosphere Interactions).

Lipenkov, V. Y., N. I. Barkov, P. Duval, and P. Pimienta, Crystalline texture of the 2083 m ice core at Vostok Station, Antarctica, *J. Glaciology*, *35*(121), 392–398, 1989.

Lliboutry, L. A., *Very slow flows of solids*, Martinus Nijhoff, Dordrecht, 1987.

Lliboutry, L. A., Ice sheet dynamics, in *Flow and creep in the Solar system: observations, modelling and theory*, edited by D. B. Stone and S. K. Runcorn, pp. 399–416, Dordrecht, etc., Kluwer Academic Publishers, 1993, (NATO ASI Series E: Applied Sciences 391).

Meier, M. F., W. B. Kamb, C. R. Allen, and R. P. Sharp, Flow of Blue Glacier, Olympic Mountains, Washington, U.S.A., *J. Glaciology*, *13*(68), 187–212, 1974.

Merry, C. J., and I. M. Whillans, Ice-flow features on Ice Stream B, Antarctica revealed by SPOT high resolution visual imagery, *J. Glaciology*, *39*(133), 515–527, 1993.

Nixon, W. A., J. A. Dowdeswell, A. P. R. Cooper, D. J. Drewry, L. G. Watts, O. Liestøl, and R. A. Smith, Applications and limitations of finite element modelling to glaciers: a case study, *J. Geophys. Res.*, *90*, 11303–11311, 1985.

Nye, J. F., The flow of a glacier in a channel of rectangular, elliptic or parabolic cross section, *J. Glaciology*, *5*, 661–690, 1965.

Oakberg, R. G., Variational methods for glacier mechanics problems, Bozeman, Montana, Department of Civil Engineering and Engineering Mechanics, Montana State University.

Paterson, W. S. B., *The Physics of Glaciers*, 3rd ed., Pergamon Press, Oxford, 1994.

Payne, A. J., and P. W. Dongelmans, Self-organization in the thermomechanical flow of ice sheets, *J. Geophys. Res.*, *102*, 12219–12233, 1997.

Raymond, C. F., Numerical calculation of glacier flow by finite element methods, *Tech. rep.*, Geophysics Program AK-50, University of Washington, Seattle, Washington 98195, 1978.

Raymond, C. F., Shear margins in glaciers and ice sheets, *J. Glaciology*, *42*(140), 90–102, 1996.

Retzlaff, R., N. Lord, and C. R. Bentley, Airborne-radar studies: Ice Streams A, B and C, West Antarctica, *J. Glaciology*, *39*(133), 495–506, 1993.

Rigsby, G. P., Crystal orientation in glacier and experimentally deformed ice, *J. Glaciology*, *3*(27), 589–606, 1960.

Rooney, S. T., D. D. Blankenship, R. B. Alley, and C. R. Bentley, Till beneath Ice Stream B. 2. structure and continuity, *J. Geophys. Res.*, *92*, 8913–8920, 1987.

Sander, B., *An Introduction to the study of fabrics of geological bodies*, Pergamon Press, Oxford, 1970.

Shabtaie, S., and C. R. Bentley, Ice thickness map of the West Antarctic ice streams by radar sounding, *Annals of Glaciology*, *11*, 126–136, 1988.

Shoji, H., and C. C. Langway, Jr., Flow-law parameters of the Dye 3, Greenland, deep ice core, *Annals of Glaciology*, *10*, 146–150, 1988.

Steinemann, S., Experimentelle Untersuchungen zur Plastizität von Eis, *Beitr. Geol. Schweiz, Ser. Geotech. – Hydrol.*, *10*, 1958.

Thorsteinsson, T., J. Kipfstuhl, and H. Miller, Textures and fabrics in the GRIP ice core, *J. Geophys. Res.*, *102*, 26583–26599, 1997.

Thwaites, R. J., C. J. L. Wilson, and A. McCray, Relationships between bore-hole closure and crystal fabrics in Antarctic ice core from Cape Folger, *J. Glaciology*, *30*(105), 171–179, 1986.

Wakahama, G., Studies of fabrics and textures in deep layers from Dome summit, Cape Folger and the Amery Ice Shelf, Antarctica, *Tech. rep.*, Japanese Science Foundation, 1974, in Japanese.

Weertman, J., Creep of ice, in *Physics and chemistry of ice*, edited by E. Whalley, S. J. Jones, and L. W. Gold, pp. 320–337, Royal Society of Canada, Ottawa, 1973.

Whillans, I. M., M. Jackson, and Y.-H. Tseng, Velocity pattern in a transect across Ice Stream B, Antarctica, *J. Glaciology*, *39*(133), 562–572, 1993.

Wilson, C. J. L., Texture and grain growth during the annealing of ice, *Textures and Microstructures*, *5*, 19–31, 1982.

Wilson, C. J. L., Deformation induced recrystallization of ice: the application of in situ experiments, in *Mineral and rock deformation: laboratory studies — the Paterson volume*, pp. 213–232, American Geophysical Union, Washington D.C., 1986, Geophysical Monograph 36.

Wilson, C. J. L., J. P. Burg, and J. C. Mitchell, The origin of kinks in polycrystalline ice, *Tectonophysics*, *127*, 27–48, 1986.